Refining the Formation of Linear Fissures on Europa

Eliana Grobe Perlman
Department of Astronomy
Mount Holyoke College

May 2, 2024

Professor Darby Dyar
Department of Astronomy
Mount Holyoke College
Thesis Advisor

Visiting Lecturer Thomas Burbine
Department of Astronomy
Mount Holyoke College
Second Reader

Professor Alan Werner
Department of Geology and Geography
Mount Holyoke College
Third Reader

Abstract

Europa is a large moon of Jupiter with an icy crust and a subsurface ocean. Europa orbits close to Jupiter and is tidally locked, so it experiences tidal forces that cause the tectonic, magmatic, and volcanic processes that shape its surface. This relationship has formed two prominent terrain types: ridged plains and chaos terrain. While the ridged plains are dominated by ridges and the chaos by pits and domes, both are home to fractures and gorges (fossae). Studying these landforms could prove useful in deciphering the subsurface's physical, chemical, and mechanical characteristics. Current models of the crust posit a two-layered system with a thinner, brittle outer layer and a thicker, ductile one. However, the exact thickness of these layers and whether this thickness varies over the surface is as controversial as their chemical compositions. Europa's subsurface processes are also debated. The many models of linear landform formation fall into two broad categories: formation via tidal tectonics and formation via indirect tidal forces like tidal heating. The maps and morphological analyses of the landforms in this thesis have contributed to the conversations regarding Europa's subsurface processes and characteristics. This thesis finds an overabundance of wavy and jagged linea compared to tectonic model predictions. It is, therefore, reasonable to assume that indirect tidal processes such as diapirism are at least partially responsible for these landforms. Bethel (2018) explains that tidal forces will preferentially deform regions of the thinner crust, while on planets with uniform crusts, tidal forces will act more symmetrically. The results of this thesis fit the ladder explanation and thus question the idea of a homogenous Europan crust. The landforms mapped in this thesis could be of speleogenic and geochemical interest. However, the quality and quantity of current Europa data have made this dataset incomplete. Thus, once better data is acquired, this list should be refined and expanded upon before it is used for geochemical or spelogenic research.

Introduction

Europa (Fig. 0.1) is the fourth largest moon of Jupiter with a diameter of just over 3000 km, similar in size to our moon. Like our moon, Europa is tidally locked with Jupiter, meaning that if viewed from the perspective of Jupiter, only one hemisphere (called the leading hemisphere) will ever be visible. Data from NASA's Voyager and Galileo missions has shown that it has a water-ice crust and likely supports a salty subsurface ocean (Carr et al. 1998). Because of its proximity to Jupiter, and incredibly fast orbit of 3.5 Earth days, tidal heating is likely responsible for the bulk of Europa's geologic features. The moon flexes and bends in response to the gravitational pull of Jupiter, generating heat and motion in the interior of Europa. Tidal heating and salt content keep the ocean liquid despite its surface temperature of -160C. These tidal forces act on the surface and ocean, similar to terrestrial tectonic processes that act on the crust and mantle. Parts of Europa's crust are squeezed together and collide to form ridges, fractures, and faults or pulled apart to form troughs and ridge complexes. Tidal heating also drives plumes of hot ocean water to break through the crust and spill onto the surface, causing discoloration and creating pitted, bumpy regions called chaotic terrain (Fagents, 2003; Nimmo, F., & Gaidos, 2002;). Much like Earth and Io Europa, has a relatively small number of confirmed impact craters because it constantly resurfaces

Fig. 0.1: The first spacecraft image of Europa ever Captured by *Pioneer 10* in December 1973. Image credit: Alexander et al. (2010) pg 9.

(Bierhaus et al. 2009). As such, its surface is between ~40 and 90 million years old, very young compared to some of its neighbors (Bierhaus et al. 2009).

The exploration of Europa began in the early 1970s with instruments like NASA's optical telescopes on Mauna Kea and Hawaii. The telescopes used spectrometry to measure the temperatures and surface composition of Europa and its fellow Galilean satellites (the other three large moons of Jupiter). Analyses of these data concluded that between 50% and 100% of the surface of Europa is water-ice (Alexander et al., 2009 pg. 7). Additionally, variations in rotation were noted in both visible and ultraviolet reflectance, suggesting Europa might be interacting with the Jovian magnetosphere (Morrison et al., 1974; Johnson & Pilcher, 1977)

Around the same time, NASA launched the first mission to leave the solar system. The Pioneer mission had three main objectives. "1) explore the inter-planetary medium beyond the orbit of Mars; (2) investigate the nature of the asteroid belt, assessing possible hazards to missions to the outer planets; and (3) explore the environment of Jupiter, including its inner magnetosphere"(Europa book hist sec, pg. 8).

Pioneer 10 was launched in 1972 (followed by Pioneer 11 in 1973), carrying two magnetometers, a plasma analyzer to examine solar wind, a charged-particle detector, and an ion detector. Despite this clear emphasis on exploring Jupiter's magnetosphere, the Pioneers also carried three rudimentary remote-sensing instruments: an imaging photopolarimeter, ultraviolet photometer, and infrared radiometer. In December of 1973, Pioneer 10 completed its weeks-long Jupiter encounter and obtained the first spacecraft view of Europa (Fig. 1). Despite its low resolution at 200 km/pixel, the image displays a world with distinct geology as interpreted from its different surface albedos. Not long

after this, Pioneer 11 measured Europa's density to be 2.99 g/cm3, much lighter than its neighbor Io, suggesting that the two had very different compositions and structures in contrast to popular hypotheses (Alexander et al., 2009 pgs. 8-10).

Pioneer data allowed scientists to infer their surface and internal compositions based on the reflectivity or albedo of the surfaces and their densities. The satellite observed that Europa has a reflectance spectrum similar to clean water ice (Fanale et al.,1977, as seen in Burns, 1977). The optical and density data was used to calculate Europa's bulk density. The ice layer was expected to be a maximum of 40 km thick with a silicate core (Fanale et al., 1977 as seen in Burns, 1977). Consolmagno (1975) also used these data to calculate that Europa is 10% water-ice and 90% silicate by weight. The thesis also calculated that Europa had a thin ice crust, water underlayer, and silicate core. At this time, some also began to theorize about the formation of the Jovian system in earnest. For Europa, the emerging view was that its history bore several similarities to Earth's (Pollack & Reynolds, 1974; Cameron & Pollack, 1976; Pollack et al., 1976).

Next came the two Voyager missions, whose imagery would provide more detailed and expansive data from Jupiter, Saturn, Uranus, Neptune, and their respective satellites. The instruments updated Europa's density to ~3.0 g/cm3, and its imagery mapped the moon's surface features more extensively. Due to its disadvantageous orbital position during both flybys, Europa was poorly imaged, with only a tiny fraction of one hemisphere mapped at 2 km/pixel. That portion was almost entirely crater-free and consisted of bright, high-albedo terrain crisscrossed by long linear markings with some short ridges up to a few hundred meters in elevation (Alexander et al., 2010 pg. 11).

Such an absence of craters and surface relief suggested recent resurfacing to Voyager-era scientists (eg. Squyers et al., 1983) while the long cracks implied a brittle crust subject to tectonic stress (eg. Parmentier & Head et al., 1981). It was also proposed that Europa may experience episodic heating analogous to the tidal forces responsible for Io's immense geologic activity. Voyager imagery also enabled surface mapping of Europa, early studies of its surficial geochemistry, and speculation about Europa's atmosphere. (Alexander et al., 2010 pgs. 10-12)

Voyager also spurred many people to speculate about the habitability of Europa. For example, American astronomer and physicist Guy Consolmagno, in the appendix of his master's thesis, remarked, "Given the temperatures of the interiors, and especially of the silicate layers through which liquid will be percolating, the possibility exists of simple organic chemistry taking place, involving either methane from the ice or carbon in the silicate phase. However, we stop short of postulating life forms in these mantles; we leave such to others more experienced than ourselves in such speculations" (Consolmagno, 1975). Novelist Arthur C. Clark also famously imagined what life might look like on Europa in his 1986 novel 2010: Space Odyssey Two, the sequel to his 1968 novel (and motion picture) 2001: A Space Odyssey Europa's habitability.

While all seemed to agree that life on the surface would be improbable given the radiation and near-vacuum conditions, Consolmagno (1975) suggested that life could be possible in the subcrustal ocean. Scientists were also beginning to understand a previously unknown type of terrestrial lifeform: autotrophs that somehow lived without the sun or oxygen. These mostly oceanic lifeforms convert chemical compounds from geothermal sources into energy, a process termed chemosynthesis. Comparable

processes are plausible in Europa's dark, likely anoxic, subsurface ocean (Chyba, 200; Chyba & Hand, 2001 add to bib later). However, quantitative discussion of biosignatures would have to wait until better geochemical data was obtained (Alexander et al., 2010, pgs 11-12).

The present era of Europa exploration began with the launch of Galileo (Fig. 0.2), which had been in the conceptualization and development stage long before the Voyager 1 launch date. The Galileo orbiter carried 16 instruments, including various remote sensing instruments such as the Solid-State-Imaging (SSI) device for optical imagery, the Near Infrared Mapping Spectrometer (NIMS) for chemical analysis, an Ultraviolet Spectrometer (UVS) to study gases and a Photo-Polarimeter Radiometer (PPR) to measure radiant and reflected energy (Alexander et al., 2010 pg. 13). Galileo was in the Jupiter system from December 1995 through September 2003, almost a full Jovian year. It achieved several flybys of the Galilean moons: Io, Ganymede, Calisto, and Europa.

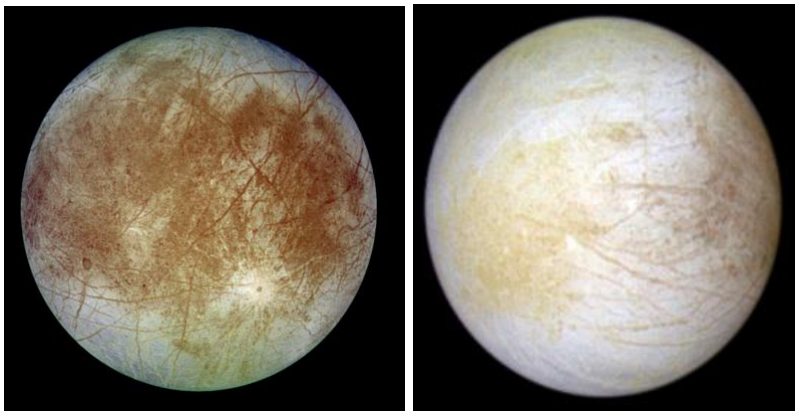

Fig. 0.2: True-color images of the trailing hemisphere (left) and leading hemisphere (right) of Europa captured by the *Galileo* satellite. Image credit: NASA image archive, PIA00502 (left) and PIA01295 (right).

For Europa, Galileo's 12 encounters obtained Global SSI imagery in resolutions comparable to its direct predecessor as well as regional views that were a few hundred m/pixel and high-resolution (tens to five m/pixel) images of key terrains and features like Conmara Chaos, fracture networks, and Cilix impact crater (examples, Fig. 0.3). The imagery from Galileo has greatly contributed to our knowledge of Europa's surface, producing innumerable papers whose ideas I will briefly summarize in the fourth section of the Background

This thesis uses *Galileo* imagery to explore an as-of-yet-overlooked aspect of Europa's geology, its shallow subsurface. By identifying and studying key features on the surface that, if studied, could hint at the dynamics and characteristics of the subsurface caves. Europa is governed by tidal forces and intrusive and extrusive cryovolcanic processes and thus, Europan SAPs are most likely tectonic and/or cryovolcanic in origin. Therefore, studying the spatial distribution and morphological variations in SAPs on Europa can provide insights into these processes. Similar to Martian missions like Curiosity and Insight, these features can serve as landing sites for future missions to Europa.

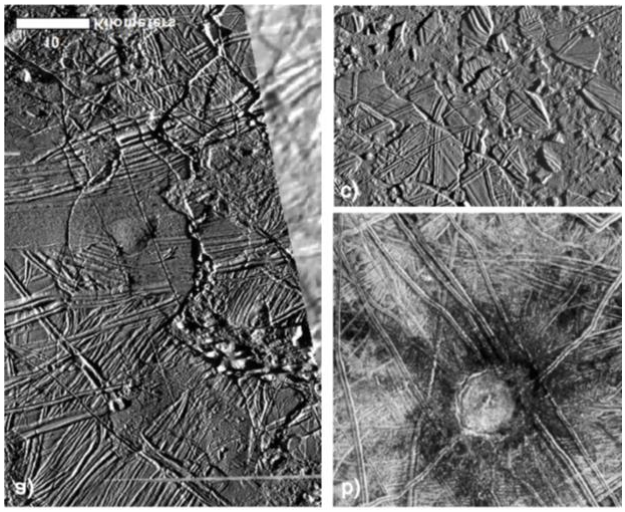

Fig. 0.3: a) a fracture network image credit: Galileo, SSI images 11E0024 (top) and 11E0026 (bottom); b) Cilix impact crater and c) Conmara Chaos, image credit: Galileo observation E6ESBRTPLN01

1. Background

Understanding this project depends on the appreciation of several critical aspects of planetary science. To identify caves on other planets, we must know what they are, how they form, and what data studying them can provide. We must also look into extraterrestrial cave exploration as a whole. Finally, we must understand the moon's geology to identify geologic features on Europa.

1.1 Caves and Speleogenisis

Most early and modern definitions of caves have tended to be very geocentric. For example, in a paper called "On the definition of a cave," Curl (1964) refers to "proper caves" as those that a human can enter and explore. This paper defines all non-dissolution caves as simply pseudokarst. On Earth, the majority of the caves that have been explored formed through karst (Wynne et al. 2022) dissolution processes that only occur in areas where rocks (i.e. limestone, dolomite, gypsum, etc.) experience dissolution due to specific geochemical conditions that are common on Earth.

These definitions are not very practical for extraterrestrial cave studies. The caves to be discussed here cannot be entered by humans, and the geochemistry of many extraterrestrial planets in the solar system and beyond lack much or all of the necessary components for karstification. Thus, for this paper, caves are essentially voids in the subsurface of a planetary body. The categories of formation, or speleogenisis, are similarly broad; caves can form via either constructive or destructive processes.

1.1.1 Destructive Speleogenisis

Destructive caves are voids formed through the removal of material. These may be created through dissolution (i.e. karst), suffusion, and mechanical transport. Tectonic and volcanic processes often form these, and they can even form in glaciers.

Destructive caves are voids formed through the removal of material. These may be created through dissolution (i.e., karst), suffusion, and mechanical transport. Tectonic and volcanic processes often form these, and they can even form in glaciers.

Karst formations

Dissolution is the most common type of speleogenisis on Earth, and it occurs through a chemical reaction called karst. A karst reaction has two main components: a rock, such as limestone or marble, that contains calcium carbonate (easily soluble minerals like calcite, halite, gypsum) and water. As illustrated in Fig. 1.1, as rain travels from the clouds to the Earth's surface, it picks up CO2 from the atmosphere, causing carbonic acid to form in the water. As a result, this

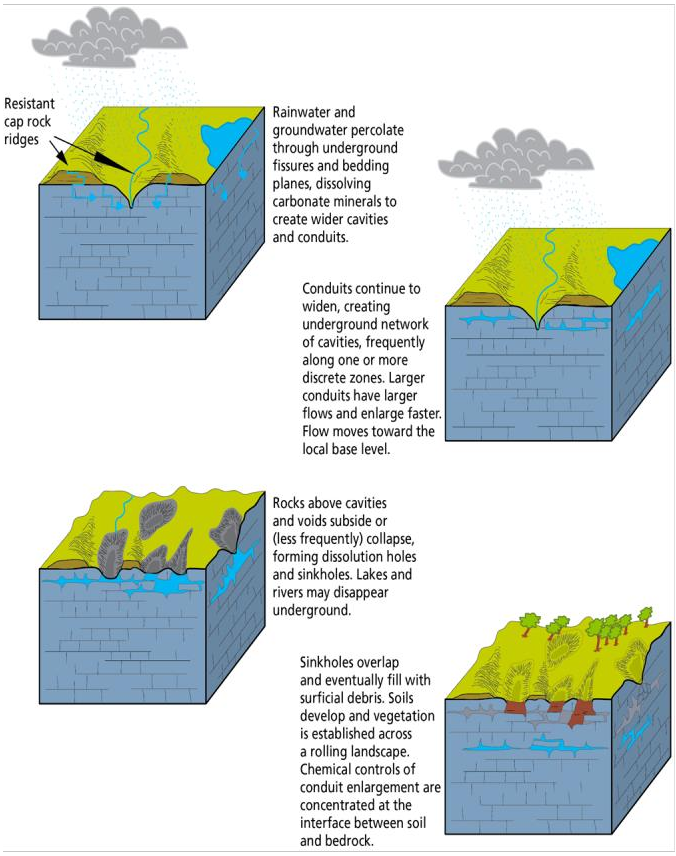

Fig. 1.1: Diagram of Karst landscape formation, Image credit: U. S National Park Service.

weakly acidic solution travels through the soil (profile picking up additional carbon dioxide) and ultimately into the bedrock below. This solution will react with these minerals and rocks, slowly dissolving them. Over time, this dissolution destabilizes the soil's foundation, forming joints, fractures, and voids. Sometimes, the voids eventually enlarge so much that their ceilings collapse, forming sinkholes and cave entrances. Water can also travel through the fracture network it creates until it bursts forth from the bedrock into a spring, another cave entrance. Water from rivers and streams can also cause this process by collecting weak acids from the soil as it travels through the subsurface, causing lakes to sink and streams to seemingly disappear (The Encyclopedia Britannica) Ground water flow is crucial to this step. If water cannot utilize the pore space of the soil and bedrock, dissolution will not happen.

Suffusion or 'piping caves' also fall into this category. Suffusion is the process of mechanically moving fine particles in pore water. Underground, fine-grained particles are transported through an existing pore (shown in Fig. 1.2). This process is similar to

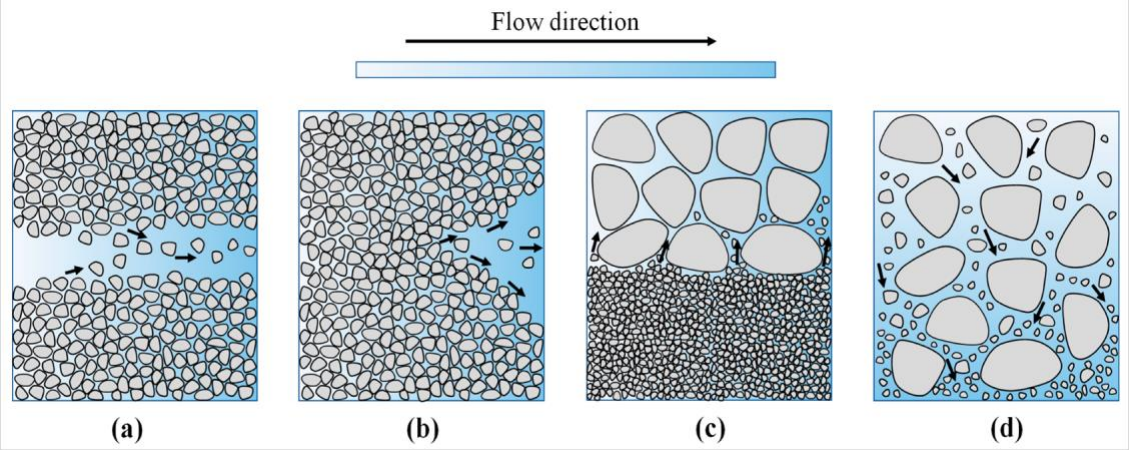

Fig. 1.2: Soil erosion and piping cave formation process image credit: Dastpack et al., (2023)

karst but also includes rocks such as sandstone or claystone that are not easily soluble. To form, they require a large amount of unconsolidated rock that is very stable in a

humid environment. On Earth, the vast majority of unconsolidated rocks are eroded by water or removed and transported to another location before they can accumulate to the quantity required for suffusion caves. As a result, terrestrial suffusion caves are very rare (Speleology: Suffosional Pseudokarst - Piping Cave - Showcaves.com)

Glacial Caves:

Glacial caves also fall into this category. As the name suggests, these form inside glaciers, created through melt. A typical glacier grows in the winter, fed by the snow, and shrinks in the summer due to the heat. As the air temperature increases, it can melt different parts of the glacier more easily than others based on their reflectivity or albedo.

A glacier's albedo is highest when covered in freshly fallen snow. The air pockets in the snow allow heat and light to bounce off of it effortlessly. As the snow compresses over time, its reflectivity decreases, but it is still relatively high (Hodgkins, 2001). As the seasons change, the snow stops accumulating and even starts to melt in some places. This differential heating can cause meltwater rivers and lakes (called moulins) to form on the glacier's surface. The warmer meltwater can then

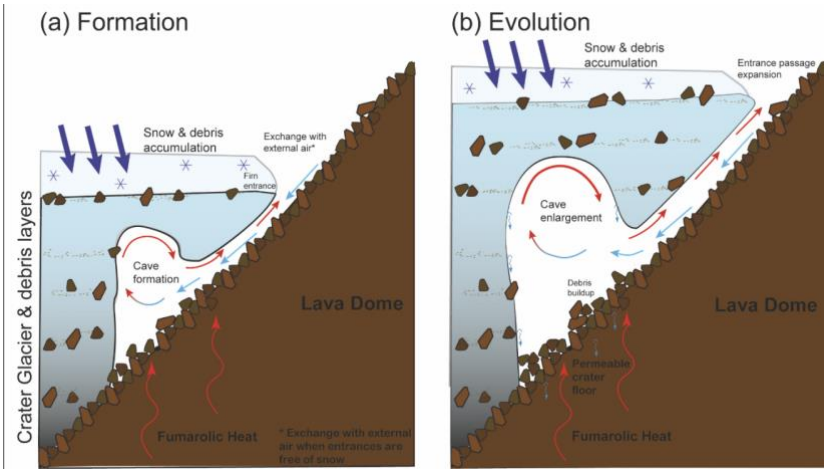

Fig 1.3: the formation and evolution of a glacial cave Formed by differential melting caused by the heat from the lava dome below the glacier. Image credit:(Sobolewski,et al.,2020)

cut troughs and holes into the glacier, and the surface can refreeze above the newly formed void, creating a cave (Speleology: Glacier Caves - Showcaves.com). They can also form at the bottom of a glacier as a hole formed by melting from a heating source below the glacier (shown in Fig 1.3).On Earth, most glacier caves do not last very long. They either close up once the melt season ends or collapse from a more significant melt during the same season. However, these caves could last longer on icy worlds like Europa or Enceladus (Wynne et al. 2022).

Tectonic and Volcanic caves:

Tectonic processes can also form destructive caves by moving large amounts of bedrock. Fissure or fracture caves possibly form through one or several tectonic processes. One hypothesis is the divergent movement of rock sections: in plate tectonics, plates, whole or in part, move away from each other, creating fissures. These can penetrate deep into the crust, but they are sometimes filled with magma from the upper mantle, resulting in dyke formation instead of caves. Another idea is uplift and subsidence, which never occurs evenly, resulting in the fracturing of harder rock layers and the folding of softer ones. The final method involves the creation of voids via the separation of rocks along pre-existing joints or fractures, which are pulled apart slowly by the movement of the tectonic plates, leaving narrow fissures behind (fracture cave). Ridges, which have narrow troughs in their center, are also counted as tectonic caves in this project. Although their entrances are typically inaccessible to humans, they are pathways to the subsurface. None of the potential caves on Europa are accessible to humans.

Caves can also form in volcanic environments, although destructive and constructive processes create them. During an eruption, lava can flow out of the vent and onto the surface like a river. The top of the flow is exposed to the elements, so it tends to solidify quickly, trapping the still-liquid lava beneath it. The now-subsurface lava river melts through to the bedrock, causing a tunnel that is left behind after the lava drains. (lava cave). Additional lava flows create more tunnels and expand the main ones by melting through the bedrock (Wynne et al., 2022). Over time, the roofs of these lava tubes can collapse, leading to pit craters by the suffusion process. Lava tubes are thus constructive, while the tunnels in the bedrock and pit craters are destructive.

1.1.2 Constructive Speleogenisis

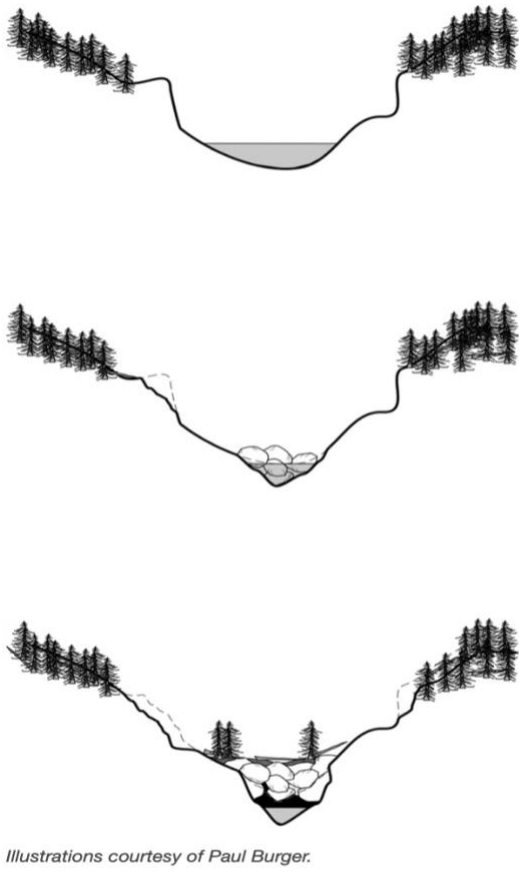

Fig 1.4: A diagram of talus cave formation, image credit: Talus Caves, NPS.com,

In contrast to the previous types, constructional caves form through material transport to the location, closing off an area to create a void. These form through tectonic, volcanic, and a few karst processes. The most common terrestrial tectonic constructive cave is a talus cave, which gets its material from rockslides. They form in three stages (shown in Fig. 1.4).

In stage one, a stream or another erosional process cuts a deep, steep valley into the ground. The combination of water from the stream and the steep slope reduces the friction,

keeping the surface together, leading to stage two, where parts of the walls collapse into the valley. As the water flows and cuts downward, a void space is created underneath the fallen rock (stage three). These stages can repeat over and over, adding material to the ceiling.

For this thesis, lava tubes (described in the previous section), pits, and volcanic vents can also be considered cave entrances, especially once the volcano becomes extinct. They are still Subsurface Access Points (SAPs) and thus cannot be separated from this list like they often are. On Earth, cryovolcanism can also create temporary cave systems on glaciers through the partial melt of the glacier, penetrating it and creating crevasses and moulins.

1.2. The History of Extraterrestrial Cave Exploration

Other studies have quantified, characterized, and explored potential cave entrances and systems on bodies from Mercury to Pluto (including Earth) (Cushing et al.,2017; Martin et al., 2017; Crown et al., 2018; Wagner & Robinson, 2021; Malaska et al.,2022; Wynne et al., 2022). These reports, summarized in Wynne et al. (2022), have found that all planets exhibit some or all of these seven cave-forming (speleogenic) processes. Volcanism (cryo and/or magmatic), fracturing (tectonic and/or impact melt), sublimation, suffusion, dissolution, phase transition, and mass-wasting.

1.2.1 The Moon

The Moon was the first solar system body on which surface caves were identified., A majority of them were imaged at a scale of 0.5-2 m/pixel by the Lunar Reconnaissance Orbiter (LRO). To date, hundreds of SAPs have been identified on its surface, the majority of which (221 out of 276) occur in impact melts (Wagner &

Robinson, 2021). Collapse pits are the most extensively researched of these caves because they could connect to extensive networks of lava tubes potentially suitable for habitation (Wynne et al., 2022). Some researchers (Fielder, 1965; Wilson et al., 2011) have also proposed that the Lunar SAPs, chiefly long narrow troughs, or grabens, were formed by the formation and expansion of subsurface fractures driven by tectonic and/or intrusive volcanism. This process is thought to have formed some of the pit craters in Hawai'i, a landscape often used as a lunar analog because of their similar geology (Okubo & Martel, 1998).

1.2.2 Mars

On Mars, over 1600 SAPs have been identified (Baioni et al., 2009; Cushing, 2017). These are compiled in the Mars Global Cave Candidate Catalog (MGC3). They include pit crater chains, lava tube skylight features, small rimless pits,(Fig 1.5)

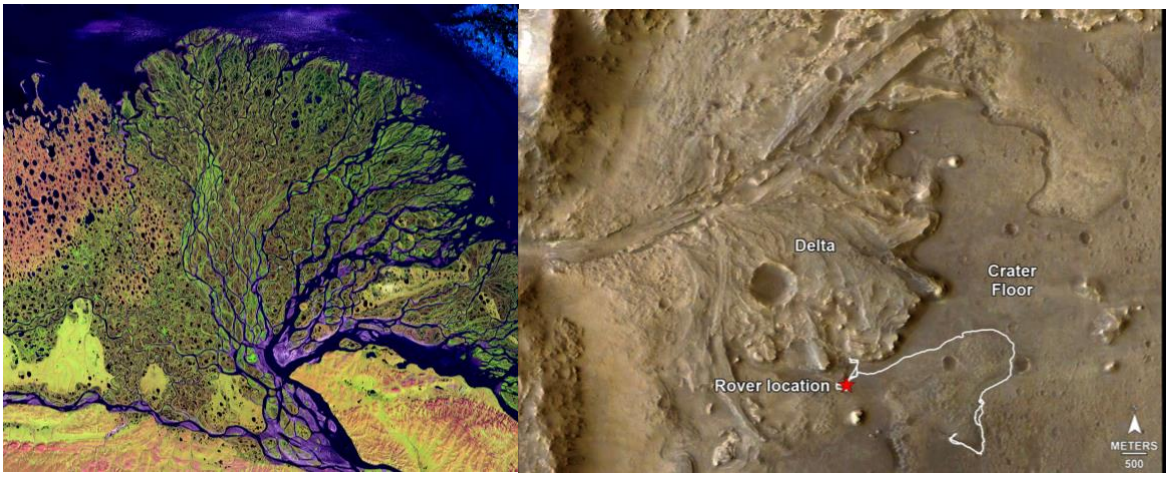

Fig. 1.5, Notice the visual similarities between a suspected Martian river delta nearby Jezero Crater, (the landing site of Perseverance Rover shown on the left. Image credit: NASA JPL) and a terrestrial river delta (Lena river delta in Russia imaged in infrared false color on the right. Image credit: USGS EROS Data Center Satellite Systems Branch, Landsat 7 Satellite, 2000).

pinholes, lateral entrances on cliffs, and deep extensional fractures (i.e., grabens) (Cushing et al., 2017).

Some pit craters may be entrances to lava tubes (Cushing et al., 2017), and others are tectonic fractures with collapsed walls that leave small holes exposing them to the surface (Okubo & Martel, 1998). Mars also has sinkholes, structures that are not possible without water. Today, Mars is a cold, desolate wasteland, but about 4 billion years ago, it was not too dissimilar from Earth. This is evidenced by the abundance of fluvial formations like deltas that litter the surface (Fig. 1.5) and the abundance of surficial calcium, magnesium sulfate, and some carbonate deposits, which commonly get left behind as water evaporates.

1.2.3 Titan

Malaska et al. (2022) used the Cassini Synthetic Aperture Radar (SAR) to identify and characterize 1,270 Subsurface Access Points (SAPs) on Titan, an icy moon of Saturn with a thick, nitrogen and methane(CH_4)-rich atmosphere. The paper found that Titan has at least one cryovolcanic and at least 370 other equatorial pits. It also analyzed older papers that catalog hundreds of depressions and valleys, some of which lie in the moon's Labyrinth terrain (Fig. 1.6).

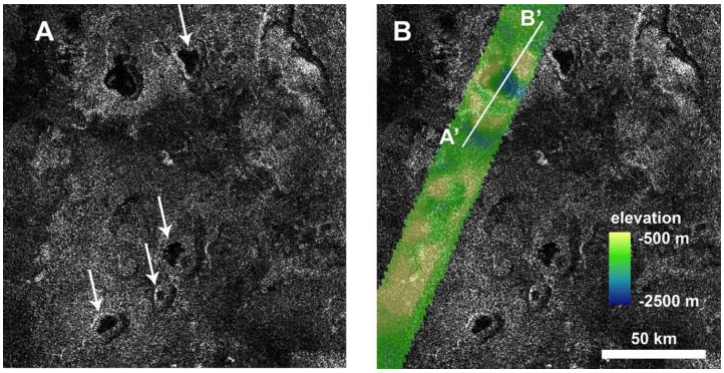

Fig. 1.6: examples of SAPs on Titan. (a) Synthetic Aperture Radar (SAR) image of an unnamed filled lake in the north polar terrain of Titan. The lowest backscatter return (darker) indicates liquid fill in parts of the lake. Several partly filled lakes are also present in this scene, indicated by white arrows. (b) Overlay of colorized Digital Elevation Model (DEM) on the SAR image. Warmer tones indicate higher elevation, colder tones indicate image and co lower relative elevation. Image and caption credit: (Malaska et al.,2022)

Data from the Cassini-Hughes mission has shown compounds like CO2, Benzene, and a variety of organic chemical compounds (Maynard-Casely et al.,2018). This chemistry means some pits could have formed through karst processes, like terrestrial sinkholes (Malaska et al., 2022). Filled lakes (Fig.1.7) were also found at northern latitudes, which might have formed similarly to the pits (Malaska et al., 2022).

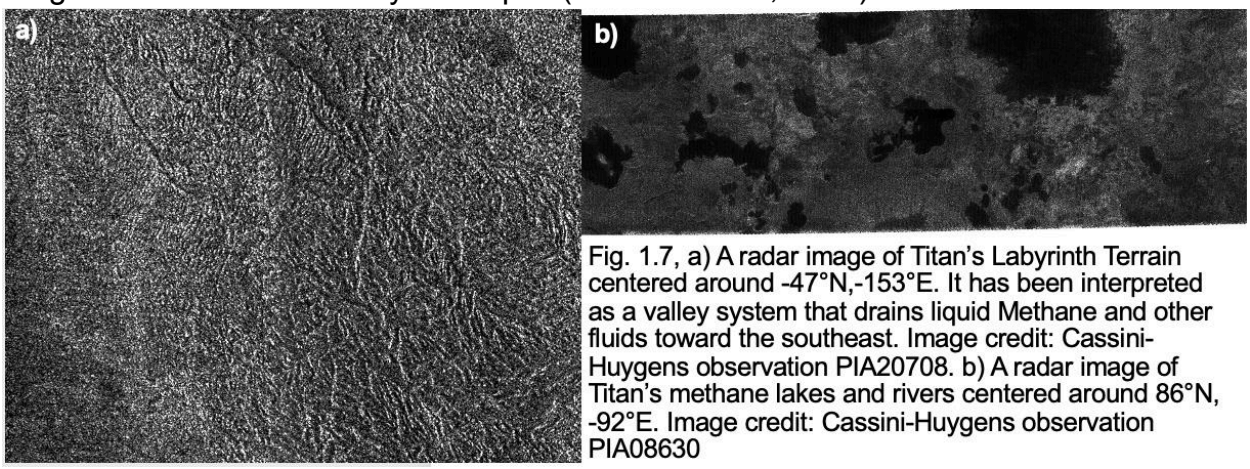

Fig. 1.7, a) A radar image of Titan's Labyrinth Terrain centered around -47°N,-153°E. It has been interpreted as a valley system that drains liquid Methane and other fluids toward the southeast. Image credit: Cassini-Huygens observation PIA20708. b) A radar image of Titan's methane lakes and rivers centered around 86°N, -92°E. Image credit: Cassini-Huygens observation PIA08630

1.2.4 Ganymede

Ganymede, the largest moon in our solar system and a fellow moon of Jupiter comprises roughly equal proportions of silicate rock and water. It is theorized to have tectonic, cryovolcanic, impact, phase transition, and sublimation SAPs. Ganymede moon has pit-crater chains (fig 1.8a), standard features of icy and rocky bodies (e.g Cushing, 2017; Martin et al., 2017) that have been previously associated with caves on Earth the Moon, and Mars (e.g. Ferrill et al., 2011; Okubo & Martel, 1998). Several chains, especially the four

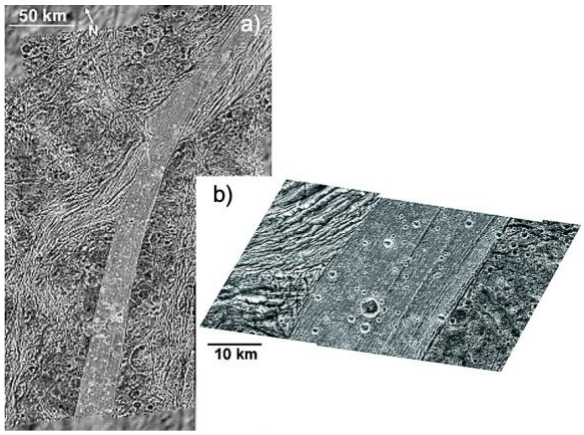

Fig 1.8: two images of suspected cave entrances on Ganymede. A potential fracture cave (a) and a chain of cryovolcanic pits (b). Image credit: Galileo SSI image mosaics (Head et al., 2002

largest, may support tectonic caves (Wynne et al., 2022). Galileo SSI imagery (Fig. 1.8b) suggests cryovolcanic vents and sources and fracture caves may also be present. These likely formed as a result of faults (Head et al., 2002) and meteor impacts (e.g., Scully et al., 2020) enlarged by freezing expansion (Boston, 2004). These processes are also possible on Europa (Wynne et al., 2022).

Ganymede's permafrost can be subject to ice sapping, a process also experienced on Earth. This process is where underground icy permafrost thaws and freezes repeatedly, leading to collapse and subsequent void formation (Wynne et al., 2022). The heat of impact events also releases volatiles trapped within the ice, forming subsurface void spaces (Boston et al., 2004). Roth et al. (2021) has also confirmed that water vapor is present in Ganymede's atmosphere, reinforcing the potential for sublimation-driven speleogenisis (Wynne et al., 2022).

1.2.5 Triton

Triton is an icy moon of Neptune with a thick atmosphere of nitrogen. Only 40% of its surface was imaged by a spacecraft, Voyager 2, during its sole visit. What was captured revealed that Triton resembles Saturn's moon, Titan. It is thought to experience cryovolcanic, tidally driven tectonic, mass-wasting, and possibly karstic speleogenisis (Wynne et al., 2022). The imagery revealed that most of the surface is smooth, geologically young, and

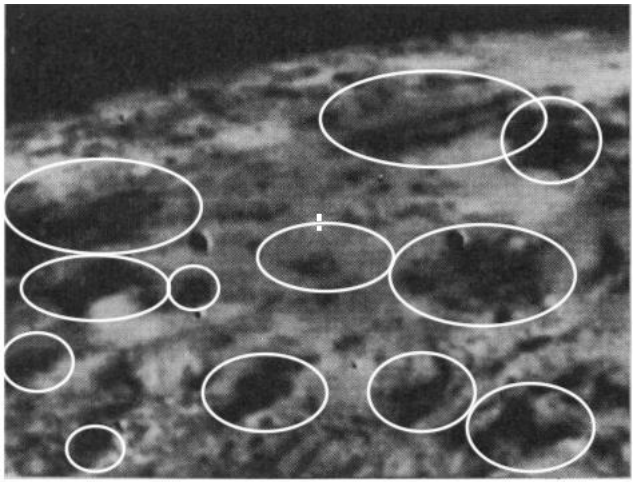

Fig. 1.9: Several plumes (circled) in the western equatorial regions of Triton (Soderblom et al.,1990)

composed of mainly erupted material. (Croft et al.,1995). Large caldera-like depressions, three active plumes (Fig. 1.9, Soderblom et al.,1990), and flow lobes (Planum) are on the surface. Therefore, cryo-lava tubes confirmed by Lunar lunar cave systems are possible cave systems on Triton (Wynne et al., 2022). Additionally, the pit crater chains, pits (standalone referred to as cavi and in clusters) (Croft et al.,1995), and pitted ridges (Croft et al., 1995) on Triton's rugged Cantaloupe Terrain (Fig. 1.10) are also possible SAPs (Wynne et al., 2022). Curvilinear ridges (Fig. 1.10) and Grid-like linear ridge networks and rugged ridges (all termed Sulci) are also present (Croft et al., 1995), implying the possibility of tectonic speleogenisis on Triton (Wynne et al., 2022). Some have also proposed that some Cantaloupe Terrain could be due to landslides and other mass-wasting processes (Smith et al., 1989). The presence of numerous scarps and irregularly shaped and distributed hills and knobs further corroborate the existence

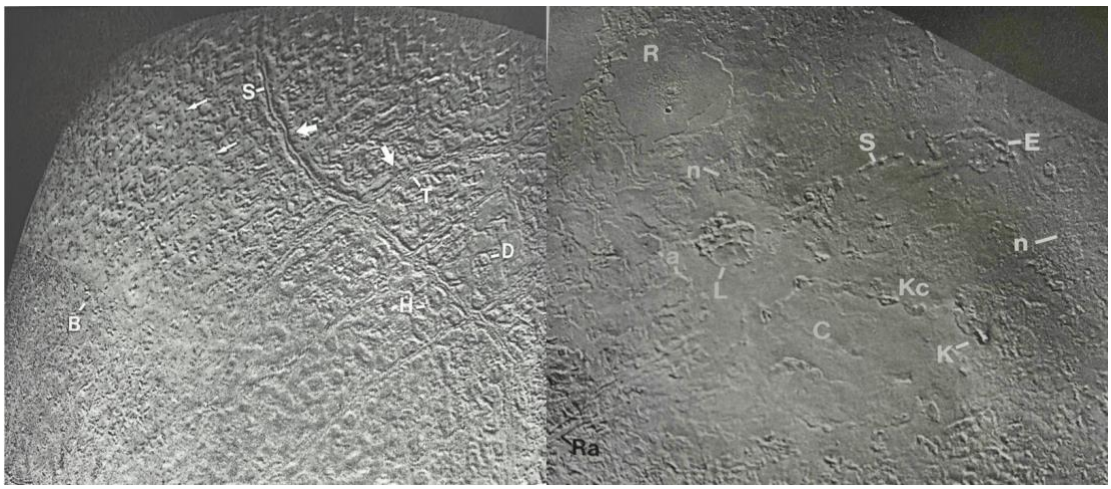

Fig. 1.10: Two images of Triton showing a variety of geologic features and terrains. On the left is cantaloupe terrain in Bubembe Regio with curvilinear and textured ridges depicted with arrows. Bheki, Dagon, and Hekt Cavi (B,D and H respectively); Slidr and Tano Sulci (S and T) are part of this terrain's characteristic look. On the right is a completely different section. Centered on Cipango planum (C), a lava plain, which is surrounded by Kibu and Leviathan Patera(K and L) irregular pits; and Set and Kraken Catena (S,E and Kc), two chains of rimless pits. Raz Fossae (Ra), and the smooth Ruach Planitia (R) are also part of this complex region. Images and descriptions : (Croft et al., 1995)

of this process and the possibility of them forming constructional, Talus talus caves as they have on Earth (e.g., California's Balconies Caves).

1.2.6 Enceladus

Several fracture networks, pit crater chains, about 2000 narrow troughs, and 100 water-ice plumes have been identified on another of Saturn's icy moons, Enceladus (see Fig. 1.11) (Wynne et al., 2022). Like Europa, Enceladus has a thin icy crust that covers its global ocean. Tidal heating is likely the primary driver of the geologic processes that produced these SAPs, tectonism, and cryovolcanism (Porco et al., 2014). The fracture networks are theorized to respond to the expansion and contraction of Saturn's gravity coupled with the heat it generates, causing water vapor to well up and crack through the surface (Lucchetti et al., 2017). Its troughs are also likely indicative of recent tectonic activity, penetrating several kilometers of the crust (Lucchetti et al., 2017).

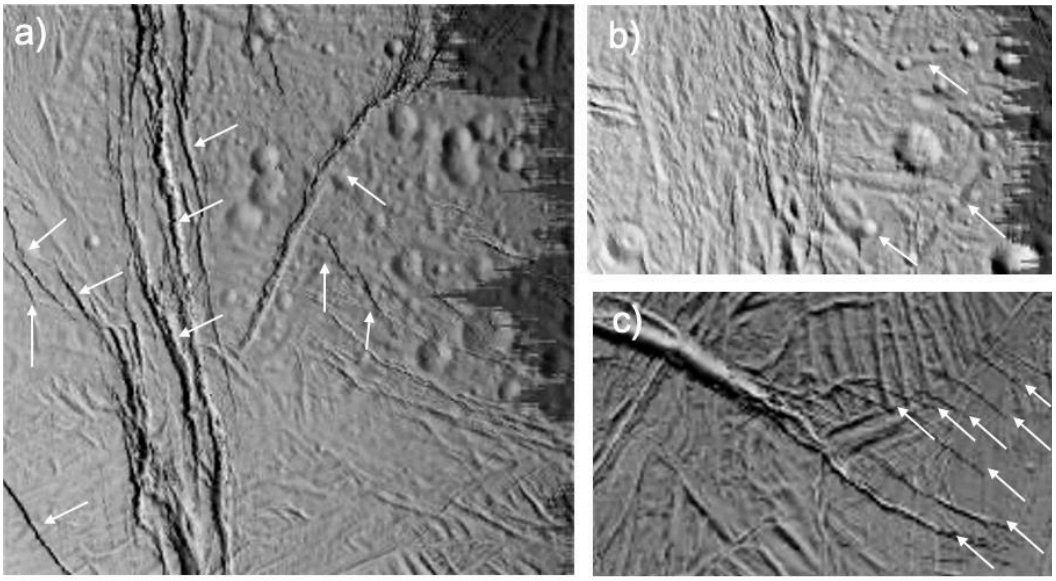

Fig. 1.11: Cassini images of Three types of potential cave entrances on Enceladus. Fractures or narrow troughs (a), isolated pits (b) and pit crater chains (c). Image credits: image N1500061838, b) image N1489050078, c) image N1487182149

1.3 The Significance of Studying Caves

Studying subsurface environments can inform scientists about planets' mineralogic and climatic histories, the movements of liquids like lava, magma, and groundwater, and even a planet’s tectonic history.

The isolation of cave environments often provides them with unique climates and atmospheric conditions very different from the surface, making them ideal targets for astrobiology and future space exploration by humans (Wynne & Titus et al.,2022). On Earth, karst caves have geologic structures called speleothems that grow from their grounds and ceilings. After a cave forms, the still-saturated groundwater can drip through cracks in the cave’s ceilings and floors, depositing these minerals in thin layers that, over time, build up to become stalactites and stalagmites. Once stalactites and stalagmites stop growing, their growth rates can be determined through radiometric dating, indicating precipitation levels in the area. They also contain archives of the climate in the ratio of oxygen isotopes stored in each layer of the minerals (How Caves Can Teach Us About Climate, NOAA.gov)

Similarly, the aforementioned geologic history of Mars makes its caves a prime target for astrobiologists and paleoclimatologists. Their isolation from the outside world could also be useful for paleoclimatic studies. They can also protect potential microfossils and other biosignatures that can degrade due to prolonged radiation exposure (Wynne & Titus et al.,2022).

On Earth, caves can provide more than just paleoclimate information. Because lava tubes are considered caves, mapping and exploring them can provide information about the volcano’s lava composition, viscosity, and the eruption rate of their parent

volcano (i.e., Webb et al.,1982; Hoang et al., 2018). Broken speleothems have been used as potential indicators of tectonic movement. Similar trends can be seen in the study of extraterrestrial caves.

A recent study on the spatial distribution of cycloid ridges (believed to be archives of polar wander and tidal forces on Europa (Rhoden et al., 2021) has revealed clusters and gaps that can be used to constrain tidal stress models. An examination of Europa pit morphology has revealed an absence of surface strain, which implies that pit shape and orientation are decided during their formation and possibly influenced by properties of the ice shell-like stress (Culha et al., 2016). Stress within the shell might change over time due to polar wander and orbital evolution, suggesting pits with similar orientations were likely formed at similar times.

Poco et al. (2014) mapped geysers on Enceladus and found apparent correlations between the locations of individual hotspots and jets and the visible thermal emission, jet activity, and tidal stresses. This suggests that they are linked to the generation and transportation of planetary heat, and thus, studying them can uncover both the current thermal state and thermal history of Enceladus. Similarly, a later analysis of fracture networks on Enceladus determined that the depth of fracture penetration increases from 31 km up to 70 km up to 75°N latitude. They used this information to determine the depth of the moon's crustal boundary (Lucchetti et al., 2016).

Caves are also frequently proposed as landing sites for future missions. They are usually flat at the bottom, making them easy to land on. They can also provide protection from radiation and cheap, easy access to the subsurface.

1.4 The Geology of Europa

Europa is a moon of Jupiter with a water-ice crust, a subsurface ocean, a silicate rock layer, and an iron-nickel core. It also has a thin oxygen atmosphere. Its equatorial diameter is 3100 km, making it about 90% the size of Earth's moon. The many fractures dotting the surface are covered in a reddish-brown material (see Fig. 0.2). Its composition is unknown. Still, it is speculated to be a mixture of salts and sulfur compounds mixed with ice that has been altered by radiation. Europa's terrain and geologic features are formed outside of its small number of impact craters through the push and pull of Jupiter's gravity (Tidal forces).

Tidal forces create tectonism on Europa akin to our plate tectonics, forming the ridges that are the most common landform on the surface. Most commonly, it takes the form of double ridges (see Fig. 1.12), comprising a pair of ridges with a central trough. These can be anywhere from a few hundred to thousands of kilometers long and 500 to 2000 meters wide (Greeley et al., 2004). Many ridges show evidence of strike-slip faulting (Hoppa et al., 1999) and extension in their morphologies through breaks and multi-ridge complexes (termed lineated bands, see Fig 1.12). Ridges can be both straight and curved. The cycloid patterns suggest that these originated as arched fractures altered by Europa's stress field (which rotates with its orbit). The straight ridges likely evolved from straighter cracks.

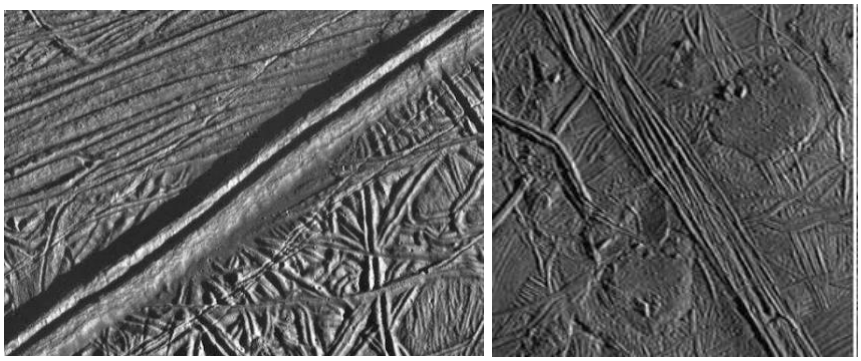

Fig. 1.12: A double ridge, (left) and a section of Agave Linea, a lineated band or ridge complex (right). Galileo imagery courtesy of NASA/JPL.

Fractures and fossae are other types of tectonic features on Europa. Fractures are narrow cracks that are thought to form through processes similar to ridges (see Fig. 1.13). Some formation models even suggest that fractures are the first step to forming double ridges. Fossae are shallow gorges or troughs formed predominantly by extensional tectonics, with some also suggesting strike-slip influences (Matteoni et al., 2023). These features can appear in straight, cycloidal shapes and hundreds of kilometers long.

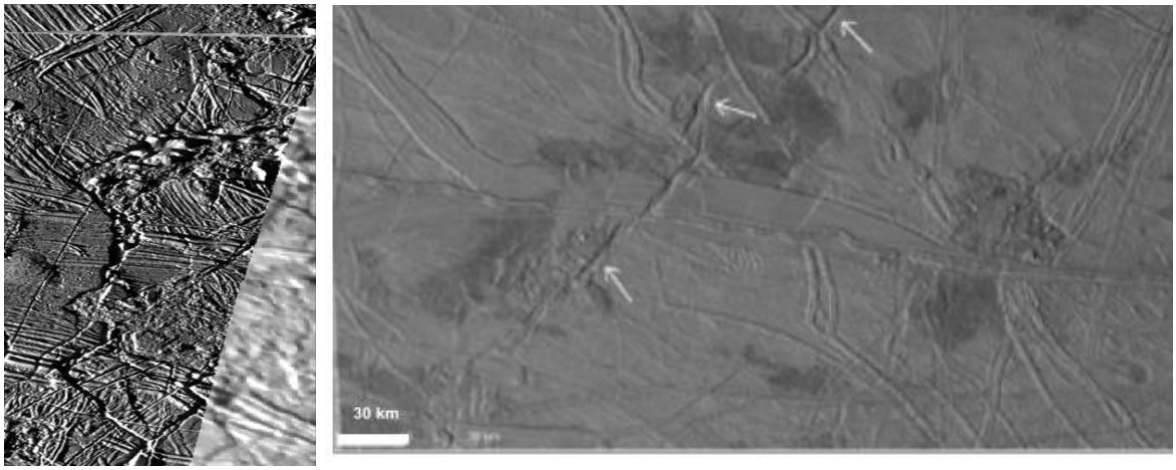

Fig. 1.13: a Europan fracture network (left) and Kermario Fossae (right)

Chaotic terrain is an enigmatic terrain that covers about 28% of Europa (Collins & Nimmo, 2009). It is characterized by having two different terrains seemingly embaying one another. A matrix of lumpy terrain with pits and domes surrounding plates of ridges and fractures (see Fig 1.13). The only thing that is certain about chaotic terrain is that it is likely the youngest type because it crosscuts all other features.

Its formation is largely unknown, but there are several models. In the melt-through model, a patch of ice is heated by tidal heating, creating a partial melt below the surface. This melt then warps the surface and refreezes over time (Greenberg et al., 1999). Another is the Diapirism model. Diapirs are vertical intrusions of rock (or, in this case, ice) that warp the surface. The final popular theory is brine mobilization, in which

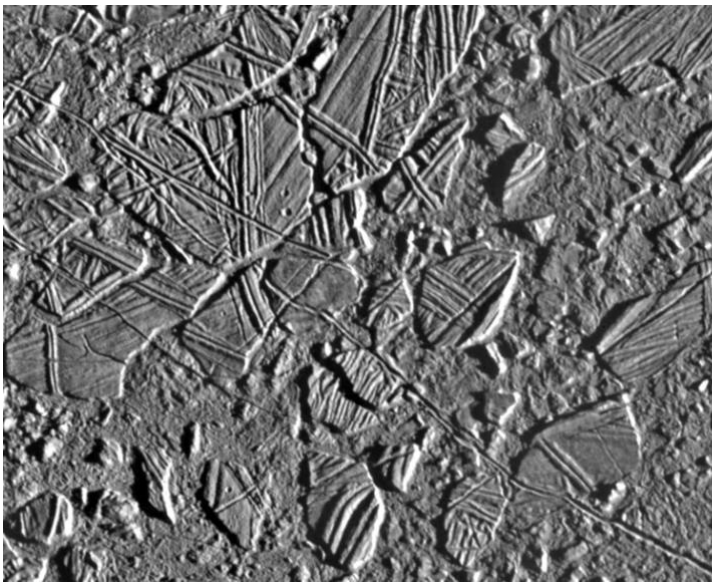

Fig. 1.14: A region of Conmara Chaos terrain courtesy of NASA/JPL.

brine (salty water) quickly moves below the surface because of its lower freezing point (Michlaut & Manga, 2014). The final hypothesis argues that these territories are due to injections of the ocean from cryovolcanic hotspots. These sills of warm ocean water soften and warp the ice above it (Collins & Nimmo, 2009).

1.4.1 Subsurface Access Point Formation on Europa

This section discusses the many hypotheses for the formation of potential subsurface access points (SAP) features and whether or not they could provide access to the shallow subsurface for any length of time. The depths and inferred geologic environments of each SAP will be speculated on based on the Earth and extraterrestrial analogs that were discussed in the background section.

1.4.1.1 Ridges and Fractures

As briefly mentioned in the background section, double ridges are likely formed by Europan diurnal tidal forces from its elliptical orbit around Jupiter. However, there is much debate among geophysicists as to the specific formation mechanism for double ridges. Five major theories discuss their formation, and two of them also involve the formation of fractures and single ridges as steps along a path that ends with double ridges, with one even involving lineated bands as a further evolution of double ridges.

Tidal Squeezing

This is the oldest of the theories first described by Greenberg et al. (1998) while *Galileo* was still imaging Europa. The process is shown in the diagram below (Fig 4.1). First, an extensional tide causes stresses that open a vertical and linear crack in the surface, implying fracture formation is the first step to forming double ridges. Liquid water from the ocean then fills up the crack to just below the surface level, and the top 0.5mm of this water freezes into an extremely thin ice cap. Following this, a tidal compression phase begins, and the ice cap fragments and thickens as the fracture narrows. The fissures in the cap expose the water underneath, and more of it starts to freeze, forming a water-ice slush. As the tidal compression continues, some slush squeezes onto the surface while the crack closes. This step forms what looks to be a single ridge with a rounded cap of material covering the linear fracture at the surface. Finally, the tidal cycle repeats, and an extensional tide reopens the fissure, forming the central trough and surrounding ridges. This cycle continues over and over, eventually creating lineated bands (see section 4.2.1 for more information)

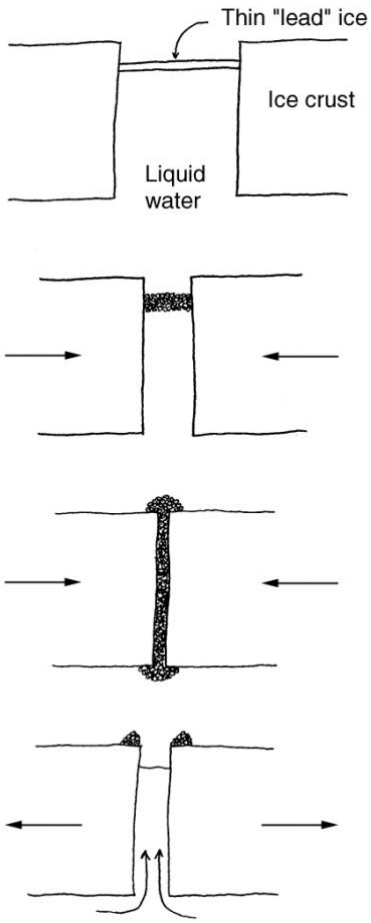

Fig. 1.15: a diagram showing the tidal squeezing process that forms double ridges. Image credit: (Greenberg et al., 1998)

The paper states that this process theoretically takes place for ten thousand to one million years, and for a small fraction of that time, a crack is open, and the ocean and subsurface are exposed. Thus, fractures and double ridges are geologically ephemeral double ridges that expose the subsurface crust and the subsurface ocean. This formation hypothesis also implies that single ridges are simultaneously remnants of previous fracture SAPS and signs that a

double ridge SAP is forming. By extension, lineated bands are remnants of previous double ridge SAPs with a narrow subsurface entrance briefly open at the center.

There is also an implication in this theory that the icy crust of Europa is very thin, even less than 10 km, which is not supported by recent literature (Greeley et al., 2004). Thus, this theory was later expanded upon in later papers.

Linear Diapirism

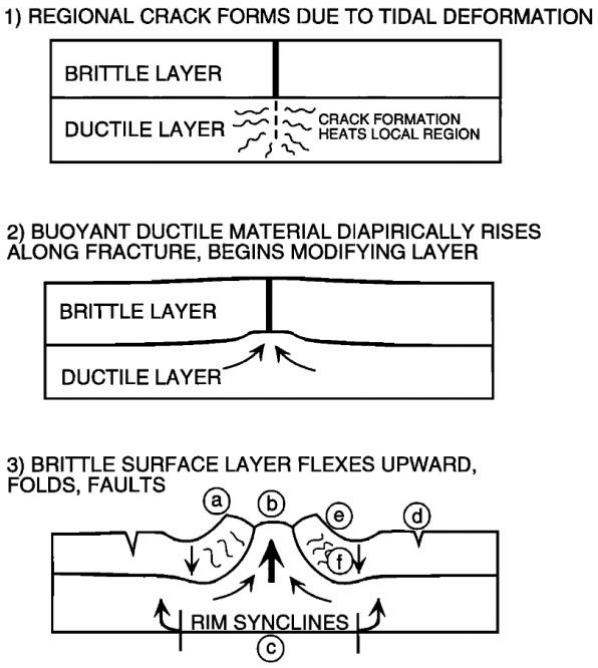

Fig. 1.16: a diagram displaying the three steps in the formation of double ridges via linear diapirism. The final step includes the possible evolutions and variations in the appearance of double ridges. "(a) The brittle layer is flexed upward along the fracture producing parallel ridges. (b) The linear diapir may reach the surface and produce a ridge. (c) Rim synclines form by subsidence following inward and upward migration of the diapir. (d) Marginal fractures and washboard texture form in response to various forces, including compression, flexure, and subsidence. (e) deformation-related changes in slope, and fracturing, cause a range of mass-wasting deposits. (f) thermal effects from the rising warm ice may cause thermal alteration, thermal migration, local melting, and, possibly, volcanism". Image credit: Head et al. (1999).

The second of the two oldest theories of double ridge formation is linear diapirism, a vertical and horizontal intrusion of ductile ice in the curst that warps the surface around it. This was proposed by Head et al. (1999) and also involves tidal forces and their resulting tectonism. This paper also presumes that Europa's crust has two layers. A thin, brittle ice layer akin to Earth's lithosphere and a thicker, ductile ice layer akin to Earth's asthenosphere.

Like the previous model, the process begins with an initial vertical and horizontal tectonic fracture. Still, instead of extending down to the ocean, this crack only breaches the boundary between the brittle and ductile layer of the crust. The ductile crust layer material fills this crack, forming a diapir and warping the brittle layer around it. Finally, the diapir breaks through the crack, widening it and drastically bending its margins,

creating the ridges surrounding the plugged trough. Further deformation and mass–wasting can cause thin linear cracks to develop at the margins of the ridge's outer walls. This process is shown in the paper's diagram above (Fig. 1.16).

Similar to the tidal squeezing model, in this theory, tectonic fracture SAPs are implied to be formed via tectonics as a step towards the formation of double ridges. However, if this theory is true, double ridges are not always SAPs because the diapir sometimes plugs their troughs. However, they can be seen as easily visible markers for the thin, surrounding fracture SAPs that are less visible at lower resolutions. Furthermore, when the diapir wells up enough in the trough, single ridges could presumably form, meaning that they could, by extension, provide the same markers for fracture SAPs as double ridges.

Shear-Heating and Thermal Compression

This theory, proposed by Nimmo and Gaidos (2002), involves strike-slip tectonics and is based on an earth analog. Like the diapirism model, it assumes the Europan crust has two layers: a thick ductile layer below a thin, brittle layer.

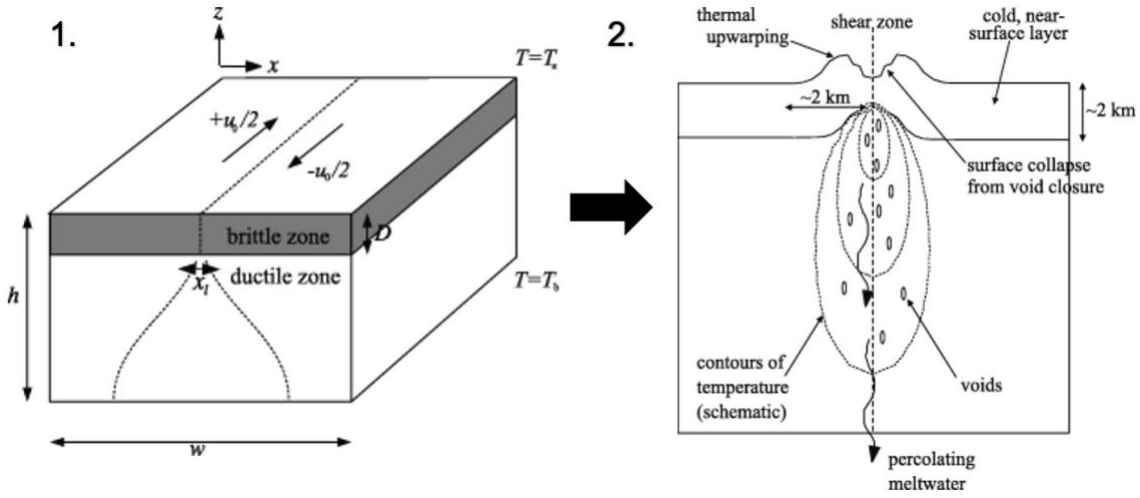

Fig 1.17: A diagram of the shear heating model." In part 1, The dotted lines show the approximate location of the shear zone. x_i is the characteristic width of the shear zone, and Ts and Tb are surface and base temperatures. In part 2, Dashed lines are schematic contours of excess temperature. The removal of water by percolation results in voids. Closure of the voids causes surface collapse; the temperature anomaly causes flexural uplift. Alternatively, inward motion of the ice due to void closure may lead to compression and uplift". Image credit: Nimmo & Gaidos (2002)

Schematics of the theoretical process are shown above (Fig. 1.17). On Earth, the movement of tectonic plates creates zones of lateral motion (termed shear zones) at transform (or strike-slip) boundaries and subduction zones. This motion causes shear heating. On Europa, this temperature change is dictated by tidal stresses and their cyclical nature. At depth, this heating causes movement and upwelling in the ductile layer, warping the brittle surface layer and creating the ridge's highlands. Subsequent heating then causes a diapir to form and push through the center of this high point, dividing it into two parallel ridges. If this theory is correct, double ridges would not be considered SAPs because their cracks never provide access to the subsurface. As shown in Fig. 4.3, the bases of their axial troughs are effectively at ground level because of the uplift caused by the double ridge formation. In this theory, they are more like valleys with hills on either side than cracks in the crust.

Shallow Water Sills

This model by Culberg et al.(2022) is based on how double ridges form in the Greenland ice sheet. Like the previous two models, this theory involves a brittle and ductile layer of Europa's crust.

The diagram above shows the terrestrial process (Fig. 1.19) In stage one, a shallow pocket (or sill) of water is emplaced in a porous matrix of soil that lies atop a thicker, impermeable layer of ice. On Europa, the porous layer is the brittle ice layer, and the impermeable ice is the ductile layer. On Earth, the emplacement process is controlled by the seasonal ablation and accumulation of ice and snow on the Greenland ice sheet (Culberg et al.,

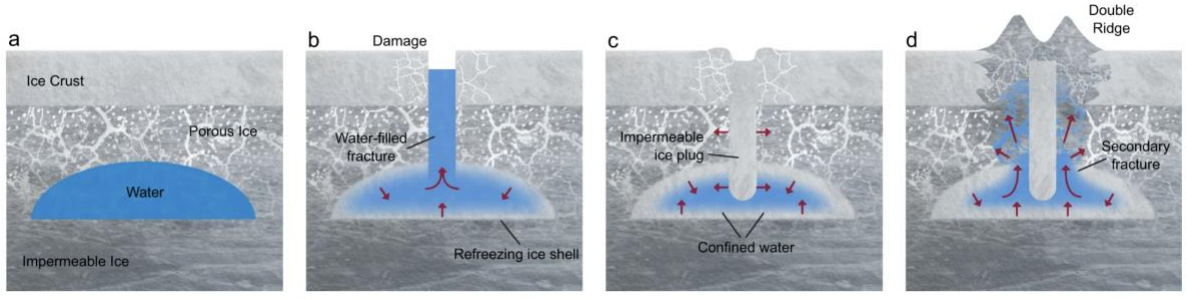

Fig. 1.19: a diagram showing the process by which double ridges are formed on Greenland, used as a Europa analog. Image credit: Culberg et al. (2022)

2022). In Europa, the process would likely be dictated by tidal forces, with the liquid water coming from a preexisting sill, a diapir, or even the subsurface ocean. In stage two, the pressure of holding the sill in the subsurface and other surface stresses fractures the surface down to the sill, causing the water to spread vertically into the crack. These stresses would likely be tidal on Europa. In the third stage, the water in the crack refreezes, forming a plug of ice that traps the remaining liquid water in the pocket. Stage 4 is when the ridge forms due to the enormous pressure buildup caused by the trapped water attempting to freeze due to the cold temperatures. This ridge starts as a single ridge, but repeated pressure causes a double ridge to form, accompanied by secondary fractures at the margins of the outer walls.

Like the tidal squeezing and linear diapirism models, this theory also involves fracture SAPs and single ridges as stepping stones to double ridge formation. Fractures also result from double ridge formation, so while double ridges are not SAPs because their troughs are plugged by ice, they are more visible markers for smaller fracture SAPs (similar to the diapirism model). Fractures would also be geologically short-lived in this model.

Ice Wedging

This is the newest of the formation models explained in Cashion et al. (2024). It is based on Europa's tides' cyclical extensional and compressional phases. Similar to the diapirism model, it does not hinge on the assumption that Europa's crust has two layers, a controversial assumption in the planetary science community.

There are five stages of this model shown in the diagram below (Fig. 1.20) . The first phase is an extensional tide, which causes a crack to open in the crust, potentially extending down to the ocean or intersecting with a preexisting diapir, or sill. Following this, water enters the crack and starts to freeze along its walls. Phase two is a compressional tide that squeezes the emplaced ice and the fracture. The pressure caused by the ice squeezing deforms the area around the crack, creating the uplift sections surrounding the fissure. The next extensional tide

reopens the crack and allows more water to enter it, and the next compressional tide makes the ridges grow taller. If this wedge gets big enough, it could form lineated bands.

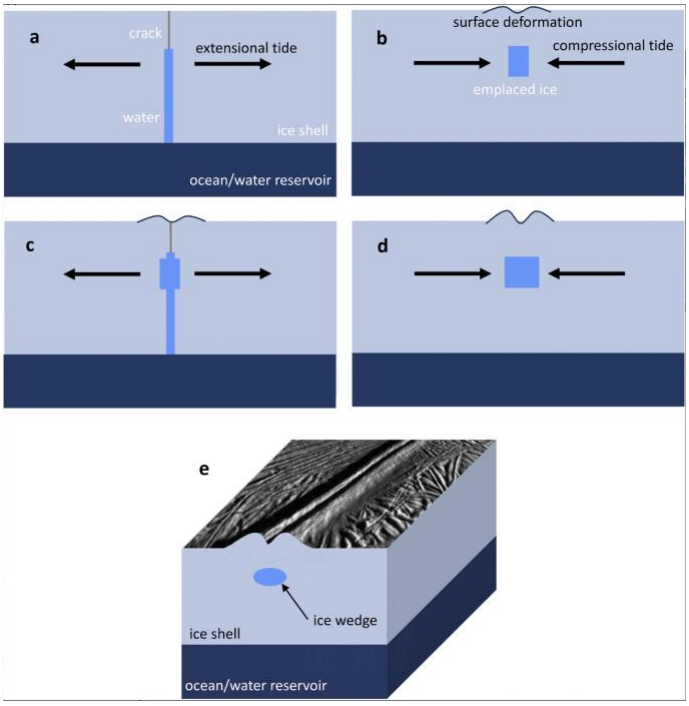

Fig 1.20: a schematic of the ice wedge formation model for double ridges. Image credit: Cashion et al.,(2024).

This model presents two SAPs. It first presents fracture SAPs as short steps to precursors to double ridges and/or lineated bands. Second, it presents double ridge SAPs as existing during the growth phase (c in Fig. 1.20) when the central crack is open. It is, however, important to note that in this model, the cracks are only open during extensional tides. Therefore, the lifetimes of these SAPs would likely be incredibly short, just over 85 hours (the time between tidal cycles on Europa).

1.4.1.2 Lineated Bands

In many lineated bands, hummocky terrain is often present in the margins of the ridges. It is also common for lineated bands to possess a prominent central fracture called an axial trough. Lineated band formation models range from lithospheric dilation to the evolution of double ridges to explosive volcanism. Just like double ridges, not all of them would result in SAPs.

Cyclic Lithospheric Dilation via Jammed Ice

This model is the same as the tidal squeezing model for forming double ridges by Greenberg et al. (1998). It posits a cycle of lithospheric deformation on Europa controlled by its diurnal tides (Manga & Sinton, 2004).

Following the creation of a double ridge via the tidal squeeze method (See section 4.1.1 for more information), the tidal cycle repeats. The central crack in the axial trough of the double

ridge opens again. This causes more water to enter the crack and freeze as its depth decreases. Some of this slush will be expelled as the compression cycle begins, and the ice at the top prevents the crack from fully closing. This incomplete closure causes more deformation, leading to the texture seen between the ridges in a band. Then, the crack opens even wider during the next tidal expansion, and the cycle begins again. Greenberg et al. (1998) also describe the formation of narrow marginal fractures on some lineated bands in response to the combination of tidal stress and surface deformation imposed by the formation of the ridge complex. These fractures could also aid in forming more ridges in the complex as they evolve with the tides (Greenberg et al., 1998).

Using this model, each lineated band can have several SAPs. The first is its axial trough, which can reveal the shallow subsurface whenever it is open during extensional tides. This trough is, unfortunately, mostly blocked by the jammed ice during compressional tides, so it might not be an SAP at these times. The marginal fissures also serve as SAPs, though they may be shallower if they form solely as a response to the stress of surface deformation rather than in response to an extensional tide. Many bands also have a reddish color attributed to the oceanic material they expel during their formation (Manga & Sinton 2004). Therefore, their surfaces may also provide useful subsurface information.

Lithospheric Dilation via Oceanic Convection Currents

Prockter et al. (2002) explains that this model is similar to the previous one, but it uses a terrestrial analog, mid-ocean ridge. The two formations share striking visual similarities so assuming they form similarly via extensional tectonics is not unreasonable (Prockter et al. 2002). The paper also asserts that lineated bands are an evolved form of double ridges and assumes the layered model of the Europan crust. The final assumption is that Europa's subsurface ocean has convective currents imposed by tidal heating, similar to the convection currents in our mantle.

This model has two theoretical processes: a slow-opening scenario and a fast-opening scenario. In the slow opening model, convective currents in the subsurface ocean cause motion in the ductile layer, exploiting a preexisting weakness in the crust. Warm ice from the ductile layer is then extruded from this new crack. Over time, as more lithospheric material is added, the brittle layer reaches sufficient thickness to fracture, and the cycle begins again until a ridge complex is formed. In this instance, the hummocky material between ridges in the complex can be caused by a pile-up of this warm ice outside the crack. A distinct trough is also left behind, as is seen in mid-ocean ridges. The fast-opening model also begins with a crack, but this time, it is caused by surface tension overwhelming the weak ice in the area. Warm ice then fills the gap and starts to upwell, but the crack closes too quickly for prominent band topography to form. Instead, a band of subdued ridges and hummocks is left behind as the warm ice freezes. The axial trough is not very prominent either.

In the slow-opening version of this model, lineated bands one SAP in their axial troughs, and unlike the previous model, they may not be short-lived. This model does not have cracks opening and closing in response to the tides, so these will stay open regardless of whether Europa is in its extensional or compressional tide. The depth and width of the cracks may depend on the directions and strengths of the oceanic convection currents.

Cyclic Lithospheric Dilation via External Forcing

Similar to the previous models, Tufts et al.(2000) argues lineated bands are formed via lithospheric stretching. However, this model does not depend on just endogenic convection or tides. It argues that instead of jammed ice, there is also an external force imposing the dilation and preventing the crack from fully closing

On a typical Europan day, a crack opens and closes in response to the tidal cycle that switches between extension and compression over 85 hours (Doggett et al., 2017). In this model, that crack is influenced by an external extensional force, which increases the dilation of the lithosphere (Tufts et al., 2000). This external force prevents the crack from fully closing in a

compressional tide, allowing warm ice and slush to keep welling up through the gap. With repeated tidal cycles, the crack is widened and narrowed but never fully closed, so the dilation increases, and more material is extruded through the gap, forming a ridge complex.

Tufts et al. (2000) gives two possibilities as to the origins of this external force. The first option is a walking strike-slip fault. These lateral faults go back and forth from exerting left-lateral and right-lateral force, thus producing an extensional force. These faults are a plausible cause for strike-slip deformation on Astypalaea Linea and smaller linea on Europa (Tufts 1998, Tufts et al. 1999). The second is potential convective currents from the subsurface ocean that cause lithospheric blocks to move, similar to the model explained by Prockter et al. (2002)

Similar to the previous models, this model would also result in at least one SAP per lineated band, its axial trough. Like Greenberg et al. (1998), Tufts et al. (2000) note the presence of marginal ridges for some bands but do not speculate on their formation. However, given that these ridges appear to be double or single ridges (Tufts et al., 2000), they might also be SAPs during extensional tides.

Explosive Cryovolcanism

This is a unique model, one that does not rely on the tidal system and may not produce any SAPs outside of the axial trough. Fagents et al. (2000) present two models of explosive volcanism, ballistic and shock. In the ballistic model, particles of condensed gas rapidly sublimate above a cryovolcanic vent. As the particles freeze, they intersect, collide, and act as ballistic projectiles, pilling up ridge-like along the surface nearby. All of the particles have similar velocities and trajectories, which would produce a uniform, subdued ridge complex topography. In the shock model, the expelled particles are gas and fluid. The addition of the fluid particles changes the velocity and density of the ridge material and allows for a more prominent topography.

In both models, the only SAP is the volcanic vent, and all other low points will be at the surface level. The volcanic plume would also provide information about the subsurface. Many

bands appear reddish or have red-brown margins. If this colored material is the plume ejecta, as the volcanism model posits, SAPs might not be the only way to study Europa's subsurface through lineated bands.

1.4.1.3 Fossae Formation

Unlike ridges and bands, there is far less research on the formation mechanisms for Europa's Fossae. However, the existing papers advocate for mechanisms controlled by tidal bulges and the response of elastic Europan crust. Like Earth, Europa has an elliptical, tidally locked orbit. However, many papers (ex, Beuthe, 2016; Rhoden et al., 2021) posit that it still experiences a polar wander despite not having an eccentric orbit. The idea is that the icy shell floats freely on the subsurface ocean, allowing it to spin in a slightly different direction than the ocean and core. So, the tidal bulges appear to wander around the globe and affect the moon's surface at slightly different angles as it orbits despite its lack of orbital eccentricity. This 'spin-pole' effect (Benthue, 2016) affects the surface deformation caused by the tides.

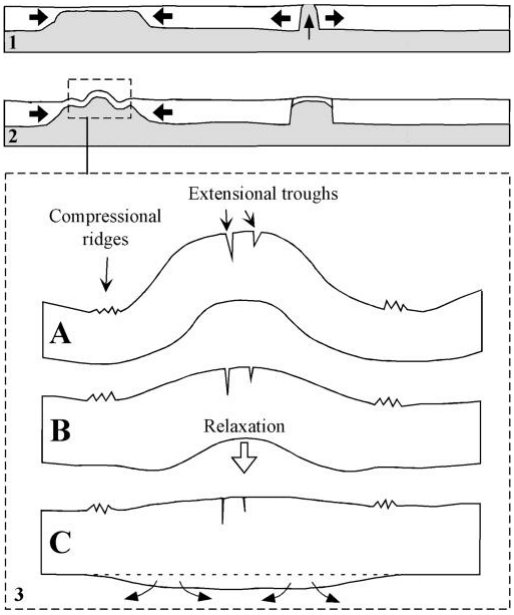

Fig 1.21: a visual diagram of how fossae form. Image credit: Prockter & Pappalardo (2002)

The prevailing model of fossae formation seems to be the theory presented by Prockter & Pappalardo (2000) via extensional tectonics and crustal folding. The process they present is explained below and above in the schematic (Fig. 1.21).

The first step is an extensional tide-causing band formation, which stretches the brittle lithosphere and allows the ductile layer to well up through the gap that forms. The tide also changes the thickness of the lithosphere, such that if two bands form with a large space between the bands themselves, they will have a thicker lithosphere than the area between them

(Prockter et al., 2000). Following this, The extensional strain is accommodated by the formation of folds in regions with a relatively warm, thin lithosphere (Such as the region between bands). Once the compression tide begins, extensional troughs (eventually termed Fossae) start to form at the center of the fold in response to the change in stress. When the compression slows, these folds flatten, and the troughs get shallower and narrower as the crust relaxes.

By this model, fossae are SAPs regardless of where they are in the formation process. However, the width and depth of the SAP do change with the tides. The strike-slip alteration also tends to be pervasive among fossae SAP (See figures 3.2 and 3.10 for examples), and most of the articles on fossae discuss the potential causes of strike-slip tectonics on Europa. Potential causes include shallow water reservoirs (Matteoni et al., 2023), polar wander (changing of Europa's tidal regime as a result of changes to its orbit) (Schenk, Matsuyama & Nimmo; 2020), an elastic crustal response to increased strain (Katterhorn, 2004), and 'tidal walking' (Preblich et al., 2007). Regardless of the cause, this alteration would influence the potential underground environment of the affected caves (see section 5 for more).

1.4.1.4 Pits & Chaos

Pits and lenticulae (small circular features on Europa with contrasting albedo including pits, domes, and chaos units (Culha & Manga, 2016) are also Europan SAP with controversial origins. Formation models include oceanic plumes and convection (Thomson & Delaney, 2001), Ice shell plumes and convection (Rathbun, Musser, & Squyers,1998), convective or tidal melt-through (Greenberg et al.,1999), and sills of warm ice and/or liquid water (Michout & Manga, 2014)

Ocean Convection and Plumes

Thomson & Delany (2001) describe the process of forming pits as follows (Fig. 1.22). First, buoyant plumes float toward the surface, transporting heat to the base of the shell where melting begins. This melting occurs above several plumes, sometimes in proximity to ice ridges. This melt fluid then spreads laterally outward from the plume core, flowing into the shape of a sphere with the tides. Excess remains in the base of the matrix in this spherical shape. This causes a density difference within the solid ice that the crust responds to by sagging, forming a pit.

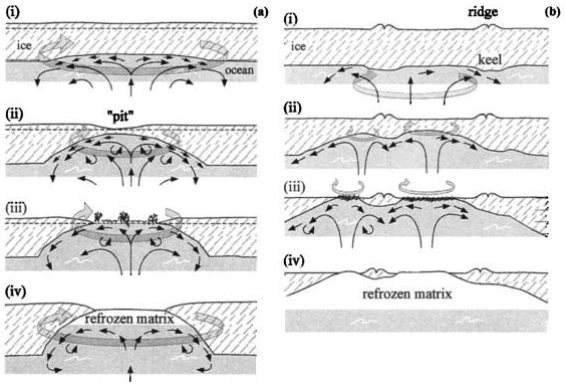

Fig. 1.22, a schematic of the ocean plume formation model of pits. Image credit: Thomas & Delaney, (2001).

Plumes and Convection Within the Ice Shell

Similar to the linear diapirism model of double ridge formation, the stages of this model are presented by Rathbun, Musser, & Squyers, (1998). A diapir rises through the surrounding crust and as it rises, its flow is modified by the cooler, elastic ice near the surface. This modification causes the flow to distort and changes the shape of the diapir into an oblate spheroid. Similar to the previous model, the heat from this spheroid of warm ice thins the brittle crustal layer, causing a pit to form. Also similar to the last model, the diapir expands as it begins to refreeze, forming a dome.

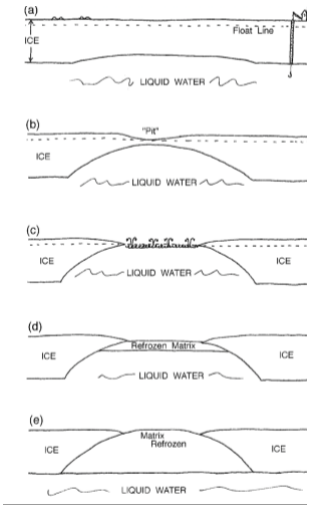

Fig 1.23, a schematic of the melt-through model. Image credit: Greenberg et al., (1999)

Melt-Through

This model was proposed and described by Greenberg et al., (1999) and displayed in Fig. 1.23 Tidal heating is not uniform on Europa, causing preferential heating of different regions of the crust or other parts of the satellite at different times. This heating can either come from

the ductile layer of the crust or originate in the rocky core and rise through the ocean. Either way, this heat melts a section of the ductile layer into water and in response to this intrusion of warm, dense water, the brittle layer begins to thin from below. Ice floats on the water ocean water because of its buoyancy and it is supported by a boundary called the float line (Greenberg et al., 1999). As the ice thins, it gets denser, causing the surface to sag. If melting stops here and the crust remains thin, a pit will be left behind. But if it thins enough for the liquid to be exposed, it will quickly freeze and boil once it is exposed to Europan surface conditions creating a chaos unit.

Shallow Water Sills

This model (Fig 1.24 is similar to the double ridge model of the same name. It starts with an intrusion of water into the ductile layer of the shell, which causes the shell to deform elastically (Michout & Manga, 2014). If the intrusion is deep enough, the ice-ocean boundary will flow slowly. After emplacement, the water sill will begin to freeze, and the heat from the sill transfers to the surrounding ductile ice layer, causing it to thin. This increase in stress disrupts the ice shell, causing it to sag downward in response to the denser water. Once the sill solidifies and expands, a dome can form.

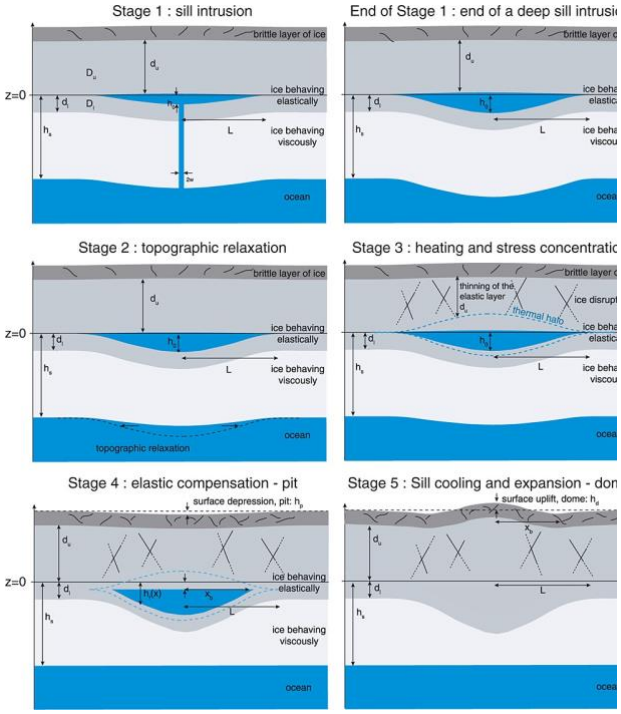

Fig. 1.24: a schematic for the sills model of pit formation. Image credit: Michout & Manga, (2014)

1.5 Summary

Not all models result in SAPs, and even when they do, their lifespans vary. The models show pits and fossae would qualify as SAPs, though they would be rather

shallow and short-lived. Some models suggest that pits have a longer lifespan if the water stops rising at a deep enough point to keep it liquid. Similarly, double ridges formed via the linear diapirism or shear heating models would not be considered SAPs because there are no void results from these models except at the beginning with the initial crack. The other double ridge models show SAP lifespans are very short, usually not longer than Europa extensional tide cycles. Lineated bands are less temporary. The three cyclical deformation models show at least one partially open SAP during compressional tides. However, the explosive volcanism model would not result in an SAP because it is implied that the initial volcanic vent does not remain open.

Different geologic processes also control the formation of these landforms. All pit models are cryomagmatic (Culha & Manga, 2016). Meanwhile, the prevailing model for fossae suggests that these are tectonic SAPs. Fracture formation models are also mostly tectonic, but they only seem to form through extensional tectonics, while bands and fossae require both extension and compression. Ridges and bands are the only landforms whose formation is dictated by several geologic processes. Models for double ridge formation are either fully tectonic or both tectonic and cryomagmatic. Likewise, lineated bands are either volcanic features or are created through convective or tidal tectonic force. There is an ongoing debate over whether or not nontidal processes play a role in fissure formation. By mapping Europa's SAPs and analyzing their morphologies, this thesis hopes to help settle this debate.

2. Methods

The landforms are mapped on a bundle of global and regional mosaics of *Galileo* SSI*. Galileo* imagery is a two-dimensional visualization of the landscape. It lacks topographic data, so any depth is inferred based on light and shadow. Only the surface is visible. Therefore, the features mapped in this thesis are considered potential cave entrances or features that may hint at a cave beneath them.

2.1 What Landforms Qualify as Potential SAPs

Features were considered cave entrances if they met one or both criteria. (1) It resembles verified cave entrances or cave-containing features on other bodies; (2) it appears to contain the entrance to a chasm or trough.

2.1.1 Pits as Potential SAPs

Pits meet both of these criteria. Pits have been classified as cave entrances on the Moon and Mars (Cushing et al., 2017, e.g., Fig. 2.1), most often as skylights in lava tubes. (cite Martian Cave catalog). Many of them are concave and have visible shadows, making them more likely to be subsurface access points.

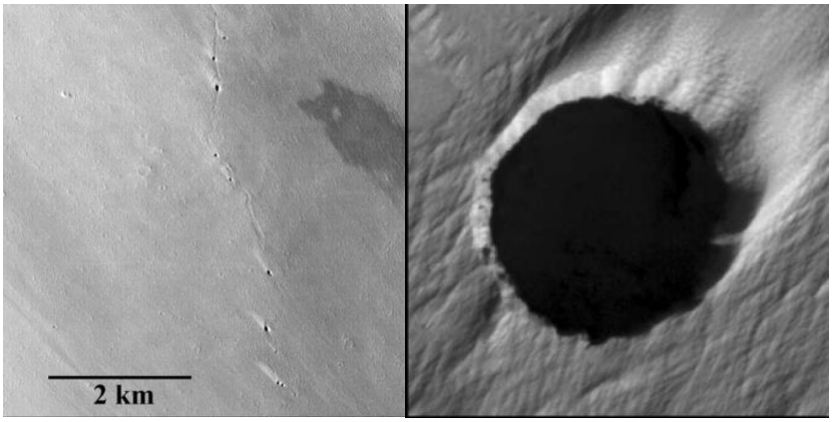

Fig. 2.1, two types of Martian candidate cave entrances. The left image shows a lava-tube rille with multiple skylight entrances (CTX: P17_007774_1757); and the right is a zoomed-in atypical pit crater (HiRISE: PSP_003647_1745).

2.1.2 Fractures and Fossae as Potential SAPs

Fractures and Fossae also meet each of these criteria. On Earth, fractures frequently occur at either cave entrances or hint at a cave underneath. For example, the Castleguard cave system in Alberta, CA, has two fissures above the cave's central portion (Ford et al., 1983). The central cave is mostly linear, and the fissure contains stalagmites (see Fig. 2.2) (Ford et al., 1983).

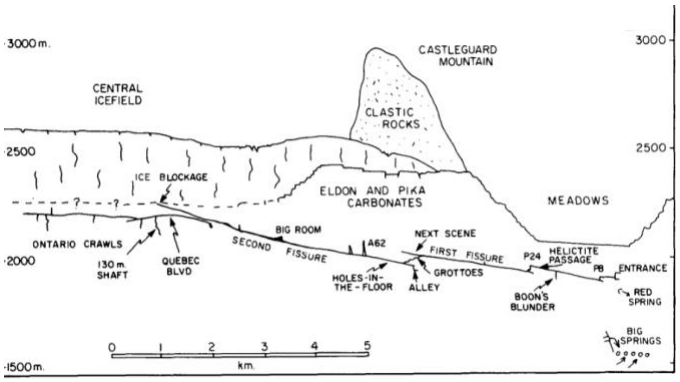

Fig. 2.2: A map of a fracture cave in Alberta, Canada. Image credit: (Ford et al.,1983)

Several grabens (the technical term for fossae on Mars) or graben-like features have been suggested as potential cave entrances on Mars (Cushing, 2017). One of these is a linear depression that flanks Arsia Mons; it was found to contain many cave entrances (Cushing et al., 2017). The former results from the cave forming along a pre-existing fault (Ford et al.,1983), and the latter shows signs of volcanic and tectonic formation (Cushing et al., 2017). On Europa, these are also sometimes associated with impact craters (Greeley et al.,2004).

2.1.3 Ridges and Bands as Potential SAPs

Double ridges and single ridges also meet the criteria for SAPs. Several shale and sandstone ridges, including the Flint Ridge, are associated with Mammoth Cave, a labyrinth of limestone caverns in KY, USA (Palmer, 2017). On Mars, the Tharsis-Ridge volcanic system has multiple lava tubes with skylights associated with cave entrances (Cushing et al.,2017). Double and single ridges on Europa may have these entrances

on them, but they are currently invisible due to the low resolution of the imagery. Double ridges especially have large troughs in the center that could be hundreds of meters deep (Greeley et al., 2004).

Lineated bands meet the second criterion. They are thought to form through processes akin to terrestrial seafloor spreading (Greeley et al.,2004), which leaves ridge complexes behind. Lava tube skylights could form in these ridges, and the troughs might also be deep enough to constitute a linear cave (Wynne et al.,2023). Some lineated bands also have an axial trough like mid-ocean ridges (Prockter et al., 2002). The bands possessing axial troughs would also meet the first criteria because the fissure would function as a linear cave entrance.

2.2 Mapping and Classifying Potential Cave Entrances

These features were identified and mapped in ArcGIS on a dataset of 92 georeferenced Galileo image-mosaics gathered from Astropedia and made by Bland et

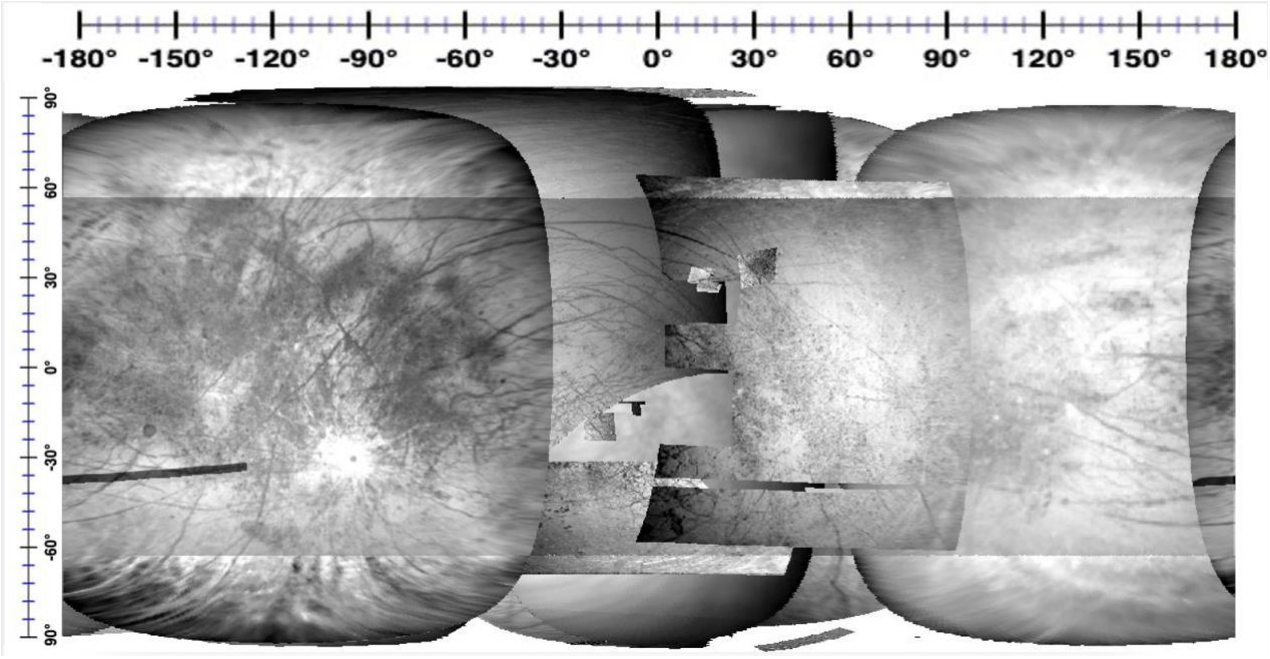

Fig 2.3: The map of Europa used in this thesis, constructed of mosaics of *Galileo* SSI imagery made by Bland et al., (2021).

al. (2021). These images were global and regional, with resolutions ranging from 14000 to 1000 m/pixel and 500 to 6 m/pixel, respectively. The mosaics were encoded with a planar coordinate system called Equirectangular Europa, which is in meters. For ease of mapping and data analysis, these were reprojected into an IAU-approved ellipsoidal projection for Europa, Europa2000, transforming the units into latitude and longitude. As a result, the map goes from -180 to 180°E longitude and 90 to -90°N latitude (Fig. 2.3).

The linear features were then mapped, and the following characteristics were recorded. Rough central location (in latitude and longitude), Length (km), Shape (linear, cycloid, or neither, termed jagged) (see Fig. 2.4), the type of terrain they are on, and what type of linear feature they are. Pit data was derived from Culha et al., (2016), a study that displayed the spatial distribution of lenticulae (dark spots) on Europa.

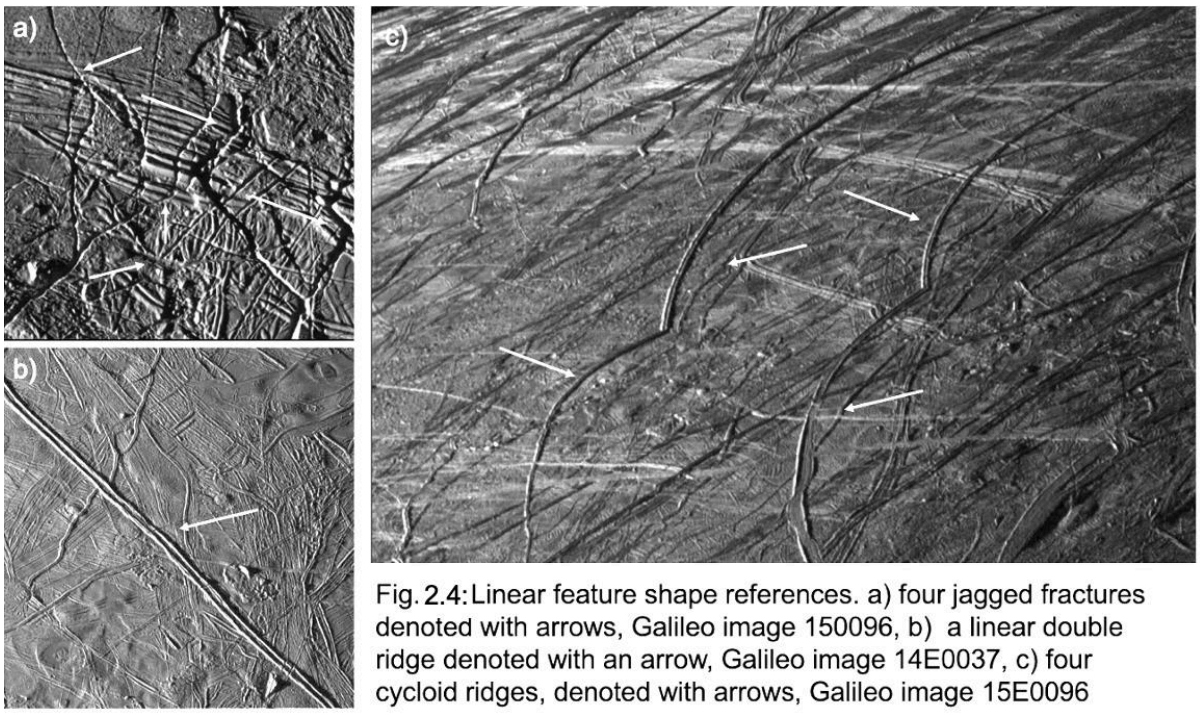

Fig. 2.4: Linear feature shape references. a) four jagged fractures denoted with arrows, Galileo image 150096, b) a linear double ridge denoted with an arrow, Galileo image 14E0037, c) four cycloid ridges, denoted with arrows, Galileo image 15E0096

Pits and other types of lenticulae are not visible at resolutions below about 500 m/pixel (Culha et al., 2016). Therefore, any region of the globe without high-resolution imagery was not mapped for pits. Linear features such as fractures and fossae are

equally invisible at low resolution, so the areas in this study and that of Culha et al., (2016), mostly overlap. These regions are largely in the northern hemisphere but select portions of the southern hemisphere also include high-resolution imagery.

2.3 Identifying Linear SAPs

Linear features were visually identified as one of the five following features. (1) Fractures (Fig. 2.5 a) are small thin cracks on the surface with negative relief. They are usually a result of tectonic activity or impact cratering (Doggett et al., 2009) (2) Single ridges (Fig. 2.5 b) are standalone ridges without a visible trough. Some of these may be more complex ridge systems (double ridges or bands) but they can only be identified as single ridges at lower resolution. These are likely tectonic or cryovolcanic features (Greeley et al., 2004). (3) Lineated bands (Fig. 2.5 c) are bands of multiple smooth and/or textured ridges. These likely form through tectonic processes akin to divergent plate movements (Prockter et al.,2009). (4) Double Ridges (Fig. 2.5 d) are ridges along which two sloping surfaces meet with a central trough. These are likely tectonic features

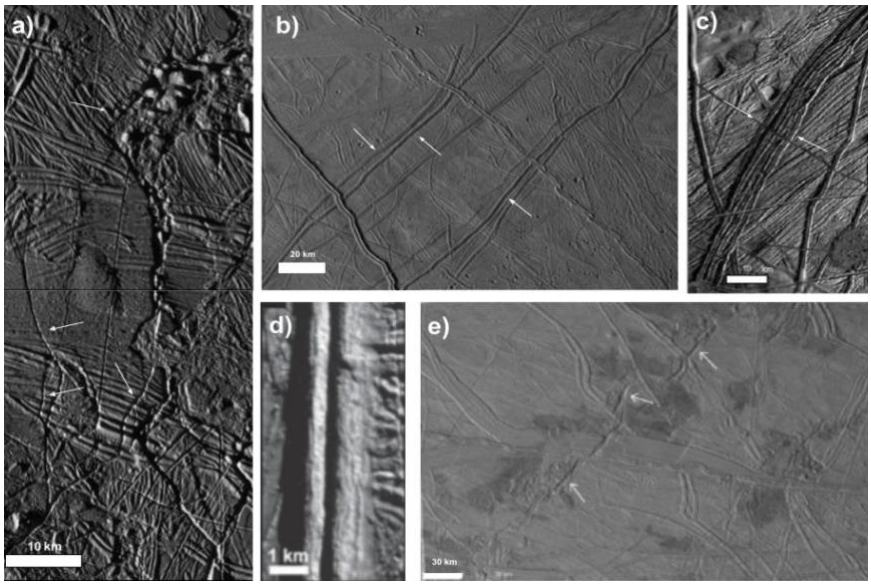

Fig 2.5**:** references for the classification of linear features. a) A fracture network, individual fractures are denoted by arrows, image credit: Galileo, SSI images 11E0024 (top) and 11E0026 (bottom). b) Three single ridges denoted with arrows, image credit: Galileo SSI 14E0035. c) A lineated band with no clear central trough, image credit: Bland et al., (2021) Equirectangular mosaic 19ESRHADM01. d) A double ridge, Androgenous Linea, image credit: Galileo Observation E6ESBRTPLN02. e) Kermario Fossae, image credit: Matteoni et al., (2023)

(Prockter et al.,2009). (5) Fossae (Fig. 2.5 e) are long narrow depressions or troughs that likely form through tectonic and impact methods (Matteoni et al., 2023).

3. Results

This section explains several groups of the SAPs mapped above (Fig. 3.1). Trends in morphology and subsurface access potential will be

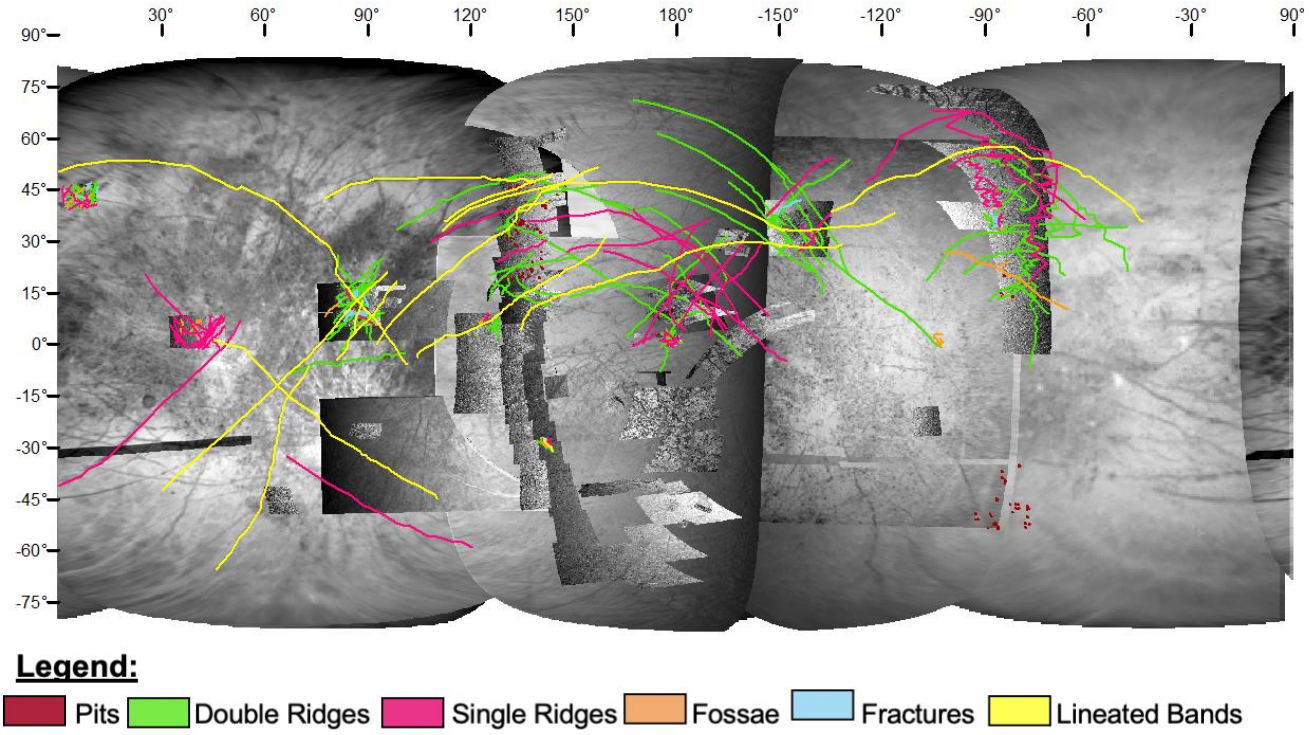

Fig.3.1: a map of all potential cave entrances found in this study by Culha & Manga (2016) on photogrammetrically controlled mosaics of *Galileo* imagery. Note the high concentration of mapped features in high-resolution areas. A longitude scale is along the top and resolution ranges from 6 to 1300 m/pixel.

speculated on, and formation hypotheses will be contemplated. A summary of the morphologies can be found in Table 1. It showcases and explains Nine landform clusters. The nature of the potential subsurface chambers is unknown. This paper assumes the presence of at least one isolated chamber. It is also

Type	Shape		
	Cycloid	**Linear**	**Jagged**
Double Ridge	**15**	**49**	**81**
Single Ridge	**12**	**11**	**44**
Fossae	**2**	**7**	**48**
Fracture	**1**	**19**	**82**
Lineated Band	**4**	**6**	**3**
Totals	**34**	**92**	**258**

Table 1: A simplified data table showing the distribution of the feature's shapes

possible that these features are not subsurface access points, and scenarios in, which the entrance is closed or the chamber is not present will be discussed below.

3.1 Cluster 1

Cluster 1 (Fig. 3.2) lies roughly 600 km northeast of Callanish Crater at the edge of Balgatan Regio, a region of high-relative albedo that is dominated by water-ice regions that have experienced tectonic alteration (Leonard, Patthoff, & Senske 2024). Even in this high-resolution image, the fine details of these ridges were difficult to discern so most of them were classified as single ridges. The more linear ridges in the eastern third of the cluster might be double ridges or fractures but their central troughs were not clear enough to classify them as such.

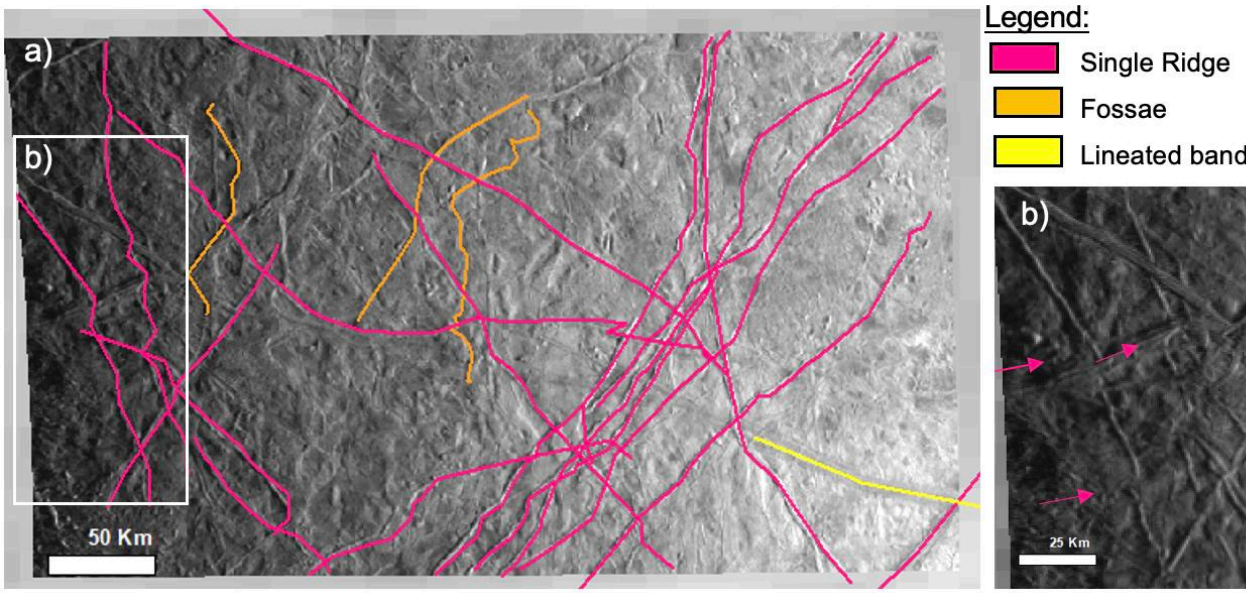

Fig. 3.2: a) Cluster 1, centered at ~ 3.709628°N, 39.210626°E, at the edge of Balgatan Regio about 600 km northeast of Callanish Crater. This cluster features several single ridge SAPs including one whose extent is longer than is shown here, three jagged fossae SAPs, and the end of one lineated band. b) A zoomed-in section of this cluster showing two single ridges that seem to exhibit strike-slip faulting (faults denoted with arrows)

Given that most of the features depicted here are over 50 km long, the lineated bands and single ridges are likely signs of subterranean environments and a cave

ceiling. These ridges exist on a largely tectonic terrain. It is equally, possibly more likely that they are either double-ridge SAPs or lineated-band SAPs, which form tectonically. In the former scenario, these are currently invisible cave openings that have formed as the evolution of a fracture during compressional tectonics (see section 4 for more details). In the second scenario, these are products of extensional tectonics, fissures in the surface that have now closed, artifacts of previously open subsurface entrances, or former cave locations.

Depending on their length, the fossae might be the entrances to one or several caves. A few jagged single ridges exhibit strike-slip faulting (Fig. 3.2b), indicating they likely experienced tectonic alteration. This alteration may have formed a tectonic cave in their vicinity via the shear heating model (see section 7), but it could also damage the chamber (section 8). It is also possible that these single ridges represent one or several cave systems.

3.2 Cluster 2

Cluster 2 (Fig. 3.3) is also a section of ridged plains, most models of Europa's geologic history state that the ridged plains formed during a massive (possibly global) tidal resurfacing therefore, these SAPs are likely tectonic. The double ridge SAPs are their troughs possibly formed through tectonic-like processes connected to the moon's cyclical tides. Some theories (see section 1.5) even posit that double ridges are an evolution of tectonic fractures (Greenberg et al., 1998; Head, Pappalardo & Sullivan, 1999; Nimmo & Gadios, 2002). The entrances would be their troughs, and, given the lengths of Androgenous Linea and Agave Linea, they are likely representative of cave systems rather than individual caves

The Fracture SAPs are also tectonic, and their environments could be similar to terrestrial fracture caves (Head, Pappalardo & Sullivan 1999) The lineated band is probably formed through extensional tectonics (Greenberg et al., 1998; Prockter et al., 2002)

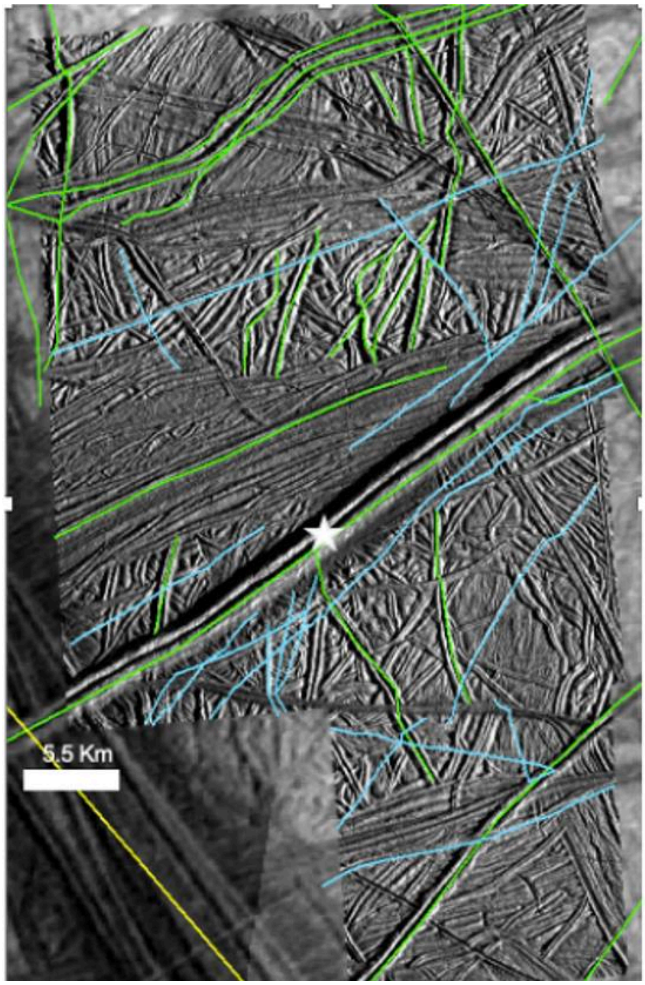

Legend:

Double Ridge

Fracture

Lineated Band

Fig.3.3: Cluster 2 is centered at ~15.023717°N, 86.780887°E and features Androgenous Linea (denoted with a star) as one of the double ridge SAPs. Like Cluster 3, this region is also bounded by Agave Linea (the lineated band on the left). The cluster showcases how the different types of Europa SAPs can intersect with and embay each other meaning many of them might be different openings to the same cave.

3.3 Clusters 3 & 4

The third and fourth clusters (Fig. 3.4 and 3.5) contain the SAPs identified on Conmara Chaos. Though chaotic terrain is possibly formed through processes that would likely fill subsurface passages with slush, the repeated pressure and force exerted on the surface in creating this terrain could create new cracks. These SAPs

would likely have formed either first through tectonic processes and later altered by cryovolcanism or solely through cryovolcanism.

The fossae in this cluster are small enough to host a single cave rather than a cave system, while the fractures are long enough to host several. They may not be as deep or continuous as others, but they still provide access to the shallow subsurface.

The double ridge and lineated band SAPs are likely artifacts of tectonic caves that have been altered by the later cryovolcanic activity that formed the chaos unit and potentially filled in or collapsed the caves.

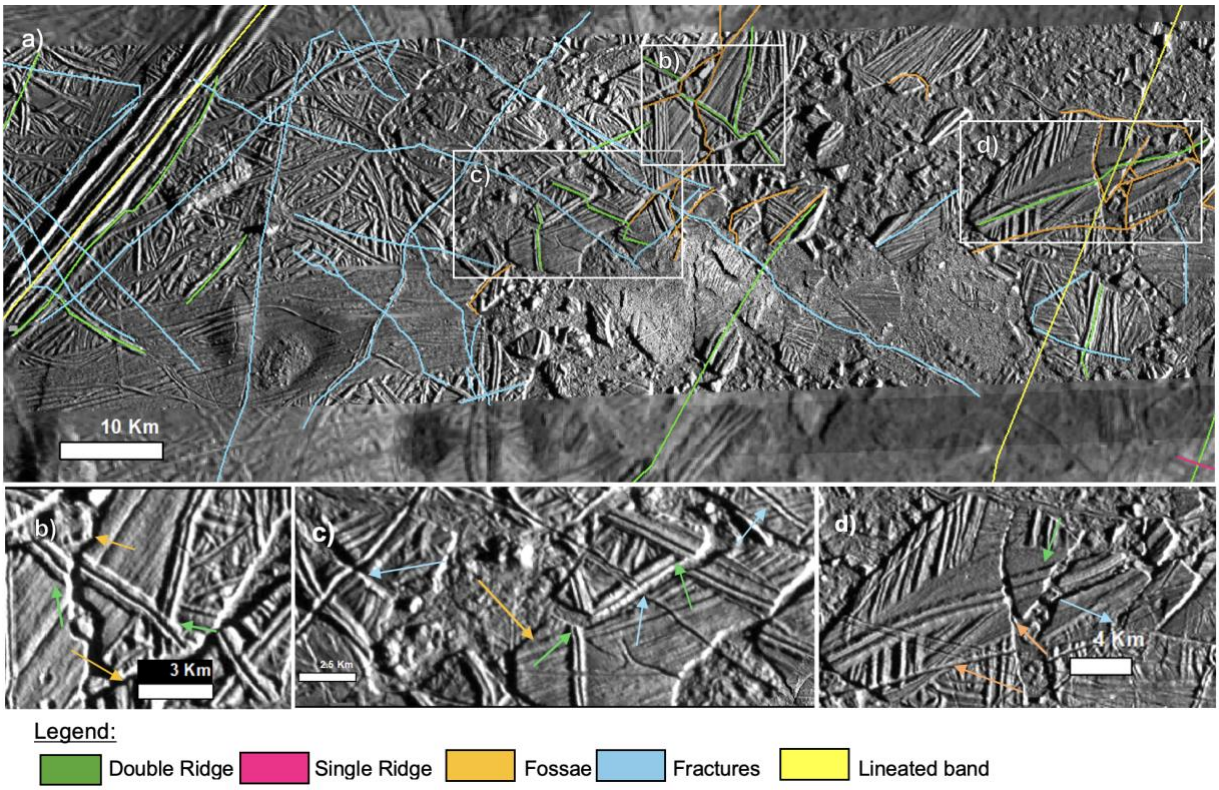

Fig.3.4 a): Cluster 3, centered at ~9.183045°N, 86.30080°E , is flanked by Asterius Linea (the lineated band on the far left) showcases the features of Conmara Chaos. Many of the double ridge and fracture SAPs are broken up by the rafts of icy ridges surrounded by an ocean of hummocky terrain. The small gaps between some of the rafts create shallow fossae. b-d are zoomed-in pictures of the chaos breaking up the features with the different features shown by arrows whose colors correspond to the legend.

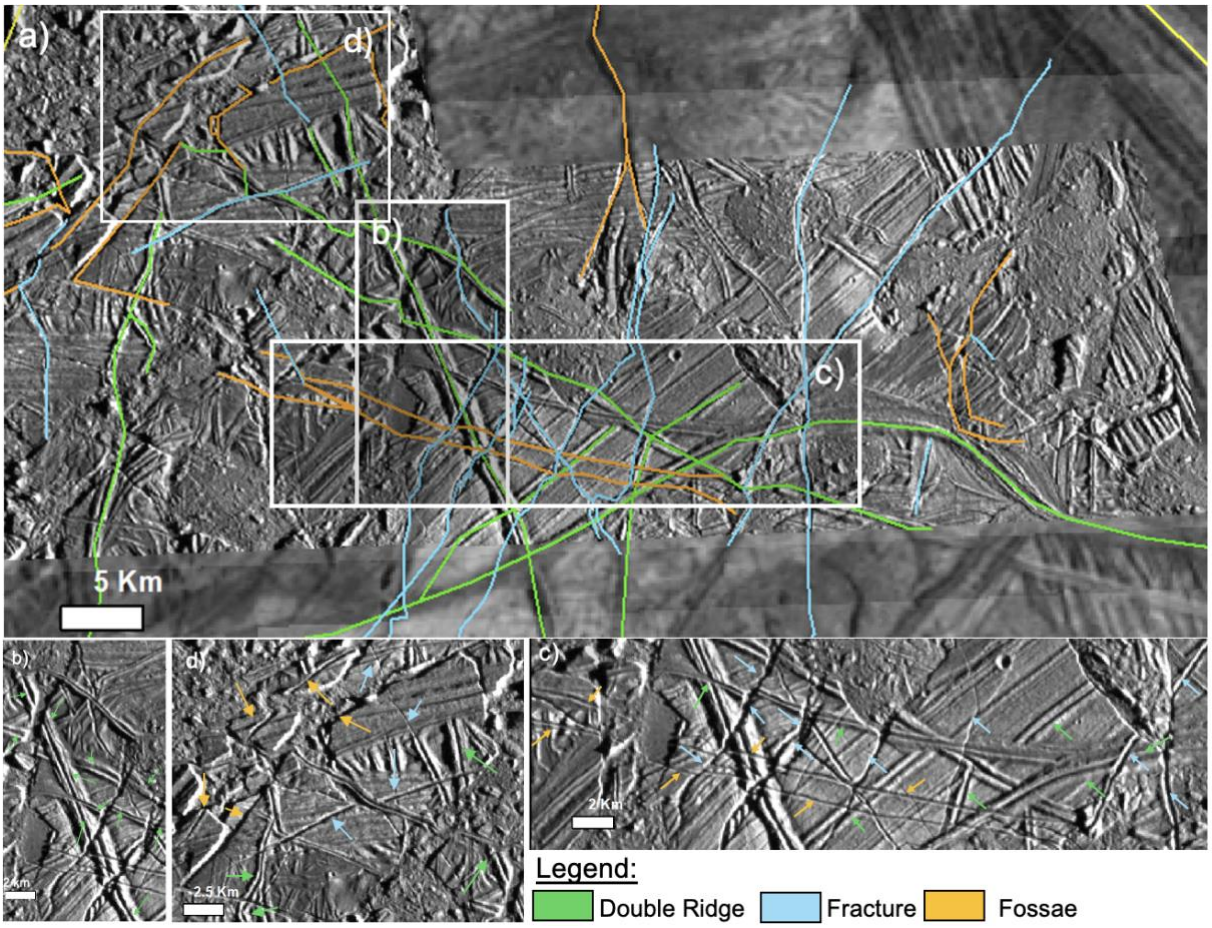

Fig.3.5 a): Cluster 4, centered at ~9.001811°N, 88.97907°E, is a section of Conmara Chaos but flanked by Agave linea (a sliver is shown as the lineated band on the far right). This section showcases more of the crisscrossing double ridge, fracture, and fossa SAPs on rafts of ridged terrain with some of the fractures and fossae bleeding into the hummocky terrain in between the rafts. b,c, and d show examples of how SAPs can be broken up by the creation of chaotic terrain.

3.4 Cluster 5, Clilix Crater

Cluster five (Fig. 3.6) showcases the SAPs surrounding Cilix Crater. These are not impact fractures but old, ridged plains formed during a previous tectonic event. Evidence of this can be seen in the stratigraphy relationship between the ridges and the crater. Because of the geologic history of ridged plains, these single ridges might also be double ridges whose troughs were filled with ejecta or just not visible. Given their

short lengths, they are unlikely to be lineated bands. The double ridges likely formed similarly to cluster one, though the crater impact may have affected the subsurface environment.

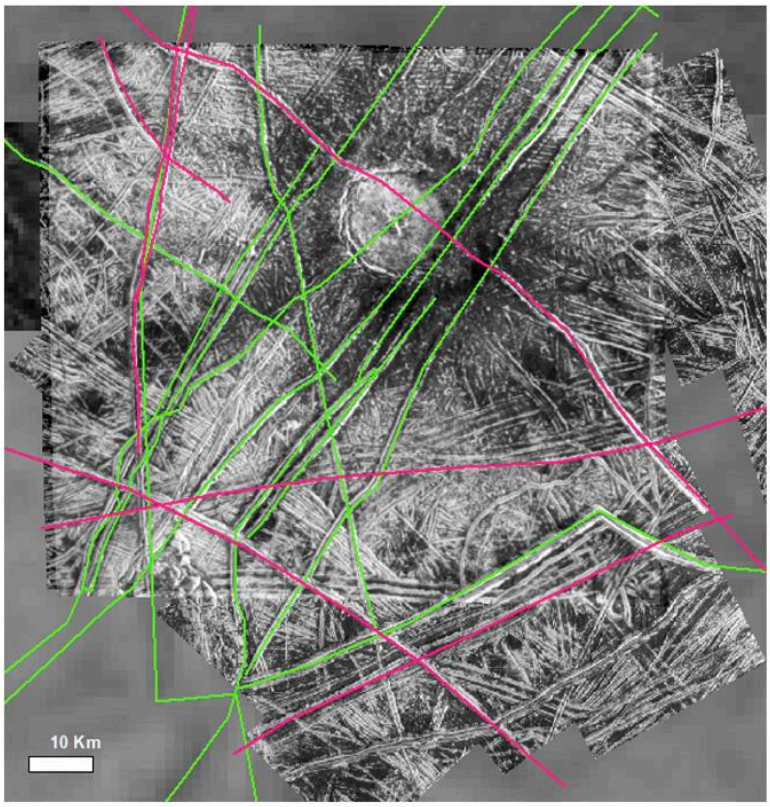

Legend:

Double Ridge

Single Ridge

Fig.3.6: Cluster 5, centered at ~2.02841°N, 177.95541°E is the cluster of SAPs on the ridged plains that Cilix Crater is super-imposed upon. The region's stratigraphy, with the crater being untouched by the ridges, suggests that these double and single ridges were not created by the Cilix impact but rather existed before it. These SAPs were not created by the impact but by a previous tectonic event.

3.5 Cluster 6

Cluster six (Fig. 3.6) is at the intersection of a chaos unit and ridged plains, meaning that the SAPs in this area were formed through cryovolcanic and tectonic processes (Leonard, Patthoff, & Senske, 2024). The double and single-ridge SAPs are likely tectonic, while the fossae are likely cryovolcanic. Some ridge features and SAPs appear to be embayed by melt material (refer to the starred features in Fig. 3.7), suggesting that these may be remnants of old caverns that are now filled and/or sealed with cryovolcanic material. The formation of the fractures is unclear. They occur in the chaos and ridged plain units so that they could have formed during both cryovolcanism

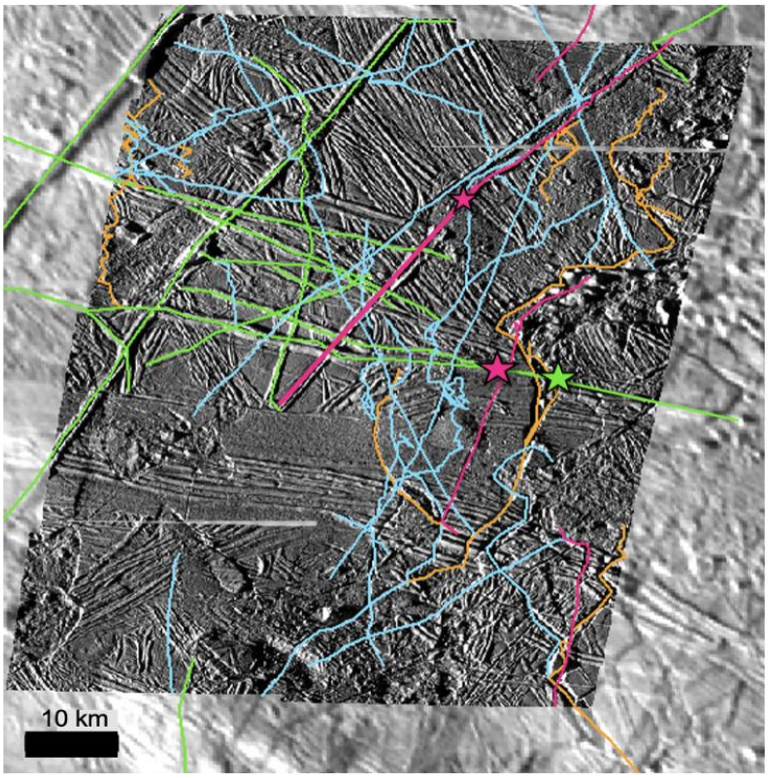

Legend
Double Ridge
Single Ridge
Fracture
Fossae

Fig. 3.7: Cluster 6 is a fracture network centered at ~35.649574°N, -86.603891°E, 300 Km west of Bress Crater. This set of SAPs includes portions of chaotic terrain and ridged plains creating a unique blend of features. The stars denote ridges that have been embayed by smooth-plain material (possibly of cryovolcanic origin or melted by cryomagmatic activity during the event or events that created the nearby chaos unit).

and tectonic events. Given their stratigraphic positions, overlapping several ridges in the plains, they are likely the youngest features and the most likely to possess open subterranean environments.

3.6 Cluster 7, The Tyre Multi-Ring Structure

At the Tyre impact structure, we see cluster seven (Fig. 3.8), which includes ridged plains and small bumpy chaos units along with smooth units and small, shallow secondary craters created by the impact's ejecta (Kadel et al., 2000). The surface includes a combination of saline hydrate and sulfate salts in the darker areas among the brighter water ice (Granahan et al., 1997, 1998; McCord et al., 1998; Fanale et al., 1999). Given their differing stratigraphy and morphologies, the ridged plains have been interpreted to form differently than the double ridges that crisscross the ring structure. The ridge and fracture on the nearby plains are the result of a compressional tectonic

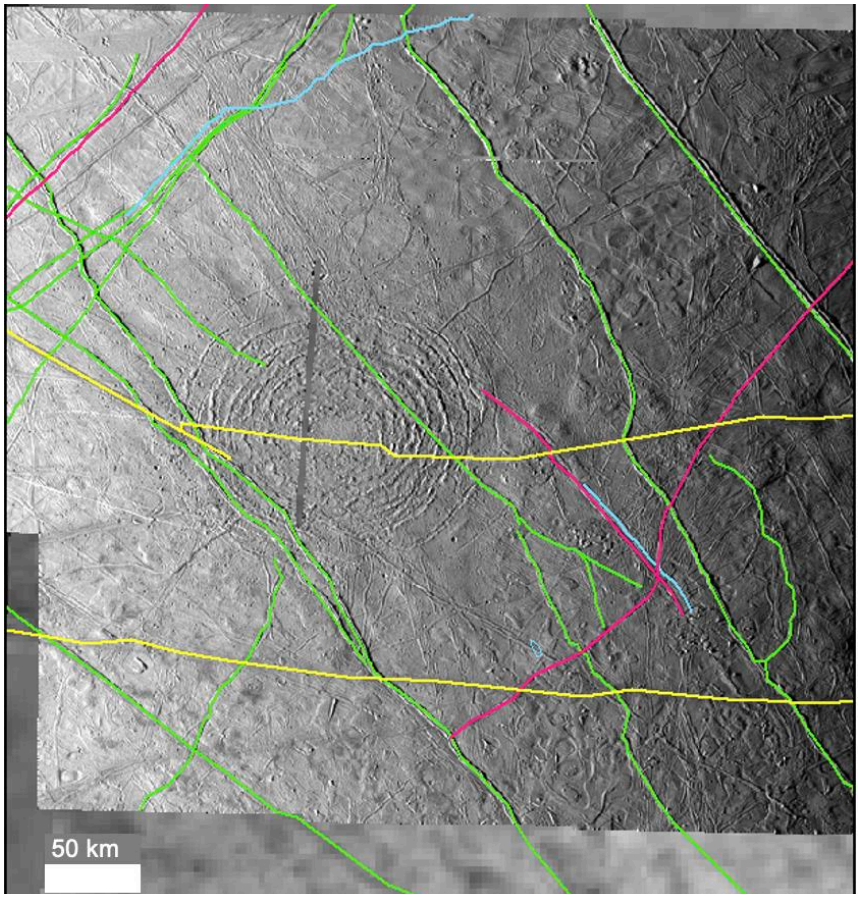

Legend
Double Ridge
Single Ridge
Fracture
Lineated Band

Fig. 3.8: Cluster 7, centered at ~ 33.5639°N, -145.3639°E shows the SAPs on and around the Tyre Multiring Structure, a large impact feature.

resurfacing event, while the isolated double ridges are from a later ridge-building event just before and after the Tyre impact (depending on their stratigraphic position relative to the ring structure) (Kadel et al., 2000).

The older smooth ridges were likely filled in by impact melt during or shortly after the impact (Kadel et al., 2000) so, were not considered SAPs. Given the presence of the lineated bands, the area around the crater has been interpreted as having thinner ice than the surrounding area such that some of the cracks and pits may have penetrated the crust fully (Kadel et al., 2000).

3.7 Cluster 8

Like cluster 6, cluster 8 (Fig. 3.9) contains both chaos and ridged plains terrain. Cluster 8 occurs on Agradnel Regio, a region of largely water ice with sulfate and saline

in the chaos. The ridges and bands in the lineated bands were similarly formed by tectonic activity, with the fossae and fractures likely cryovolcanic, given their placement on a chaos unit and overlapping the ridges.

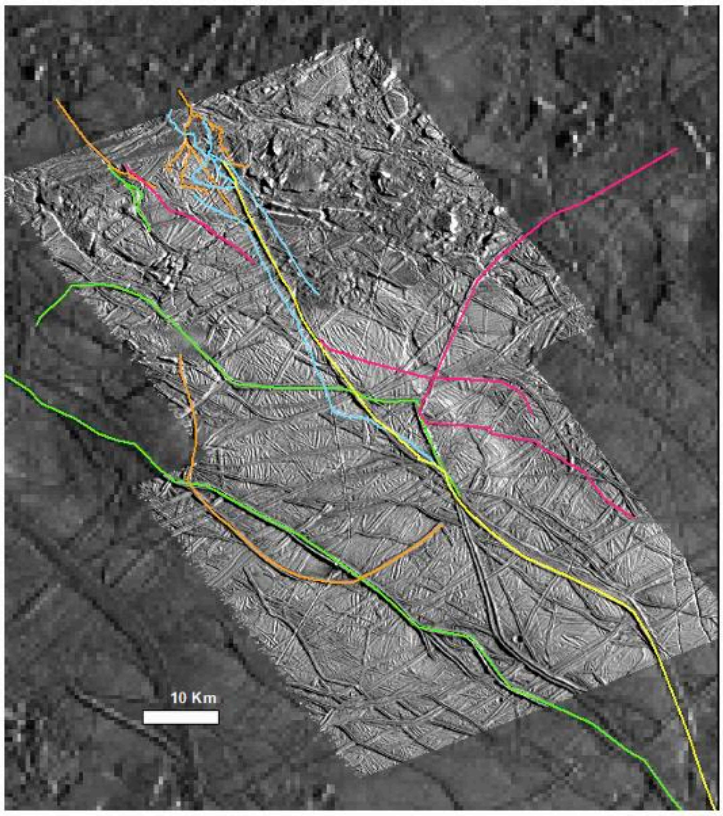

Legend
Double Ridge
Single Ridge
Fracture
Lineated Band
Fossae

Fig. 3.9: cluster 8 is a section of Agradnel Regio centered at ~ -28.688838 °N, 142.0162857°E. These SAPs are located at the intersection of a ridged plain and chaotic terrain meaning that both tectonic and volcanic processes played a role in cave formation.

3.8 Cluster 9

Cluster 9 (Fig. 3.10) is a section of Annwn Regio consisting of low-brightness chaos material, formed through cryomagmatic activity, surrounded by lighter ridged plains. As with the previous examples, the color difference reflects a change in surface chemistry (Leonard et al., 2024). The plains ridges and fractures on the plains are due to tectonic activity. The youngest feature and SAP are the fossae highlighted in Fig. 3.10

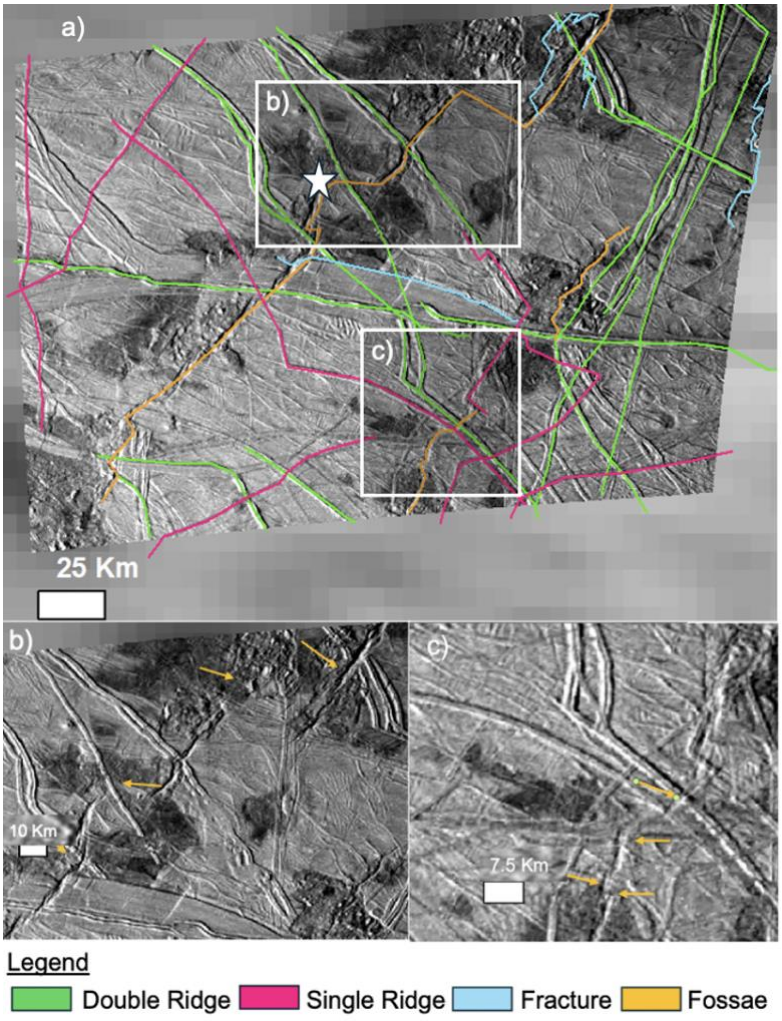

Fig. 3.10 a) Cluster 9 is centered at ~ 43.5430°N, 5.73973°E, part of Annwn Regio. It features Kenmario Fossae (indicated by a star) an SAP that exhibits signs of alteration by strike-slip faulting (highlighted in b and c)

a and b, which exhibit strike-slip tectonic alteration. This is a potentially tectonic feature, but given the darker and lighter bumpy chaos patches surrounding it, it could also be a product of cryovolcanism. It could be a cryovolcanic vent that opened via extensional tectonics and later altered by strike-slip faulting.

In contrast, the cycloidal double ridges were almost entirely between 100° and -132° longitude but on both chaotic terrain and ridged plains. The linear double ridges, meanwhile, occur in one of four regions. The first is around the intersection point of two lineated bands, Agave and Asterius linea, where many ridges intersect. The second includes Murias Chaos, a significant fracture network centered around 35.5°N,-86.0°E, and various intersecting ridges. The third region is the Tyre multi-ring structure, in, which a few of the double ridges appear to intersect. The fourth region includes the Cilix crater, parts of Harmonia, and

Radamanthys Linea. The linear and cycloidal single ridges are scattered around the globe in similar regions to the double ridges.

In contrast to the linear and cycloidal ridges, jagged ridges occur in essentially the same areas as the cycloidal and linear ridges except for the easternmost regions. The highest concentration of high-resolution imagery is outside of these ranges. So, it is also possible that some of the ridges mapped in these two regions are not as straight or cycloidal as they appear.

The most significant number of fossae and fractures are either surrounding or inside clusters 1, 3, 4, and 6 (Figs 3.2, 3.4, 3.5, and 3.9, respectively). They also seem to occur in similar regions to double ridges. Almost all occurred on chaotic terrain or ridged plains, aligning with their predicted formation theories. However, neither were identified in the many regions of the map with imagery greater than 200 m/pixel resolution, so this is far from an extensive list. There may be more fractures and fossae in these regions, but due to their smaller dimensions, they will remain invisible until these regions are imaged at a higher resolution.

The vast majority of the lineated bands were over 1000 km. Lineated bands are the widest, most distinctive linea and they can be identified at any resolution. By contrast, single ridges were mostly 400 km or less, double ridges were mostly 200 km or less, and fossae and fractures were mostly less than 50 km long, with fossae being longer than fractures on average. This means that the majority of fracture and fossae SAPs are likely single caverns, while ridges and bands represent cavern systems.

Mapping this area for SAPs led to five conclusions. (1) Cryovolcanic, tectonic, and otherwise tidal processes are all involved in forming SAPs on Europa. (2) Lineated

bands and single ridges are among the longest SAPs, while fossae and fractures are the shortest. (3) Fossae and Fracture SAPs seem almost exclusive to this hemisphere's chaotic terrain. (4) Ridge SAPs are the only types that appear on plain terrain. (5) Double ridge SAPs are evenly distributed throughout the mapped area, while Fossae and fractures appear in clusters.

This thesis identifies 493 potential cave entrances or features that could host caves (Fig. 3.1) termed Subsurface Access Points (SAPs). This includes 145 double ridges, 109 pits, 102 fractures, 67 single ridges, 57 fossae, and 17 lineated bands (Table 1). Most of them were jagged (neither entirely linear nor fully cycloid), which is not predicted by purely tidal tectonic models. The following section will show that this morphologic trend significantly impacts the current models for Europa's crust and subsurface processes.

4. Cluster Reinterpretations

This next section will reanalyze the ten clusters with these new perspectives. This section will also discuss the potential effects of tectonic alteration on the SAPs in each cluster based on Earth and extraterrestrial analogs.

4.1 Clusters 1 & 2

As discussed in Section 6, clusters 1 and 2 (Fig. 3.2, and 3.3) lie on high albedo ridged plains dominated by tectonic structures (Leonard, Patthoff, & Senske, 2024). Cluster 1 is mostly single ridges (two exhibiting signs of strike-slip faulting) with three jagged fossae and part of one lineated band. Cluster 2 mostly has double ridges and fractures with one lineated band. It is unlikely that the SAPs in this area were formed through extrusive cryovolcanism; this activity leaves dark albedo residue behind (Leonard, Patthoff, & Senske, 2024).

Section 1.4 discussed two models that involve the creation of single ridges: The tidal squeezing model and the linear diapirism model. They both list these as steps in the evolution of double ridges and evolutions of fractures (Greenberg et al., 1998; Head, Pappalardo, & Sullivan, 1999), meaning they are not currently SAPs but were in the past. These theories seem like options for forming these single ridges. However, because the tidal squeezing model still involves the extrusion of subsurface ocean material, it is likely to be the less viable of the two models. However, even if the single ridges are not SAPs, the linear diapirism model involves the upwelling of ductile ice from the subsurface. Therefore, studying these ridges could still provide information on the material and mechanics of Europa’s subsurface ductile crust layer.

The double ridges in cluster 2 also could have formed via the ice wedging model, which does not involve extrusive volcanism (Cushion et al., 2024). If they are in the right stage of this model, the central trough might even be deep enough to reach the subsurface ocean, though this would not last long.

The fractures were likely formed through extensional tectonics (Greenberg et al., 1998; Head, Pappalardo, & Sullivan, 1999), and given their proximity to ridges, they might become ridges in the future. The lineated band was also likely tectonic (see section 1.4.2), and the generally bright terrain can rule out the cryovolcanism model. Most SAPs in these clusters are ephemeral, except the lineated band. In this case, the single ridges would not be considered SAPs because their troughs are closed. However, they could also be double ridges or fractures with invisible central troughs.

Two single ridges in the first cluster appear to have strike-slip faults. If these are double ridges, they might have formed through the shear-heating model. This strike-slip faulting could have also caused a myriad of changes to the subsurface chamber, including but not limited to ceiling collapse, deformed the cave walls, and altered the topography of the subsurface chamber(s) (Kim & Sanderson, 2010; Szcygiel et al. 2021). If the ceiling did collapse, these ridges would no longer qualify as SAPs because they would not provide access to the subsurface.

4.2 Clusters 3, 4 & 8

These SAPs occur on chaotic terrain, so they have likely experienced cryovolcanic alteration. These clusters also have some dark albedo regions, so cryomagmatism is a possible formation style for these SAPs. The double and single ridges could have been formed through any of the processes in section 4. However,

according to the stratigraphic history, the area was likely ridged plains before the chaos developed (Leonard et al., 2024) and thus would have experienced tectonic resurfacing first. The ridges would have likely formed via tidal squeezing or ice wedging model. They could have also formed through the shallow sill model. Shallow sills of water are also a theorized contributor to the formation of chaotic terrain which is also present in these regions. The fractures are likely also tectonic because they are often broken up by the chaos terrain, indicating that they formed before the event that created the chaos.

However, the fossae seem to only exist because of the chaotic terrain. There are three main models of chaotic terrain formation: melt-through, diapirism, and shallow sills. These are all cryomagmatic processes, so these potential fossae likely formed through one of these methods. The most commonly accepted model for fossae formation is that they form in response to uneven crust thinning (Prockter et al., 2002). This could have happened through the shallow sill model, also known to thin the lithosphere. In this scenario, the lineated bands flanking the chaotic terrain act as lithospheric thickeners.

4.3 Cluster 5, Cilix crater

This is the cluster of SAPs in the Cilix Crater region. As mentioned in section 6, the crater is the youngest feature, so the area was just ridged plains before the Cilix impact event occurred. This means the double and single-ridge SAPs were likely not formed volcanically like the first two clusters. Given their proximity to double ridges, the single ridges in this cluster may be double ridges whose troughs have been obscured by the resolution or incidence angle of the image. If this is the case, the shear heating

and thermal compression model could also be feasible, though any SAPs in the area would have closed up by now if it was. Otherwise, the linear diapirism model is also feasible.

The placement of Cilix crater overtop the SAPs means a crater impact could influence them. The impactor was likely small because the crater has a small diameter (18 km) and is only about 400 m deep (NASA/JPL Cilix DEM). Models for icy bodies such as Europa predict that small impactors such as that of Cilix do not cause pervasive fractures (Harriss & Burchell, 2017). Therefore, new SAPs would not have been created by this impact. However, the force of the impact could have shaken the subsurface enough to cause alterations similar to those caused by strike-slip tectonics.

4.4 Cluster 6

This cluster occurs at the intersection of regional plains and bright chaos. Much of the double and single-ridge SAPs occurred on the plains terrain and were thus formed during successive tectonic events (Leonard et al., 2024). The many different orientations represent different tides resulting from ice wedging, linear diapirism, and tidal squeezing models. The linear fracture SAPs on the regional plains are likely formed by the same processes.

The fossae are the borders of the bright chaos, so they were probably not tectonic. They might result from cryomagmatic activity (like linear diapirism) freezing and expanding inside the crust, overwhelming the above crust, and causing it to crack. The abundance of domes and the overall convex shape of the chaos unit further support this hypothesis—the jagged fracture SAPs and especially the fractures on

chaos terrain possibly formed via a similar method. Though jagged fracture SAPs also appear on regional plains, their shapes do not match those of tidal models.

4.5 Cluster 7, The Tyre Multi-ring Structure

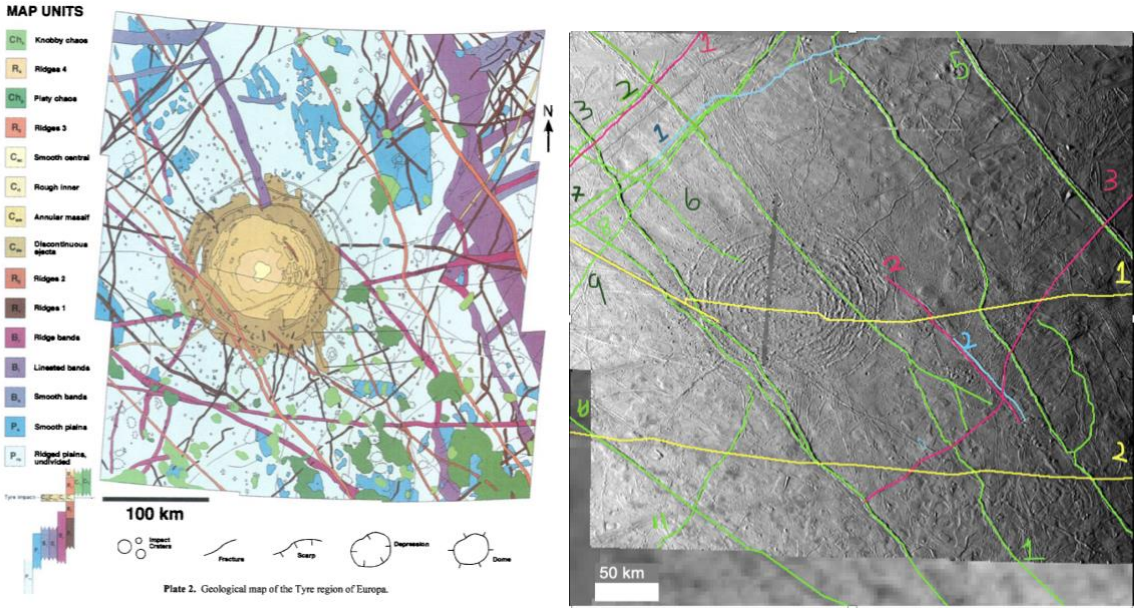

Fig.5.1: a side-by-side display of cluster 7 and a geologic map of the Tyre multi-ring structure. SAPs are numbered for ease of geologic interpretation. Geologic map credit: Kadel et al., (2000)

This is one of the most complex clusters. Each SAP will be referred to with an acronym corresponding to their type (Dr. = double ridge, Sr. = single ridge, Lb. = lineated band) and a number (Fig. 5.1) for ease of interpretation. The SAPs sit on a unit of ridged plains (Kadel et al., 2000), also called regional plains (Leonard et al., 2024), a terrain shaped by tectonic resurfacing. Given their stratigraphic positions, the fracture SAPs on it were likely formed during the event that created this terrain via extensional tectonics.

The smooth plains units are next in the geologic history (Kadel et al., 2000) and are interpreted in two ways. The units whose topography is not visible have been interpreted as products of cryovolcanic extrusion. These are the units near Dr. 4, at the intersection of Dr. 10 & Lb. 2, the north end of Dr. 3, 8, & 9, and at the south end of Sr.

1. The units in, which subtle regional plain topography is visible have been interpreted as either regional plains that have suffered extreme thermal degradation or a lineated band obscured by low resolution and poor incidence angle (Kadel et al., 2000) If they are the former, they were formed possibly through melt-through or some other internal process that produces heat. The ladder scenario would involve lithospheric dilation of some kind. These events should not affect the subterranean environments because all SAPs are stratigraphically younger than these units.

Following the above events is the formation of the Ridged bands, Lb. 1 & 2 and Sr. 2. Despite their differing morphologies, if they were all formed via the models presented in Greenberg et al. (1998), they could have formed at the same time (as suggested by their stratigraphic positions). This means that Lb. 1 & 2 were likely formed by a cyclic deformation model (See sections 4.2.1 and 4.2.2), and the Single ridge was likely a product of the tidal squeezing model. Further evidence of the cyclic deformation model can be seen in the lack of axial symmetry exhibited by the lineated bands. This is a property required by the other models in section 7 (Prockter et al., 2002). Dr. 1 was formed directly after the event that formed the ridged bands (Kadel et al., 2000) as a product of a tidal or lithospheric stress event just before the Tyre impact.

The Tyre impact leaves behind a complex crater, and its outer two units, the Annular Massif unit, and the Discontinuous Ejecta unit, affect some of the SAPs. The Annular Massif unit is disrupted blocks of pre-existing crust, disrupting Lb. 1, Dr. 1, 3, 6, 8, & 11. Despite the crater's much larger diameter of 150km, recent models show that the force required to produce a crater of this size would not be strong enough to fully rupture the crust of Europa (Harriss & Burchell, 2017). However, given that the impact

was strong enough to disrupt the surface to some extent, its movement and heat might have caused alterations similar to strike-slip faulting. The discontinuous ejecta layer affects Dr. 1 and the tip of Sr. 2. The ejecta might have filled the entrances to these chambers. Lb. 1 would have likely suffered the most damage from the impact because it is partially enveloped, unlike the other SAPs affected by the crater (see Fig. 5.1). Therefore, a whole or partial cave-in is likely for this SAP.

Shortly after the crater, the third ridge-building event occurs (Kadel et al., 2000), and Dr. 3, 4, 5, 8, and 10 are formed. These SAPs are oriented in the same direction, which implies that they were likely created by tidal forces imposed in that direction in the tidal squeezing model (Kadel et al., 2000). The ice wedging and linear diapirism models also begin with an extensional tide opening the initial fracture, so these models cannot be ruled out either. The shallow sill model also involves the tides, but they are only involved in the placement of the sill and do not influence the orientation of the resulting double ridge (Culberg, Schroder & Steinberg, 2022).

Chaos units were created last; two types are shown in Fig. 5. Knobby chaos is covered in lenticulae, and Platy chaos is populated by rafts or plates of old crust (Kadel et al., 2000). Later maps have split chaos units further into dark and light albedo categories (Leonard et al.,, 2024). Knobby chaos is thought to be a result of the injection of warmer ice material as evidenced by its convex features, with extrusion of this slurry being the cause of the darker albedos (Kadel et al., 2000), and platy chaos is thought to be due to the extrusion of salty brines with the melt-through model forming the brighter terrain. The ends of Dr. 4 and Dr. 1 & Sr. 3 intersection are disrupted by bright knobby chaos likely from some form of intrusive cryovolcanism. Given the

placement of these units, the heat produced during this event could have closed the SAP by filling the chamber with warm ice. The same could have happened to the center of Dr. 4, the southern tip of Sr. 2, and Dr. 10 & 11, which are disrupted by bright platy chaos. The center of Dr. 3 and the western end of Lb. 2 are enveloped in dark knobby chaos. During the cryovolcanic event(s) that formed the chaos units, the listed sections of these SAPs may have partially or filled with the extruded material.

4.6 Cluster 9

This cluster occurs on a ridged plain with spots of dark, chaotic terrain. Kermario Fossae is likely the youngest feature because it crosscuts several ridges and chaos units. It is near some lineated bands, but it is also possible that the compression needed to form these fossae came from forming one of the several double ridges in this area. Some double ridges that flank the fossae could also be steps in the evolution of lineated bands via any formation models discussed in section 4. The chaos units and fossae are younger than the ridges, so, likely, this area was also originally ridged plains, meaning the ridge SAPs are also tectonic.

The fossae experienced strike-slip faulting, which could have caused changes to any subterranean environment underneath it. Similar to the single ridges in cluster 1, this fossa would not be an SAP if the walls or ceiling collapsed due to this alteration. The status of these fossae as SAPs is also called into question by their proximity to the chaos units in the area. Chaos terrain is theorized to form through cryomagmatic or impact processes which could have altered or filled some or all of the subsurface chamber(s)

5. Discussion

The abundance of jagged features calls some of the formation theories discussed in the next section into question, particularly the idea that tidal forces are solely responsible for creating these features. They also bolster the idea that Europa's crust is not homogenous in thickness or rigidity.

'Jagged' is a broad category encompassing features that were neither fully linear nor fully cycloid. These landforms fell into two broad categories (shown in Fig. 4.1 below): Those resembling connected arcs (type 1) and those that change direction more randomly, meandering like rivers, or in a more abrupt manner (type 2). The shapes of the type 1 features can be partially explained by polar wander.

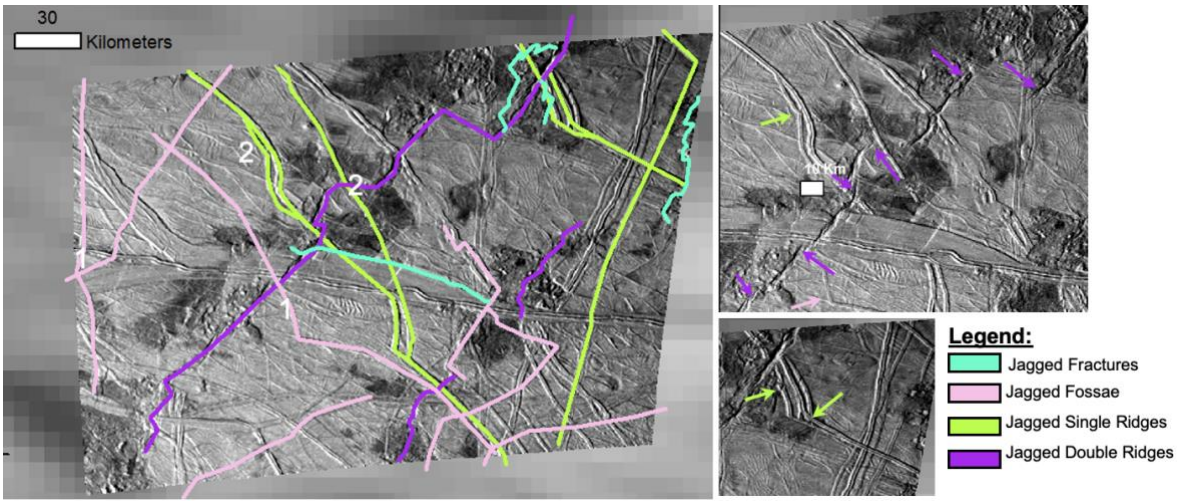

Fig. 4.1: This cluster displays both types of jagged ridges (numbered). The images at the right are zoomed in to a scale of 10km to show the changes in direction (the locations of the temperature changes are marked with arrows). more clearly.

Rhoden et al., (2021) conducts an inventory of cycloidal fissures on Europa. The standard model for cycloid formation is that they form in response to daily variations in the principle tidal stressors on Europa (Greenberg et al., 1998). A crack eventually forms in response to increasing regional tidal stress. This crack then propagates slowly in a path following the direction of the tidal force until the tidal stress decreases and the

crack stops propagating. The crack then remains dormant till tidal forces increase again, and a new arc segment is formed beginning at the termination of the previous one (Rhoden et al., 2021). This forms the kink or cusp connecting arcs (see Fig. 4.2 for an example). The standard model states that tidal forces should form neat concentric arcs whose orientation matches the direction of tidal stress at the time of its formation (Rhoden et al., 2021).

However, Rhoden et al.'s 2021 results could not be explained by tidal eccentricity alone. Cycloid distribution alone did not correlate as well with tidal stress maps as the theory proposed. The paper explains this discrepancy by noting that other factors, such as crustal rigidity and/or thickness variations, polar wander, and obliquity, influence cycloid location. Similarly, the results of this thesis seem to support the conclusion that non-tidal forces create and influence the morphology of linear features on Europa.

Type 2 jagged linea tend to change direction for one or more of the following reasons. Strike-slip faulting (shown in Fig. 3.2) is most common in jagged fossae, although some ridges exhibit this. This phenomenon is often attributed to shallow water reservoirs (Matteoni et al., 2023), polar wander (Schenk, Matsuyama & Nimmo; 2020), an elastic crustal response to increased strain (Katterhorn, 2004), and 'tidal walking' (Preblich et al., 2007). Some also change direction after being crosscut by another feature (Fig. 3.12). In either case, these changes are often associated with evidence of surface disruption, such as the crack stopping and starting or being filled in by debris. This suggests that these fissures did not initially form with this path. Instead, their shape was altered after formation.

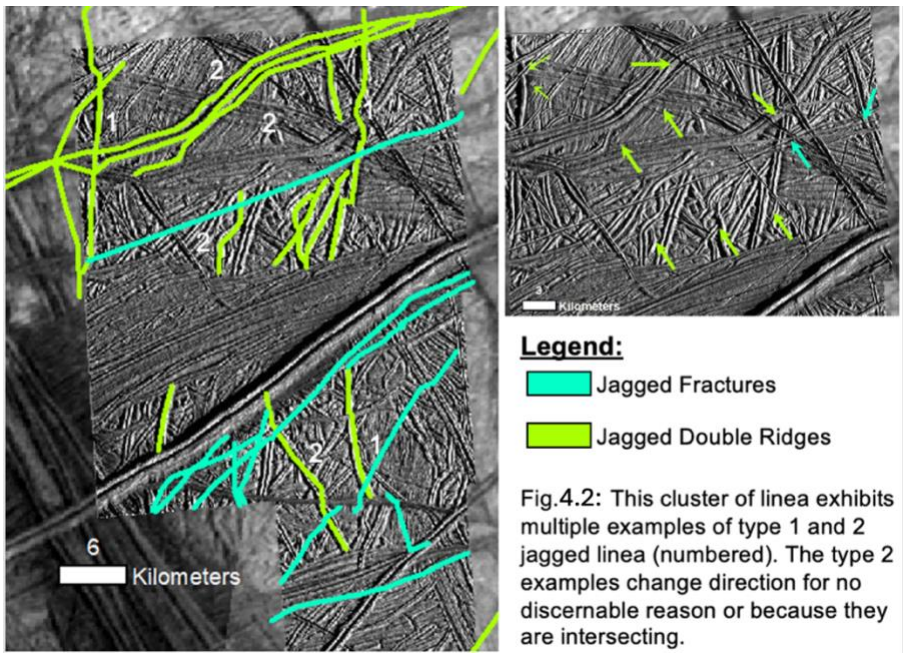

Fig.4.2: This cluster of linea exhibits multiple examples of type 1 and 2 jagged linea (numbered). The type 2 examples change direction for no discernable reason or because they are intersecting.

Some type 2 jagged linea seem to change direction while forming. These changes sometimes happen around nearby features like chaos units or pits, as if the ridge is swerving to avoid hitting them like a car avoiding an obstruction. They also sometimes change when one ridge branches into several or two or more combine into one (See Fig, 3.2 & 3.3). Another peculiarity is when ridges change direction for no discernable reason (ex, the sizeable double ridge complex in Fig. 3.3). They meander like a river, changing direction gradually with little to no signs of surficial disruption. The lack of disruption suggests that these linea formed with these jagged shapes rather than altering their paths.

This revelation calls into question the idea that the formation of linear features is dictated by tidal forces alone. Landforms whose morphology is governed chiefly by variations in tidal stress will form concentric arcs (Rhoden et al., 2021). While the morphology of type 1 jagged linea can be partially explained by orbital factors, the same cannot be said about the type 2 wavy linea. No purely tidal models predict the morphology reflected in these results. Thus, the results of this thesis suggest that the formation of double ridges and similar features cannot be explained by tidal stressors

alone. Other factors, such as variations in crustal thickness (Rhoden et al., 2021) and cryomagmatic processes, must be involved in forming Europan fissures.

Variations in crustal thickness might help explain the abundance of wavy linea. Beuthe (2018) found that on planets with varying crustal thickness, the effects of stress are enhanced where the crust is thin. So, it stands to reason that the jaggedness observed in this study is partially due to the cracks preferentially propagating along paths of thinner crust. However, it does not explain why the changes in direction are so relatively abrupt.

Rhoden et al. (2021) explain that the orientation of the cusps of cycloids should correlate to the angle at, which tidal forces are exerted on the crust. This angle appears to change despite Europa's orbit being tidally locked (having little to no obliquity) because Europa's crust is essentially floating atop the ocean and can thus spin in a different direction than the rest of the moon. This creates changes in direction that are reflected in the cusps. The ridges described and mapped by Rhoden et al. (2021) have hundreds of kilometers apart cusps. In contrast, the meandering ridges mapped in this thesis appear to experience changes in direction at much smaller intervals, just several kilometers. This is faster than predicted by the models in Rhoden et al. (2021), and therefore, there must be some other stressor creating these lines.

Convection currents due to tidal heating would explain the shape better. In addition to tidal tectonics, Europa also experiences tidal heating, which can create convection currents in its ocean and, in some models, the ductile layer of the lower crust. In the tidal heating model presented by Tobie et al, (2003), the tidal heating that Europa experiences creates convection currents in the lower crust. They are much

smaller than tidal forces so they could explain these abrupt changes. However, recent models do not show convection causing large-scale deformation as we have observed on Europa (Showman & Han, 2004). Despite this, many papers argue that tidal heating could create warm upwellings called diapirs that deform the crust (Pappalardo & Sullivan, 1999; Sotin et al., 2002; Culberg et al.,2022). Therefore, the abundance of jagged linea presented in this thesis would make sense if the formation of linea involved heating and diapirism rather than tidal compression and extension alone.

6. Conclusions

On Earth, studying caves is fruitful enough to warrant its own discipline, speleology. The study of cave formation has largely been restricted to karst, a subset of processes that are very common on Earth. Karst processes are possible elsewhere on bodies such as Titan, but many other ways of forming caves exist. Tectonic, volcanic, and impact processes can also form subsurface access points on virtually all rocky celestial bodies. Thus, studying subterranean environments can teach us about the paleoclimate, hydrology, magmatism, volcanism, and tectonics of our planet and other planets' moons and asteroids.

Image resolution is a major factor in identifying SAPs. It is for this reason that this list is likely incomplete. The SAPs classified as single ridges could be double ridges, lineated, or textured bands. However, the features that distinguish these and other types of linea are not visible at resolutions lower than about 500 m/pixel. Equally, pits can only be identified with certainty at resolutions at or above 200 m/pixel (Culha & Manga, 2016). At lower resolutions, the various types of lenticulae become indistinguishable (Greenberg et al., 2003). This resolution issue is why only 70% of the northern hemisphere was mapped in this study.

This thesis explores Europa's subsurface processes by mapping and analyzing its linear SAPs. In doing this, it also contributed to the ongoing debate over the role of nontidal processes in forming ridges on Europa. A morphological analysis of these linear SAPs revealed an abundance of wavy or jagged linea, much more than purely tidal models would predict. Therefore, it is reasonable to assume that nontidal forces like diapirism are at least partially responsible for forming Europan linear fissures. The results

of this thesis also raised questions about the homogeneity of Europa's crust. If tidal extension and compression acted on a planet with uniform thickness, it would produce more symmetrical linea. Benthul (2018) found that on planets with crusts of variable thickness, thinner areas experience differentially stronger tidal stress. Therefore, the abundance of wavy linea would make sense if the cracks initiated by tidal forces were preferentially propagating in regions with thinner crust.

This thesis also shows some of the features of speleogenic interest in Europa. Tectonic, cryomagmatic, and cryovolcanic processes create these ridges, bands, troughs, and pits. Analyzing the current list of features could provide insight into subsurface and geologic processes. Rhoden et al. (2021) examine the spatial distribution of cycloid ridges and reveal clusters and gaps that can be used to constrain tidal stress models. Culha & Manga (2016) analyze the morphology of pits and point out the absence of signs of surface strain. The absence of strain implies that pit shape and orientation are decided during their formation and possibly influenced by properties of the ice shell, like stress. Stress within the shell might change over time due to factors like polar wander and orbital evolution, meaning that pits with similar orientations are likely to form at similar times (Culha & Manga, 2016).

When better data are obtained from Europa Clipper or JUCIE, these features will likely be studied further to uncover more about Europa's subsurface processes and habitability. Depending on how deep Clipper's radar instrument measures their cracks, they could also provide insights into the geochemistry of the ductile layer or even the subsurface ocean (ref). It would be much easier and cheaper to sample and study the ocean from inside these fissures. They could also be landing sites for future in-situ

missions to Europa, like Jezero crater for the Mars Curiosity Rover. SAPs appear to have flat bases, making them easy to land on compared to the uneven topography of Europa's surface terrain, especially the wider cracks like fossae or pits. The walls might also provide some protection from Jupiter's ionizing radiation. However, this list is far from extensive, so when better data is obtained, this experiment should be conducted on the features presented in this thesis and similar landforms on the remainder of the globe.

7. Acknowledgements:

First, I would like to thank Dr. Jut Wynne, who responded to my emails and gave me this project. I would not have written this thesis without him. I would also like to thank Dr. Elodie Lesage and Dr. Erin Leonard, who helped me find the imagery I needed to start this project and gave me ideas on how to analyze it. Thank you to Cansu Culha for allowing me to use your data in this thesis and for helping me understand this topic more deeply.

I would also like to thank Eugenio Marcano for teaching me how to use ArcGIS and Eric Spellman for helping me fix the initial projection problem with some images and how to reproject the mosaics. I would also like to thank Eric Perlman, and my thesis committee: Darby Dyar, Thomas Burbine, and Alan Werner for their endless support and advice during this incredibly challenging year. Drs. Dyar and Perlman also taught me scientific writing; I would not have written this thesis without their help. Dr. Perlman also helped me understand the geophysics concepts I needed to properly comprehend the papers, which helped me come to my conclusion. I'm not a physicist, so that help was invaluable.

References:

Alexander, C., R. Carlson, G. Consolmagno, R. Greeley, and D. Morrison. 2017. “The Exploration History of Europa.” In *University of Arizona Press eBooks*, 3–26. https://doi.org/10.2307/j.ctt1xp3wdw.7.

Beuthe, Mikael. “Enceladus’s Crust as a Non-Uniform Thin Shell: I Tidal Deformations.” *Icarus* 302 (March 2018): 145–74. https://doi.org/10.1016/j.icarus.2017.11.009.

Bierhaus, E. B., K. Zahnle, and C. R. Chapman. 2017. “Europa’s Crater Distributions and Surface Ages.” In *University of Arizona Press eBooks*, 161–80. https://doi.org/10.2307/j.ctt1xp3wdw.13.

Bruesch, L. S., and Erik Asphaug. 2004. “Modeling Global Impact Effects on Middle-sized Icy Bodies: Applications to Saturn’s Moons.” *Icarus* 168 (2): 457–66. https://doi.org/10.1016/j.icarus.2003.11.007.

Culha, Cansu, and Michael Manga. "Geometry and Spatial Distribution of Lenticulae on Europa." *Icarus 271*, (2016): 49-56. https://doi.org/10.1016/j.icarus.2015.12.052.

Cashion, Melissa D., Brandon C. Johnson, Harry G. Gibson, E. P. Turtle, Michael M. Sori, and H. J. Melosh. 2024. “Europa’s Double Ridges Produced by Ice Wedging.” *Journal of Geophysical Research. Planets* 129 (2). https://doi.org/10.1029/2023je008007.

Collins, G. C., and F. Nimmo. 2017. “Chaotic Terrain on Europa.” In *University of Arizona Press eBooks*, 259–82. https://doi.org/10.2307/j.ctt1xp3wdw.17.

Culberg, Riley, Dustin M. Schroeder, and Gregor Steinbrügge. 2022. “Double Ridge Formation Over Shallow Water Sills on Jupiter’s Moon Europa.” *Nature Communications* 13 (1). https://doi.org/10.1038/s41467-022-29458-3.

Cushing. 2017. “Mars Global Cave Candidate Catalog (MGC^3) V1.” USGS Astrogeology Science Center. 2017. https://astrogeology.usgs.gov/search/map/Mars/MarsCaveCatalog/mars_cave_catalog.zip.

Cushing, G. E. 2012. “Candidate Cave Entrances on Mars.” *Journal of Caves and Karst Studies/Journal of Cave and Karst Studies* 74 (1): 33–47. https://doi.org/10.4311/2010ex0167r.

Dastpak, Pooya, Rosiléa Alves De Sousa, and Daniel Dias. 2023. “Soil Erosion Due to Defective Pipes: A Hidden Hazard Beneath Our Feet.” *Sustainability* 15 (11): 8931. https://doi.org/10.3390/su15118931.

Doggett, T., R. Greeley, P. H. Figueredo, and K. Tanaka. 2017. “Geologic Stratigraphy and Evolution of Europa’s Surface.” In *University of Arizona Press eBooks*, 137–60. https://doi.org/10.2307/j.ctt1xp3wdw.12.

Fagents, S. A., R. Greeley, Robert Sullivan, R. Pappalardo, and L. M. Prockter. 2000. “Cryomagmatic Mechanisms for the Formation of Rhadamanthys Linea, Triple Band Margins, and Other Low-Albedo Features on Europa.” *Icarus (New York, N.Y. 1962)* 144 (1): 54–88. https://doi.org/10.1006/icar.1999.6254.

Fanale, F. P., J. C. Granahan, R. Greeley, R. Pappalardo, J. W. Head, James H. Shirley, R. W. Carlson, et al. 2000. “Tyre and Pwyll: Galileo Orbital Remote Sensing of Mineralogy Versus Morphology at Two Selected Sites on Europa.” *Journal of Geophysical Research* 105 (E9): 22647–55. https://doi.org/10.1029/1999je001102.

Fannin, R. J., and P. Slangen. 2014. “On The Distinct Phenomena of Suffusion and Suffosion.” *Géotechnique Letters* 4 (4): 289–94. https://doi.org/10.1680/geolett.14.00051

Ferrill, David A., D. Y. Wyrick, and Kevin J. Smart. 2011. “Coseismic, Dilational-fault and Extension-fracture Related Pit Chain Formation in Iceland: Analog for Pit Chains on Mars.” *Lithosphere* 3 (2): 133–42. https://doi.org/10.1130/l123.1.

Fielder, G. (1965). *Lunar geology*. Lutterworth Press.

Ford, Derek, Peter L. Smart, and R. O. Ewers. 1983. “The Physiography and Speleogenesis of Castleguard Cave, Columbia Icefields, Alberta, Canada.” *Arctic and Alpine Research* 15 (4): 437. https://doi.org/10.2307/1551231.

Granahan, J. C., et al., Galileo's multi-instrument spectral view of Tyre Macula (abstract), *Eos Trans. AGU*, **78**, Fall Meet. Suppl., F417, 1997.

Granahan, J., et al., A composition study of Europa's impact scars (Tyre and Pwyll) as seen by Galileo NIMS and SSI (abstract), *Div. Planet. Sci.*, **30**38.02, 1084, 1998

Greeley, R., P. H. Figueredo, D. A. Williams, F. C. Chuang, J. E. Klemaszewski, S. D. Kadel, L. M. Prockter, et al. 2000. “Geologic Mapping of Europa.” *Journal of Geophysical Research* 105 (E9): 22559–78. https://doi.org/10.1029/1999je001173.

Greeley, Ronald, Christopher F. Chyba, Head, Thomas B. McCord, William B. McKinnon, Robert T. Pappalardo, and Patricio H Figueredo. 2006. “Geology of Europa.” In *Jupiter: The Planet, Satellites, and Magnetosphere*, edited by Fran Bagenal, Timothy E. Dowling, William B. McKinnon, and William McKinnon. Cambridge University Press.

Greenberg, R., P. E. Geissler, G. V. Hoppa, B. R. Tufts, D. D. Durda, R. Pappalardo, J. W. Head, R. Greeley, Robert Sullivan, and M. H. Carr. 1998. “Tectonic Processes on Europa: Tidal Stresses, Mechanical Response, and Visible Features.” *Icarus* 135 (1): 64–78. https://doi.org/10.1006/icar.1998.5986.

Greenberg, R., G. V. Hoppa, B. R. Tufts, P. E. Geissler, Jeannemarie Riley, and S. D. Kadel. 1999. “Chaos on Europa.” *Icarus* 141 (2): 263–86. https://doi.org/10.1006/icar.1999.6187.

Greenberg, Richard, Martha A. Leake, Gregory V. Hoppa, and B.R Tufts. "Pits and Uplifts on Europa." *Icarus 161*, no. 1 (2003): 102-126. Accessed April 15, 2024. https://doi.org/10.1016/S0019-1035(02)00013-1.

Gulley, Jason, and Andrew G. Fountain. 2019. “Glacier Caves.” In *Elsevier eBooks*, 468–73. https://doi.org/10.1016/b978-0-12-814124-3.00056-x.

Harriss, Kathryn, and M. J. Burchell. 2017. “Hypervelocity Impacts Into Ice-topped Layered Targets: Investigating the Effects of Ice Crust Thickness and Subsurface Density on Crater Morphology.” *Meteoritics & Planetary Science* 52 (7): 1505–22. https://doi.org/10.1111/maps.12913.

Head, J. W., R. T. Pappalardo, and Robert Sullivan. 1999. “Europa: Morphological Characteristics of Ridges and Triple Bands From Galileo Data (E4 and E6) and Assessment of a Linear Diapirism Model.” *Journal of Geophysical Research* 104 (E10): 24223–36. https://doi.org/10.1029/1998je001011.

Hobbs, Horton H., III, Rickard A Olson, Elizabeth G Winkler, and David C. Culver. 2017. *Mammoth Cave: A Human and Natural History*. Springer.

Hoppa, G. V., B. R. Tufts, R. Greenberg, and P. E. Geissler. 1999. “Strike-Slip Faults on Europa: Global Shear Patterns Driven by Tidal Stress.” *Icarus* 141 (2): 287–98. https://doi.org/10.1006/icar.1999.6185.

“How Can Caves Teach Us About Climate?” 2016. National Centers for Environmental Information (NCEI). June 13, 2016. https://www.ncei.noaa.gov/news/how-can-caves-teach-us-about-climate.

Kadel, S. D., F. C. Chuang, R. Greeley, and Jeffrey M. Moore. 2000. “Geological History of the Tyre Region of Europa: A Regional Perspective on Europan Surface Features and Ice Thickness.” *Journal of Geophysical Research* 105 (E9): 22657–69. https://doi.org/10.1029/1999je001203.

“Karst Landscapes - Caves and Karst (U.S. National Park Service).” n.d. https://www.nps.gov/subjects/caves/karst-landscapes.htm.

Kattenhorn, S. A., and T. A. Hurford. 2017. “Tectonics of Europa.” In *University of Arizona Press eBooks*, 199–236. https://doi.org/10.2307/j.ctt1xp3wdw.15.

Kim, Young, and David J. Sanderson. "Inferred Fluid Flow through Fault Damage Zones Based on the Observation of Stalactites in Carbonate Caves." *Journal of Structural Geology 32*, no. 9 (2010): 1305-1316. https://doi.org/10.1016/j.jsg.2009.04.017.

Leonard, Erin, D. A. Patthoff, D. A. Senske, and G. C. Collins. 2024. “Global Geologic Map of Europa.” *Scientific Investigations Map (Print)*, January. https://doi.org/10.3133/sim3513.

Lucchetti, Alice, Riccardo Pozzobon, Francesco Mazzarini, G. Cremonese, and Matteo Massironi. 2017. “Brittle Ice Shell Thickness of Enceladus From Fracture

Distribution Analysis." *Icarus* 297 (November): 252–64. https://doi.org/10.1016/j.icarus.2017.07.009.

Manga, Michael, and Antoine Sinton. 2004. "Formation of Bands and Ridges on Europa by Cyclic Deformation: Insights From Analogue Wax Experiments." *Journal of Geophysical Research* 109 (E9). https://doi.org/10.1029/2004je002249.

Matteoni, Pietro, A. Neesemann, R. Jaumann, Jon K. Hillier, and F. Postberg. 2023. "Ménec Fossae on Europa: A Strike-Slip Tectonics Origin Above a Possible Shallow Water Reservoir." *Journal of Geophysical Research. Planets* 128 (7). https://doi.org/10.1029/2022je007623.

Malaska, Michael J., Ashley Schoenfeld, J. Judson Wynne, K. L. Mitchell, O. L. White, A. D. Howard, Jeffrey M. Moore, and O. M. Umurhan. 2022. "Potential Caves: Inventory of Subsurface Access Points on the Surface of Titan." *Journal of Geophysical Research. Planets* 127 (11). https://doi.org/10.1029/2022je007512.

Maynard-Casely, Helen E., Morgan L. Cable, Michael J. Malaska, Tuan Vu, Mathieu Choukroun, and Robert Hodyss. 2018. "Prospects for Mineralogy on Titan." *The American Mineralogist* 103 (3): 343–49. https://doi.org/10.2138/am-2018-6259.

McCord, T. B., G. B. Hansen, F. P. Fanale, R. W. Carlson, D. L. Matson, T. V. Johnson, W. D. Smythe, et al. 1998. "Salts on Europa's Surface Detected by Galileo's Near Infrared Mapping Spectrometer." *Science* 280 (5367): 1242–45. https://doi.org/10.1126/science.280.5367.1242.

Michaut, Chloé, and Michael Manga. 2014. "Domes, Pits, and Small Chaos on Europa Produced by Water Sills." *Journal of Geophysical Research. Planets* 119 (3): 550–73. https://doi.org/10.1002/2013je004558.

Morrison, David, and D. P. Cruikshank. 1974. “Physical Properties of the Natural Satellites.” *Space Science Reviews* 15 (5). https://doi.org/10.1007/bf00175241.

NASA/JPL-Caltech/ASI team. (2016). Cassini Orbiter SSA Radar 5 BIDR V1.0 [Data set]. NASA Planetary Data System Geosciences Node. https://doi.org/10.1789/1520231

NASA/JPL/DLR-Berlin team. (1997). Galileo Orbital Operations Solid State Imaging Raw EDR V1.0 [Data set]. NASA Planetary Data System Geosciences Node. https://doi.org/10.1789/152025

NASA/JPL/Space Sciences Institute team. (2005) Cassini Orbiter Saturn ISSNA/ISSWA 2 EDR Version 1.0 [Data set]. NASA Planetary Data System Geosciences Node. https://doi.org/10.171891520177

Nimmo, F. 2002. “Strike-slip Motion and Double Ridge Formation on Europa.” *Journal of Geophysical Research* 107 (E4). https://doi.org/10.1029/2000je001476.

Okubo, C. H., & Martel, S. J. (1998). Pit crater formation on Kilauea volcano, Hawaii. *Journal of Volcanology and Geothermal Research*, *86*(1–4), 1–18. https://doi.org/10.1016/s0377-0273(98)00070-5

Parmentier, E. M., and J. W. Head. 1981. “Viscous Relaxation of Impact Craters on Icy Planetary Surfaces: Determination of Viscosity Variation With Depth.” *Icarus* 47 (1): 100–111. https://doi.org/10.1016/0019-1035(81)90095-6.

“Photo (U.S. National Park Service).” n.d. https://www.nps.gov/media/photo/view.htm?id=2F14E8C1-E95A-469E-9D9A-69059531053F.

Preblich, B., R. Greenberg, J. Riley, and D. O'Brien. "Tidally Driven Strike–Slip Displacement on Europa: Viscoelastic Modeling." *Planetary and Space Science 55*, no. 10 (2007): 1225-1245. https://doi.org/10.1016/j.pss.2007.01.018.

Porco, C. C., D. DiNino, and F. Nimmo. 2014. "How The Geysers, Tidal Stresses, and Thermal Emission Across the South Polar Terrain of Enceladus Are Related." *The Astronomical Journal* 148 (3): 45. https://doi.org/10.1088/0004-6256/148/3/45.

Prockter, Louise M., James W. Head, Robert T. Pappalardo, Robert J. Sullivan, Amy E. Clifton, Bernd Giese, Roland Wagner, and Gerhard Neukum. "Morphology of Europan Bands at High Resolution: A Mid-ocean Ridge-type Rift Mechanism." *Journal of Geophysical Research: Planets 107*, no. E5 (2002): 4-1-4-26. https://doi.org/10.1029/2000JE001458.

Prockter, L. M., and G. W. Patterson. 2017. "Morphology and Evolution of Europa's Ridges and Bands." In *University of Arizona Press eBooks*, 237–58. https://doi.org/10.2307/j.ctt1xp3wdw.16.

Rathbun, J. A., George Musser, and S. W. Squyres. 1998. "Ice Diapirs on Europa: Implications for Liquid Water." *Geophysical Research Letters* 25 (22): 4157–60. https://doi.org/10.1029/1998gl900135.

Rhoden, Alyssa R., Kyle J. Mohr, Terry A. Hurford, Wade Henning, Stan Sajous, D. A. Patthoff, and David Dubois. "Obliquity, Precession, and Fracture Mechanics: Implications of Europa's Global Cycloid Population." *Journal of Geophysical Research: Planets 126*, no. 3 (2021): e2020JE006710. https://doi.org/10.1029/2020JE006710.

Šebela, Stanka. 2008. “Broken Speleothems as Indicators of Tectonic Movements.” *Acta Carsologica* 37 (1). https://doi.org/10.3986/ac.v37i1.159.

Schenk, Paul, Isamu Matsuyama, and Francis Nimmo. "A Very Young Age for True Polar Wander on Europa From Related Fracturing." *Geophysical Research Letters 47*, no. 17 (2020): e2020GL088364. https://doi.org/10.1029/2020GL088364.

Sobolewski, Linda, Thor H. Hansteen, Edgar U. Zorn, Christian Stenner, Lee J. Florea, Sarah Burgess, Anda Ionescu, Eduardo Cartaya, and Andreas Pflitsch. 2023. “The Evolving Volcano-ice Interactions of Crater Glacier, Mount St. Helens, Washington (USA).” *Bulletin of Volcanology* 85 (4). https://doi.org/10.1007/s00445-023-01632-5.

Squyres, S. W., R. T. Reynolds, P. Cassen, and S. J. Peale. 1983. “Liquid Water and Active Resurfacing on Europa.” *Nature* 301 (5897): 225–26. https://doi.org/10.1038/301225a0.

Szczygieł, Jacek, Michał Gradziński, Pavel Bella, Helena Hercman, Juraj Littva, Maciej J. Mendecki, Przemysław Sala, and Wojciech Wróblewski. "Quaternary Faulting in the Western Carpathians: Insights into Paleoseismology from Cave Deformations and Damaged Speleothems (DemäNová Cave System, Low Tatra Mts)." Tectonophysics 820, (2021): 229111. https://doi.org/10.1016/j.tecto.2021.229111.

Tachihara, Hiroshi, Toshio Honda, Lương Thị Tuất, Bui Van Thom, Nguyễn Văn Hoàng, Yuriko Chikano, Katsuji Yoshida, et al. 2018. “Geological Values of Lava Caves

in Krongno Volcano Geopark, Dak Nong, Vietnam." *Vietnam Journal of Earth Sciences* 40 (4): 299–319. https://doi.org/10.15625/0866-7187/40/4/13101.

"Talus Caves - Caves and Karst (U.S. National Park Service)." n.d. https://www.nps.gov/subjects/caves/talus-caves.htm.

The Editors of Encyclopaedia Britannica. 1998a. "Karst | Limestone, Sinkholes & Caves." Encyclopedia Britannica. July 20, 1998. https://www.britannica.com/science/karst-geology.

Thomson, Richard E., and John R. Delaney. 2001. "Evidence for a Weakly Stratified Europan Ocean Sustained by Seafloor Heat Flux." *Journal of Geophysical Research* 106 (E6): 12355–65. https://doi.org/10.1029/2000je001332.

Tufts, B. R. 1998. Lithospheric Displacement Features on Europa and Their Interpretation. Doctoral thesis, Univ. of Arizona, Tucson

_____, R. Greenberg, G. V. Hoppa, and P. E. Geissler. 1999. "Astypalaea Linea: A Large-Scale Strike-Slip Fault on Europa." *Icarus* 141 (1): 53–64. https://doi.org/10.1006/icar.1999.6168.

———. 2000. "Lithospheric Dilation on Europa." *Icarus (New York, N.Y. 1962)* 146 (1): 75–97. https://doi.org/10.1006/icar.2000.6369.

Wagner, R. V., & Robinson, M. S. (2021).Occurrence and origin of lunar pits: Observations from a new catalog. In Lunar and Planetary Science Conference. Abstract #2530, LPI Contributions No. 2548

Webb, J. A., E. B. Joyce, and N. C. Stevens. "Lava caves of Australia." In The Proceedings of the Third International Symposium on Vulcanospeleology, Oregon, pp. 74-85. 1982.

Wilson, L., Hawke, B. R., Giguere, T. A., & Petrycki, E. R. (2011). An igneous origin for Rima Hyginus and Hyginus crater on the Moon. *Icarus*, *215*(2), 584–595. https://doi.org/10.1016/j.icarus.2011.07.003

Wynne, J. Judson, T. N. Titus, Ali–akbar Agha–mohammadi, Armando Azúa-Bustos, Penelope J. Boston, Pablo De León, Cansu Demirel-Floyd, et al. 2022. "Fundamental Science and Engineering Questions in Planetary Cave Exploration." *Journal of Geophysical Research. Planets* 127 (11). https://doi.org/10.1029/2022je007194.

8. Appendix

8.1 SAP Data:

This section will house the full data tables. Each linear SAP was mapped, numbered (ID column), and classified by type (Frac_Type column), the approximate coordinates of its center (Latitude and longitude in decimal degrees in the Europa2000 coordinate reference system), shape (Frac_Style column), length, terrain type (Near_Feat Column), and whether it intersects with other linea (Y = yes, N = no, P = possible or unclear, obscured by incidence angle or poor resolution).

Note: if there is more than one type of linea in the Frac_Type column, the fissure looked like it could have been more than one type of SAP. This is likely because the images were mosaics so the incidence angle was not held constant for the entirety of every region. Those with multiple type classifications were ultimately classified based on how they looked for the majority of their length. Pull-apart terrain is the old terminology for the ridged plains but that was not known to me until after the data collection process was complete.

Table 1: Single Ridges

ID	FRAC_TYPE	LONG	LAT	FRAC_STYLE	LENGTH_GEO (KM)	NEAR_FEAT	LINEA_INTERESECT
0	Single Ridge	-141.541	32.208401	Linear	169.070343	Impact Crater	Y
1	Single Ridge	-138.79201	34.081699	Linear	416.199067	Impact Crater	Y
2	Single Ridge	141.229	-27.785801	Linear	22.543213	Chaos Terrain	P
3	Single Ridge	142.16299	-28.5042	Jagged Linear	48.027463	Chaos Terrain	P
4	Single and Double Ridge	142.272	-28.7523	Jagged	86.621047	Chaos Terrain	N

5	Single Ridge	124.109	7.48052	Jagged Linear	102.087304	Chaos Terrain	P
6	Single Ridge	44.920799	1.97164	Jagged Linear	237.70688	Chaos Terrain	N
7	Single Ridge/Fossa	25.7169	-19.6327	Cycloid	1688.867156	Impact Crater+ Chaos Terrain	N
8	Single Ridge	44.341801	3.6555	Cycloid	284.326011	Chaos Terrain	N
9	Single Ridge	43.940601	5.20354	Jagged	240.251079	Chaos Terrain	P
10	Single Ridge	42.665401	1.45012	Jagged Linear	196.919286	Chaos Terrain	P
11	Single Ridge	43.796902	3.51163	Jagged Linear	326.764939	Chaos Terrain	P
12	Single Ridge	-163.07201	19.5044	Jagged	874.724443	Impact Crater	P
13	Single and Double Ridge	-179.59801	5.13922	Linear	464.575206	Impact Crater + Pull apart Terrain	Y
14	Single Ridge	-178.63699	5.3551	Linear	33.292005		N
15	Single Ridge and Possible Fossa	178.325	18.75	Cycloid	868.740495		P
16	Single or Double Ridge and Possible Fossa	175.411	10.2158	Jagged Linear	643.718867	Impact Crater + Pull apart Terrain	Y
17	Single Ridge	172.668	2.32174	Jagged Cycloid	202.469379	Impact Crater + Pull apart Terrain	N
18	Single and Double Ridge	176.579	2.77048	Linear	123.033405	Impact Crater	P
19	Single Ridge	176.526	2.28475	Linear	79.86385	Impact Crater	N
20	Single Ridge	-168.326	7.60023	Jagged	330.346866	Possible Impact Crater	N
21	Single Ridge	-145.92799	45.545101	Linear	610.392266		Y
22	Single Ridge	36.4207	8.22779	Jagged	687.685249	Possible Impact Crater + Chaos Terrain	
23	Single Ridge	135.487	27.435499	Cycloid	408.63995	Chaos Terrain+ Pull apart Terrain	Y
24	Single Ridge	84.452599	14.7614	Jagged	98.675995	Chaos Terrain+ Pull apart Terrain	Y

25	Single Ridge	-85.8097	34.674801	Jagged Linear	22.707619	Pull apart Terrain +Chaos Terrain	Y
26	Single Ridge	-86.215401	35.536598	Jagged Linear	42.532286	Pull apart Terrain +Chaos Terrain	Y
27	Single Ridge/Lineated Band	-81.284698	57.519901	Jagged Linear	557.342183	Pull apart Terrain+Possible Impact Crater	P
28	Single Ridge	-92.3433	46.098499	Jagged Linear	175.762275	Pull apart Terrain+Possible Impact Crater	P
29	Single Ridge	-88.019699	46.6647	Jagged Linear	269.834743	Pull apart Terrain+Possible Impact Crater	P
30	Single Ridge	-87.448402	65.211899	Cycloid	628.464818	Pull apart Terrain+Possible Impact Crater	P
31	Single Ridge	-86.301201	58.188202	Jagged Linear	706.318256	Pull apart Terrain+Possible Impact Crater	P
32	Single Ridge	-78.466202	54.319901	Jagged Cycloid	663.373661	Pull apart Terrain+Possible Impact Crater	P
33	Single Ridge	-72.6483	51.7533	Jagged	528.70193	Pull apart Terrain+Possible Impact Crater	P
34	Single and Double Ridge	-86.230103	36.582699	Jagged Linear	64.315325	Pull apart Terrain+Possible Impact Crater	P
35	Single Ridge	89.092201	6.81139	Linear	177.331109	Pull apart Terrain+Chaos Terrain	Y
36	Single Ridge	90.098198	7.02822	Jagged	236.911548	Pull apart Terrain+Chaos Terrain	Y
37	Single Ridge	-75.044502	20.873199	Jagged	75.90063	Pull apart Terrain + Chaos Terrain	P

38	Single Ridge	174.60927	34.010339	Cycloid	2130.760839	Pull apart Terrain + Chaos Terrain	Y
39	Single Ridge	121.9121	35.773951	Linear	760.693183	Chaos terrain	N
40	Single Ridge	89.094653	-47.001028	Cycloid	1658.406261	Chaos terrain + Impact crater	N
41	Single Ridge	169.52601	29.676044	Cycloid	1166.505879	Chaos Terrain	Y
42	Single Ridge	178.76698	18.98388	Cycloid	1192.162011	Chaos Terrain	Y
43	Single Ridge	-170.22647	25.195271	Jagged Cycliod	1396.854937	Chaos Terrain	Y
44	Single Ridge	-161.32291	5.793718	Jagged Cycloid	940.233678	Chaos Terrain	Y
45	Single Ridge	45.213969	4.956707	Jagged	232.90025	Impact Crater, mannan	Y
46	Single Ridge	45.201297	4.361159	Jagged	308.314887	Impact Crater, mannan	Y
47	Single Ridge	33.718778	3.139926	Jagged	166.069838	Impact Crater, mannan	Y
48	Single Ridge	34.284397	4.931855	Jagged	219.784089	Impact Crater, mannan	Y
49	Single Ridge	35.374191	2.755835	Jagged	148.78317	Impact Crater, mannan	Y
50	Single Ridge	41.071772	2.419411	Jagged	246.968912	Impact Crater, mannan	Y
51	Single Ridge	40.876748	0.680231	Jagged	107.552289	Impact Crater, mannan	Y
52	Single Ridge	46.925882	7.655364	Jagged	54.706244	Impact Crater, mannan	N
53	Single Ridge	47.040172	8.146832	Jagged	24.748969	Impact Crater, mannan	N
54	Single Ridge	40.24659	0.92002	Jagged	174.773928	Impact Crater, mannan	Y
55	Single Ridge	36.437751	0.072898	Jagged	92.536233	Impact Crater, mannan	Y
56	Single Ridge	35.635361	1.751925	Jagged	151.156012	Impact Crater, mannan	Y
57	Single Ridge	37.744311	3.453425	Jagged	346.617943	Impact Crater, mannan	Y
58	Single Ridge	177.08668	0.803422	Cycloid	118.000341	Impact Crater Cilix	Y

59	Single Ridge	178.54712	0.323274	Linear	87.964356	Impact Crater Cilix	Y
60	Single Ridge	176.60225	3.16882	Cycloid	34.21091	Impact Crater Cilix	Y
61	Single Ridge	178.72194	1.254181	Cycloid	146.049135	Impact Crater Cilix	Y
62	Single or Double Ridge	1.221892	43.636565	Jagged Cycloid	143.377071	Chaotic pull apart terrain	Y
63	Single or Double Ridge	2.476623	44.809687	Jagged Linear	126.623694	Chaotic pull apart terrain	Y
64	Single or Double Ridge	4.771863	41.994193	Jagged Cycloid	222.432597	Chaotic rafts and pull apart terrain	Y
65	Single or Double Ridge	9.413348	40.494636	Jagged Linear	89.728189	Chaotic Pull apart terrain	Y
66	Single Ridge to Fossae	8.464649	41.1067	Jagged	124.979433	Chaotic rafts and pull apart terrain	Y
67	Single Ridge to Fossae	8.077008	42.83068	Jagged	93.73974	Chaotic rafts and pull apart terrain	Y
68	single Ridge	4.639249	40.321218	Jagged Cycloid	98.940279	Chaotic rafts and pull apart terrain	Y

Table 2: Lineated Bands

Id_1	Frac_type	Long	Lat	Frac_style	LENGTH_GEO (Km)	Near_Feat	Linea_intersect
62	Lineated Band	61.971001	-34.649101	Partial Cycloid	1850.943447	Chaos Terrain	P
63	Lineated Band	172.363998	46.875	Cycloid	2873.056343	Impact Crater	Y
64	Lineated Band	105.872002	48.277699	Partial Cycloid	1424.718427	Chaotic Terrain	Y
65	Lineated Band	133.423996	48.1217	Jagged	287.381038	Chaos Terrain	Y
66	Textured Lineated Band	137.445999	40.8395	Partial Cycloid	215.7788	Chaos Terrain	Y
67	Lineated Band	-132.207	34.318699	Linear	943.904218	Impact Crater, Tyre	Y

68	Lineated Band	178.643997	24.5606	Cycloid	2777.147283	Chaos Terrain+Impact Crater, Tyre	Y
69	Lineated Band	50.613899	45.9081	Cycloid	3519.795512	Chaos Terrain	Y
70	Lineated Band	90.759003	7.91139	Linear	828.252006	Chaos Terrain	P
71	Lineated Band	133.306	13.7853	Partial Cycloid	1832.985459	Chaos Terrain	Y
72	Double Ridge and/or Lineated Band	129.462997	44.380001	Jagged Cycloid	1041.043749	Chaos Terrain	N
73	Double Ridge and/or Lineated Band	142.033005	-28.729401	Linear	121.187981	Chaos Terrain	Y
74	Lineated Band	63.570999	-11.9454	Linear	2433.553746	Chaos Terrain	N
75	Single Ridge/Lineated Band	-81.284698	57.519901	Jagged Linear	557.342183	Pull apart Terrain+ Impact Crater,Tyre	P
76	Lineated Band	119.983236	27.187999	Cycloid	2334.395454	Chaos terrain	Y
77	Lineated Band	66.053921	-8.43126	Linear	2493.137073	Pull apart Terrain	Y
78	Lineated Band	86.978837	8.753401	Linear	268.870383	Pull apart chaotic terrain	Y

Table 3: Fractures

Id	Frac_type	Long	Lat	Frac_style	LENGTH_GEO (Km)	Near_Feat	Linea_intersect
79	Fracture	-140.646	31.348301	Linear	92.332164	Impact Crater	Y
80	Fracture	141.264999	-27.584299	Jagged	13.981218	Chaos Terrain	N
81	Fracture	141.128006	-27.343599	Jagged	15.268555	Chaos Terrain	P
82	Fracture and Double Ridge	141.464005	-27.6548	Jagged Linear	29.605812	Chaos Terrain	P
83	Fracture	122.178001	5.19885	Jagged	52.056383	Chaos Terrain	P
84	Fracture	-149.30299	39.804901	Jagged	140.152638	Chaos Terrain	Y
85	Fracture	82.0709	12.482	Jagged	19.851829	Chaos Terrain	N
86	Fracture	-86.517303	34.841702	Jagged	137.654476	Pull apart Terrain +Chaos Terrain	Y

87	Fracture	-86.6483	34.996101	Cycloid	14.034834	Pull apart Terrain +Chaos Terrain	Y
88	Fracture	-86.147301	34.893101	Jagged	23.044968	Pull apart Terrain +Chaos Terrain	Y
89	Fracture	-85.751999	36.381699	Jagged Linear	9.356913	Pull apart Terrain+Chaos Terrain	Y
90	Fracture	-86.225197	36.076698	Linear	45.446883	Pull apart Terrain +Chaos Terrain	Y
91	Fracture	-86.479797	36.465	Linear	67.192785	Pull apart Terrain +Chaos Terrain	Y
92	Fracture	-87.171402	37.080002	Linear	25.02222	Pull apart Terrain+Chaos Terrain	Y
93	Fracture	-86.987602	36.972099	Jagged	48.020127	Pull apart Terrain+Chaos Terrain	Y
94	Fracture	-86.660599	35.895802	Linear	52.828436	Pull apart Terrain+Chaos Terrain	Y
95	Fracture	-85.835197	36.923199	Linear	42.785135	Pull apart Terrain+Chaos Terrain	Y
96	Fracture	-86.5243	37.016899	Jagged Linear	21.981357	Pull apart Terrain+Chaos Terrain	Y
97	Fracture	-86.3591	37.158699	Jagged Linear	12.152344	Pull apart Terrain+Chaos Terrain	N
98	Fracture	-87.247803	37.161598	Jagged Linear	11.67417	Pull apart Terrain+Chaos Terrain	Y

99	Fracture	-86.267097	36.435699	Jagged	18.997225	Pull apart Terrain+Chaos Terrain	Y
100	Fracture	-85.992897	36.4249	Jagged	13.204734	Pull apart Terrain+Chaos Terrain	Y
101	Fracture	-86.313904	36.071999	Jagged Cycloid	29.538561	Pull apart Terrain+Chaos Terrain	Y
102	Fracture	-86.346603	35.400501	Jagged Cycloid	13.077399	Pull apart Terrain+Chaos Terrain	Y
103	Fracature	-86.552696	35.397499	Jagged	22.985132	Pull apart Terrain+Chaos Terrain	Y
104	Fracture	-86.669296	35.659801	Linear	6.384274	Pull apart Terrain+Chaos Terrain	P
105	Fracture	-86.3778	34.721199	Jagged Linear	30.564607	Pull apart Terrain+Chaos Terrain	Y
106	Fracture	-87.466599	34.7369	Jagged Linear	55.932196	Pull apart Terrain+Chaos Terrain	Y
107	Fracture	-87.2286	36.206001	Jagged	11.463839	Pull apart Terrain+Chaos Terrain	Y
108	Fracture	-87.2995	36.574902	Linear	21.196135	Pull apart Terrain+Chaos Terrain	Y
109	Fracture	-86.655403	36.2393	Jagged	3.840768	Pull apart Terrain+Chaos Terrain	Y
110	Fracture	-87.619797	36.706001	Jagged	9.642112	Pull apart Terrain+Chaos Terrain	P
111	Fracture	-86.690498	36.195099	Jagged Linear	17.141745	Pull apart Terrain+Chaos Terrain	Y

112	Fracture	-87.580803	36.8423	Jagged Cycloid	4.303137	Pull apart Terrain+Chaos Terrain	Y
113	Fracture	-87.513199	36.757198	Jagged	11.894494	Pull apart Terrain+Chaos Terrain	P
114	Fracture	-87.288803	36.8283	Jagged	6.559141	Pull apart Terrain+Chaos Terrain	P
115	Fracture	-85.804199	37.077	Jagged Linear	10.131379	Pull apart Terrain+Chaos Terrain	Y
116	Fracture	89.493599	12.8227	Linear	83.711965	Pull apart Terrain+Chaos Terrain	N
117	Fracture	141.455002	-27.880501	Linear	22.806744	Chaos Terrain	P
118	Fracture	85.720261	9.13489	Jagged	63.930639	Pull apart Terrain	Y
119	Fracture	84.851039	9.23606	Jagged	50.466027	Pull apart Terrain	Y
120	Fracture	84.105169	8.433205	Jagged	91.370729	Pull apart Terrain	Y
121	Fracture	84.89183	8.800206	Jagged	19.321195	Pull apart Terrain	Y
122	Fracture	84.923193	8.53475	Jagged	2.98183	Pull apart Terrain	N
123	Fracture	84.933418	8.694595	Jagged	4.499257	Pull apart Terrain	Y
124	Fracture	84.617076	8.786108	Jagged	19.059505	Pull apart Terrain	Y
125	Fracture	84.365853	8.956016	Jagged	5.459983	Pull apart Terrain	Y
126	Fracture	85.003718	8.501693	Jagged	6.433949	Pull apart Terrain	Y
127	Fracture	85.637441	9.085724	Jagged	9.951214	Pull apart Terrain	Y
128	Fracture	89.285407	9.127404	Jagged	36.010039	Pull apart Terrain	Y

129	Fracture	89.148183	8.97634	Jagged	34.680724	Pull apart Terrain	Y
130	Fracture	89.40644	8.743894	Jagged	4.590382	Pull apart Terrain	N
131	Fracture	88.627954	8.83939	Jagged	43.306136	Pull apart Terrain	Y
132	Fracture	88.353358	8.618889	Jagged	25.183125	Pull apart Terrain	Y
133	Fracture	88.512045	8.864508	Jagged	5.933969	Pull apart Terrain	Y
134	Fracture	88.290259	8.750373	Jagged	26.591082	Pull apart Terrain	Y
135	Fracture	87.940184	9.358422	Jagged	15.441108	Pull apart Terrain	Y
136	Fracture	88.37559	9.18187	Jagged	8.031827	Pull apart Terrain	Y
137	Fracture	88.588058	8.79864	Jagged	17.388045	Pull apart Terrain	Y
138	Fracture	87.019422	8.86642	Jagged	7.673569	Pull apart Terrain	Y
139	Fracture	87.076526	8.665387	Jagged	9.796487	Pull apart Terrain	Y
140	Fracture	87.440087	9.08061	Jagged	14.411869	Pull apart Terrain	Y
141	Fracture	86.527019	9.119468	Jagged	9.682086	Pull apart Terrain	N
142	Fracture	84.100533	9.524431	Jagged	10.475278	Pull apart Terrain	Y
143	Fracture	84.473691	9.391571	Jagged	13.490423	Pull apart Terrain	Y
144	Fracture	83.922614	9.222449	Jagged	45.003374	Pull apart Terrain	Y
145	Fracture	84.65194	9.713319	Jagged	2.73827	Pull apart Terrain	Y
146	Fracture	84.595721	9.720496	Jagged	10.742233	Pull apart Terrain	Y
147	Fracture	84.549043	9.645023	Jagged	9.001226	Pull apart Terrain	Y

148	Fracture	85.499435	9.357623	Jagged	15.029626	Pull apart Terrain	Y
149	Fracture	85.116991	9.237955	Jagged	24.959274	Pull apart Terrain	Y
150	Fracture	84.680973	9.02931	Jagged	20.238433	Pull apart Terrain	Y
151	Fracture	83.521108	9.041727	Jagged	32.767956	Pull apart Terrain	Y
152	Fracture	83.430198	8.970064	Jagged	29.626191	Pull apart Terrain	Y
153	Fracture	83.328531	9.007142	Jagged	13.813093	Pull apart Terrain	Y
154	Fracture	83.496993	9.275681	Jagged	21.24929	Pull apart Terrain	Y
155	Fracture	83.362681	9.65805	Jagged	21.276209	Pull apart Terrain	Y
156	Fracture	83.70943	9.523584	Jagged	4.319294	Pull apart Terrain	Y
157	Fracture	86.700797	14.675245	Jagged	17.424102	Pull apart Terrain	Y
158	Fracture	86.398421	14.275657	Jagged	8.801438	Pull apart Terrain	Y
159	Fracture	86.499265	14.326826	Linear	13.918834	Pull apart Terrain	Y
160	Fracture	86.703743	14.347095	Jagged	7.393097	Pull apart Terrain	Y
161	Fracture	86.153017	14.489641	Jagged	5.729395	Pull apart Terrain	N
162	Fracture	86.187645	14.555555	Linear	6.306985	Pull apart Terrain	N
163	Fracture	86.219151	14.55693	Jagged	8.831335	Pull apart Terrain	Y
164	Fracture	86.206997	14.565246	Jagged	13.472824	Pull apart Terrain	Y
165	Fracture	86.013962	14.512322	Jagged	9.383375	Pull apart Terrain	N
166	Fracture	86.086368	14.541191	Jagged	12.345024	Pull apart Terrain	Y

167	Fracture	86.630325	14.975526	Jagged	20.914855	Pull apart Terrain	Y
168	Fracture	86.714847	15.001516	Jagged	14.628739	Pull apart Terrain	Y
169	Fracture	85.956116	14.692348	Linear	13.771	Pull apart Terrain	Y
170	Fracture	85.877849	15.282782	Linear	8.193743	Pull apart Terrain	Y
171	Fracture	86.213834	15.406536	Jagged	36.234294	Pull apart Terrain	Y
172	Fracture	86.794816	15.599619	Linear	16.327299	Pull apart Terrain	Y
173	Fracture	86.788651	15.418513	Linear	8.761298	Pull apart Terrain	Y
174	Fracture	86.731246	15.269916	Linear	28.377465	Pull apart Terrain	Y
175	Fracture	86.640153	15.176196	Linear	6.514877	Pull apart Terrain	Y
176	Fracture	86.609759	14.113703	Jagged	18.827949	Pull apart Terrain	Y
177	Fracture	86.511981	15.413356	Linear	12.07246	Pull apart Terrain	Y
178	Fracture or fossae	11.278319	44.865603	Jagged	72.927565	Chaotic pull apart terrain	Y
179	Fracture or fossae	8.978359	45.914572	Jagged	28.540449	Chaotic pull apart terrain	Y
180	Fracture or fossae	8.426679	46.271998	Jagged	71.962012	Chaotic pull apart terrain	Y
181	Fracture or fossae	6.41421	43.132862	Jagged Cycloid	95.563845	Chaotic pull apart terrain	Y

Table 4: Double Ridges

Id	Frac_type	Long	Lat	Frac_style	LENGTH_GEO (Km)	Near_Feat	Linea_intersect
178	Double Ridge	140.570007	-28.076099	Jagged	71.728281	Chaos Terrain	Y
179	Double Ridge	131.136002	32.941002	Linear	59.866801	Chaos Terrain	Y

180	Double Ridge	130.363007	34.480701	Jagged Cycloid	134.318187	Chaos Terrain	Y
181	Double Ridge	136.212006	48.302601	Jagged Cycloid	2039.173292	Chaos Terrain	Y
182	Double Ridge	157.919006	20.6791	Linear	1774.003147	Chaos Terrain	Y
183	Double Ridge	-176.218	32.254101	Partial Cycloid	1268.156052	Chaos Terrain	Y
184	Double Ridge	-155.513	39.1231	Linear	737.587754	Impact Crater	Y
185	Double Ridge	-152.502	38.412102	Cycloid	1960.670748	Impact Crater	N
186	Double Ridge	-157.05299	57.507198	Cycloid	3287.940319	Impact Crater	Y
187	Double Ridge	-140.179	40.014	Partial Cycloid	1147.669569	Impact Crater	N
188	Double Ridge	-157.97701	33.744801	Partial Cycloid	1613.008739	Impact Crater	Y
189	Double Ridge	-137.74001	31.2866	Jagged	141.613736	Impact Crater	Y
190	Double Ridge	-140.88001	27.639799	Jagged	306.973231	Impact Crater	Y
191	Double Ridge	-141.17101	30.794201	Linear	38.952274	Impact Crater	Y
192	Double Ridge	-141.79401	31.0956	Jagged	83.013811	Impact Crater	Y
193	Double Ridge	-146.401	35.3494	Linear	270.864195	Impact Crater	N
194	Double Ridge	-149.148	28.2932	Linear	168.879293	Impact Crater	N
195	Double Ridge	132.126007	48.851002	Jagged	85.705889	Chaos	P
196	Double Ridge	141.654999	-29.308599	Linear	165.957348	Chaos Terrain	N
197	Double Ridge	140.570007	-28.076099	Jagged	71.728281	Chaos Terrain	Y
198	Double Ridge	136.425995	49.891499	Jagged	323.800416	Chaos Terrain	N
199	Double Ridge	141.264008	-29.2152	Jagged	51.031424	Chaos Terrain	P
200	Double Ridge	-177.608	19.8918	Cycloid	1625.066531	Chaos Terrain + impact crater	P
201	Double Ridge	176.477997	0.532205	Linear	247.942682	Impact Crater	Y
202	Double Ridge	127.814003	2.18665	Jagged	104.778706	Chaos Terrain	Y
203	Double Ridge	127.851997	4.30232	Jagged	50.51805	Chaos Terrain	N
204	Double Ridge	127.428001	6.53382	Linear	85.514237	Chaos Terrain	Y
205	Double Ridge/Textured Band	132.251999	14.8748	Jagged Cycloid	571.004173	Chaos Terrain	N
206	Double Ridge	177.128006	0.257822	Jagged	98.14706	Impact Crater	P
207	Double Ridge	179.580002	18.930099	Linear	1242.965952	Pull apart Terrain	N
208	Double Ridge	177.807999	1.83572	Jagged Linear	72.990121	Impact Crater	Y
209	Double Ridge	178.279999	2.62129	Linear	191.356215	Impact Crater	Y
210	Double Ridge	177.503998	2.12807	Linear	98.355876	Impact Crater	P

211	Double Ridge and/or Textured Band	176.531006	2.58586	Linear	76.799199	Impact Crater	Y
212	Double Ridge and/or Textured Band	177.074005	2.19165	Linear	55.696088	Impact Crater	Y
213	Double Ridge	176.373993	0.905207	Linear	27.899879	Impact Crater	P
214	Double Ridge and/or Textured Band	176.190002	0.531156	Jagged Cycloid	216.147266	Impact Crater+ Pull apart Terrain	Y
215	Double Ridge	-179.368	7.07274	Jagged	489.143839	Impact Crater	P
216	Double Ridge	168.735992	16.9368	Jagged Cycloid	998.234108	Pull-apart Terain	N
217	Double Ridge	-152.127	37.246399	Jagged Linear	83.517524	Impact Crater	Y
218	Double Ridge	-150.68401	38.2514	Jagged Linear	64.284785	Impact Crater	Y
219	Double Ridge	-145.202	43.647499	Jagged Linear	720.325142	Impact Crater	Y
220	Double Ridge	-145.83501	41.393299	Jagged LInear	114.096114	Impact Crater	N
221	Double and Single Ridge	-152.177	39.337101	Linear	136.575489	Impact Crater	Y
222	Double Ridge	-151.075	37.3839	Jagged	189.267174	Impact Crater	Y
223	Double and Single Ridge	-150.74699	37.541698	Linear	256.804686	Impact Crater	Y
224	Double Ridge	133.274002	20.664301	Jaggd Cycloid	494.280117	Chaos Terrain	N
225	Double Ridge	131.727997	17.140301	Jagged	232.070199		N
226	Double Ridge	136.973007	24.7162	Linear	511.416047	Chaos Terrain+ Pull apart Terrain	Y
227	Double Ridge	142.128006	14.8108	Jagged Cycloid	287.837451	Chaos Terrain+ Pull apart Terrain	Y
228	Double Ridge	130.917999	36.361301	Jagged Cycloid	1031.542191	Chaos Terrain+ Pull apart Terrain	Y
229	Double Ridge	135.602005	15.0639	Jagged	104.216379	Chaos Terrain+ Pull apart Terrain	Y
230	Double Ridge	130.917999	36.361301	Jagged Cycloid	1031.542191	Chaos Terrain+ Pull apart Terrain	Y

231	Double Ridge	87.482399	15.5736	Linear	342.284197	Chaos Terrain+ Pull apart Terrain	N
232	Double Ridge	84.588799	12.3643	Jagged	247.53205	Chaos Terrain+ Pull apart Terrain	N
233	Double Ridge	85.306702	12.5208	Linear	373.643048	Chaos Terrain+ Pull apart Terrain	P
234	Double Ridge	85.307098	13.1784	Jagged Linear	81.033836	Chaos Terrain+ Pull apart Terrain	P
235	Double Ridge	84.254501	13.9171	Jagged Partial Cycloid	111.056481	Chaos Terrain+ Pull apart Terrain	N
236	Double Ridge	81.880096	12.9978	Partial Cycliod	63.615839	Chaos Terrain+ Pull apart Terrain	Y
237	Double Ridge	85.976601	17.759001	Jagged Linear	478.762164	Chaos Terrain+ Pull apart Terrain	Y
238	Double Ridge	83.2603	16.382	Jagged Partial Cycloid	110.869434	Chaos Terrain+ Pull apart Terrain	Y
239	Double Ridge	-71.561501	48.851601	Jagged Cycloid	880.073056	Pull apart Terrain	P
240	Double Ridge	-85.6604	39.732498	Jagged Linear	438.668289	Pull apart Terrain	Y
241	Double Ridge	-79.519203	34.249901	Linear	686.064475	Pull apart Terrain	P
242	Double Ridge	-88.368401	36.9016	Cycloid	112.588992	Pull apart Terrain +Chaos Terrain	P
243	Double Ridge	-88.337196	34.828499	Linear	103.790418	Pull apart Terrain+Chaos Terrain	Y
244	Double Ridge	-86.9123	36.799702	Linear	41.911991	Pull apart Terrain+Chaos Terrain	P

245	Double Ridge	-88.596397	36.170799	Jagged	65.75535	Pull apart Terrain+Chaos Terrain	P
246	Double Ridge	-86.923302	35.885201	Jagged Linear	47.553677	Pull apart Terrain+Chaos Terrain	Y
247	Double Ridge	-87.100601	36.359798	Jagged LInear	29.15831	Pull apart Terrain+Chaos Terrain	Y
248	Double Ridge	-86.923103	36.174301	Linear	31.57339	Pull apart Terrain+Chaos Terrain	Y
249	Double Ridge	-86.945297	35.977501	Linear	33.596535	Pull apart Terrain+Chaos Terrain	P
250	Double Ridge	-87.405899	34.174099	Jagged Linear	18.56664	Pull apart Terrain+Chaos Terrain	Y
251	Double Ridge	-86.991302	36.2346	Jagged	22.04817	Pull apart Terrain+Chaos Terrain	Y
252	Double Ridge	-87.074898	36.008301	Linear	26.009032	Pull apart Terrain+Chaos Terrain	Y
253	Double Ridge	-76.493202	40.8867	Jagged Linear	371.018888	Pull apart Terrain+Possible Impact Crater	Y
254	Double Ridge	-84.604698	53.170799	Jagged	891.64416	Pull apart Terrain+Possible Impact Crater	Y
255	Double Ridge	-85.359398	37.304298	Partial Cycloid	24.324988	Pull apart Terrain+Chaos Terrain	Y
256	Double and Single Ridge	-85.622498	37.5961	Jagged	36.124666	Pull apart Terrain+Chaos Terrain	Y
257	Double Ridge	79.786499	4.77707	Jagged Cycloid	243.038269	Pull apart Terrain+Chaos Terrain	Y

258	Double Ridge	83.451797	6.17885	Jagged	331.335055	Pull apart Terrain+Chaos Terrain	Y
259	Double Ridge	90.930199	7.14275	Jagged Linear	333.183307	Pull apart Terrain+Chaos Terrain	Y
260	Double Ridge	91.953903	6.87759	Linear	554.630996	Pull apart Terrain+Chaos Terrain	Y
261	Double Ridge	89.156097	7.48819	Linear	564.398829	Pull apart Terrain+Chaos Terrain	Y
262	Double Ridge	87.5625	13.7215	Linear	549.950507	Pull apart Terrain+Chaos Terrain	Y
263	Double Ridge	87.077599	16.148899	Jagged Linear	106.444038	Pull apart Terrain+Chaos Terrain	P
264	Double Ridge	87.959801	16.4848	Linear	42.829588	Pull apart Terrain+Chaos Terrain	P
265	Double Ridge	89.979202	19.298599	Jagged Linear	276.329857	Pull apart Terrain+Chaos Terrain	P
266	Double Ridge	88.666199	17.469	Linear	43.822782	Pull apart Terrain+Chaos Terrain	N
267	Double Ridge	90.439003	16.5846	Partial Cycloid	147.530764	Pull apart Terrain+Chaos Terrain	P
268	Double Ridge	89.4842	16.8321	Jagged Partial Cycloid	109.110761	Pull apart Terrain+Chaos Terrain	P
269	Double Ridge	90.834	16.6602	Jagged Linear	87.691455	Pull apart Terrain + Chaos Terrain	P
270	Double Ridge	89.860497	16.433599	Linear	67.648968	Pull apart Terrain + Chaos Terrain	P

271	Double Ridge	-78.298798	20.8529	LInear	510.844281	Pull apart Terrain + Chaos Terrain	Y
272	Double Ridge	-78.243301	27.573799	Linear	762.75523	Pull apart Terrain + Chaos Terrain	Y
273	Double Ridge	-81.241699	17.0474	Jagged Linear	398.8564	Chaos Terrain+Pull apart Terrain	Y
274	Double Ridge	-81.709801	17.372	Jagged Linear	249.975412	Pull apart Terrain + Chaos Terrain	Y
275	Double Ridge	-81.552696	16.8386	Linear	261.114239	Pull apart Terrain + Chaos Terrain	P
276	Double Ridge	90.3918	17.2626	Jagged Cycloid	160.488788	Pull apart Terrain + Chaos Terrain	P
277	Double Ridge	85.777571	9.503712	Jagged	18.398685	Pull apart Terrain	Y
278	Double Ridge	85.438933	9.403035	Linear	7.310772	Pull apart Terrain	Y
279	Double Ridge	85.904021	9.611612	Linear	10.482911	Pull apart Terrain	Y
280	Double Ridge	85.160472	9.068146	Jagged	6.359812	Pull apart Terrain	Y
281	Double Ridge	85.433088	9.124564	Jagged	13.012845	Pull apart Terrain	N
282	Double Ridge	83.754199	9.17552	Jagged	32.576618	Pull apart Terrain	Y
283	Double Ridge	83.616602	8.716154	Linear	9.836077	Pull apart Terrain	Y
284	Double Ridge	87.149094	9.254002	Jagged	23.857305	Pull apart Terrain	Y
285	Double Ridge	87.13351	8.717881	Jagged	9.237962	Pull apart Terrain	Y
286	Double Ridge	87.587782	8.462424	Jagged	38.353155	Pull apart Terrain	N

287	Double Ridge	87.673678	9.151376	Jagged	10.594482	Pull apart Terrain	Y
288	Double Ridge	88.073925	9.437502	Linear	3.849707	Pull apart Terrain	Y
289	Double Ridge	88.135612	9.272466	Jagged	25.185185	Pull apart Terrain	Y
290	Double Ridge	88.660163	8.943715	Jagged	44.640174	Pull apart Terrain	Y
291	Double Ridge	88.990878	8.822676	Jagged	67.139332	Pull apart Terrain	Y
292	Double Ridge	88.76755	8.708372	Jagged	21.419429	Pull apart Terrain	Y
293	Double Ridge	88.483898	8.655959	Jagged	16.058375	Pull apart Terrain	Y
294	Double Ridge	84.02459	8.935145	Linear	8.732824	Pull apart Terrain	Y
295	Double Ridge	83.222572	9.37344	Linear	20.609183	Pull apart Terrain	Y
296	Double Ridge	86.097267	14.99515	Linear	25.969699	Pull apart Terrain	Y
297	Double Ridge	85.702614	15.615682	Jagged	25.563163	Pull apart Terrain	Y
298	Double Ridge	86.065865	15.663922	Jagged	39.963788	Pull apart Terrain	Y
299	Double Ridge	86.207825	15.312511	Linear	9.550326	Pull apart Terrain	Y
300	Double Ridge	86.145861	15.291055	Jagged	7.925412	Pull apart Terrain	Y
301	Double Ridge	86.375081	14.525143	Jagged	16.15393	Pull apart Terrain	Y
302	Double Ridge	85.923883	14.689377	Jagged	6.032247	Pull apart Terrain	Y
303	Double Ridge	85.565765	15.528532	Jagged	23.375116	Pull apart Terrain	Y
304	Double Ridge	85.550886	15.722814	Linear	24.508012	Pull apart Terrain	Y
305	Double Ridge	86.265347	15.822356	Jagged	29.785525	Pull apart Terrain	Y

306	Double Ridge	86.55353	15.693844	Jaggged	23.946752	Pull apart Terrain	Y
307	Double Ridge	86.473937	15.787231	Jagged	6.04261	Pull apart Terrain	Y
308	Double Ridge	86.413878	15.773405	Linear	3.31528	Pull apart Terrain	Y
309	Double Ridge	86.457485	15.352926	Jagged	9.043458	Pull apart Terrain	Y
310	Double Ridge	86.381934	15.323316	Jagged	8.841082	Pull apart Terrain	Y
311	Double Ridge	86.366448	15.296727	Jagged	8.025947	Pull apart Terrain	Y
312	Double Ridge	86.544495	14.640144	Jagged	12.058303	Pull apart Terrain	Y
313	Double Ridge	178.412223	2.212017	Linear	121.897764	Cilix Crater	Y
314	Double Ridge	179.184366	0.997574	Jagged	130.7759	Cilix Crater	Y
315	Double Ridge to fossae	4.513443	42.954878	Linear	175.499734	Chaotic and pull apart terrain	Y
316	Double Ridge	8.714174	42.315055	Linear	139.018426	Chaotic and pull apart terrain	Y
317	Double Ridge to Single Ridge	3.977027	40.480419	Partial Cycloid	76.323621	Chaotic and pull apart terrain	Y
318	Double Ridge to Single Ridge	2.813086	40.094098	Partial Cycloid	27.641864	Chaotic and pull apart terrain	Y
319	Double Ridge to Single Ridge	5.021748	40.251443	Linear	49.994317	Chaotic and pull apart terrain	Y
320	Double Ridge	4.928506	43.847074	Jagged	173.418444	Chaotic and pull apart terrain	Y
321	Double Ridge	4.322436	44.365731	Jagged	56.562826	Chaotic and pull apart terrain	Y
322	Double Ridge	6.397062	42.906888	Jagged Cycloid	214.766342	Chaotic and pull apart terrain	Y
323	Double Ridge	6.303821	45.121377	Partial Cycloid	113.868899	Chaotic and pull apart terrain	Y
324	Double Ridge	10.336522	45.004825	Linear	127.916403	Chaotic (raft) and pull apart terrain	N

325	Double Ridge	8.852426	41.228538	Partial Cycloid	222.073292	Chaotic (raft) and pull apart terrain	Y
326	Double Ridge	8.852426	41.228538	Partial Cycloid	97.187148	Chaotic (raft) and pull apart terrain	Y
327	Double Ridge and lineated band	10.209031	43.850787	Jagged Linear	205.399974	Chaotic Pull apart terrain	Y
328	Double Ridge and lineated band	9.994809	45.12592	Jagged Linear	85.848905	Chaotic Pull apart terrain	Y
329	Double Ridge and lineated band	8.9543	45.809392	Jagged Linear	59.030249	Chaotic Pull apart terrain	Y

Table 5: Fossae

Id	Frac_type	Long	Lat	Frac_style	LENGTH_GEO (Km)	Near_Feat	Linea_intersect
315	Fossa	140.669998	-27.377899	Linear	18.129751	Chaos Terrain	N
316	Fossa	141.264999	-27.287201	Jagged	19.206051	Chaos Terrain	P
317	Fossa	141.229996	-27.527599	Linear	18.647391	Chaos Terrain	N
318	Fossa	141.104996	-27.497999	Jagged	10.840908	Chaos Terrain	N
319	Fossa	141.074005	-27.439699	Jagged	5.458488	Chaos Terrain	N
320	Fossa	140.869003	-27.631001	Jagged	17.927872	Chaos Terrain	N
321	Fossa	121.935997	4.17319	Jagged	14.211871	Chaos Terrain	P
322	Fossa	122.778999	6.29444	Jagged	15.445484	Chaos Terrain	P
323	Possible Fossa	35.821701	4.96839	Jagged	79.51125	Chaos Terrain	N
324	Possible Fossa	39.979698	3.72288	Jagged	151.594667	Chaos Terrain	P
325	Possible Fossa	-177.269	18.935801	Linear	50.207005		P
326	Possible Fossa	39.3396	4.11236	Jagged	140.358896	Chaos Terrain	P
327	Fossa/Fracture	80.201797	11.2605	Jagged Linear	114.701669	Chaos Terrain+ Pull apart Terrain	Y
328	Fossa/Fracture	81.382797	12.0576	Jagged Cycloid	33.722701	Chaos Terrain+ Pull apart Terrain	N

329	Fossa	-85.348701	33.757801	Jagged	68.358709	Pull apart Terrain + Chaos Terrain	P
330	Fossa	-86.636803	35.424999	Cycloid	32.957271	Pull apart Terrain+Chaos Terrain	Y
331	Fossa	-86.010399	35.756699	Jagged Cycloid	38.978098	Pull apart Terrain+Chaos Terrain	Y
332	Possible Fossa	-85.756798	36.225399	Jagged Cycloid	30.614789	Pull apart Terrain+Chaos Terrain	P
333	Fossa	-86.625504	36.904999	Linear	38.35419	Pull apart Terrain+Chaos Terrain	Y
334	Fossa	-87.588898	36.856098	Jagged	33.270153	Pull apart Terrain+Chaos Terrain	Y
335	Fossa	-87.412399	36.698799	Jagged	6.220184	Pull apart Terrain+Chaos Terrain	P
336	Possible Fossa	-85.603203	36.547699	Jagged	34.944966	Pull apart Terrain+Chaos Terrain	Y
337	Fossae	-85.955704	36.729301	Jagged Cycloid	20.561633	Pull apart Terrain+Chaos Terrain	Y
338	Possible Fossa	-84.348602	23.404499	Jagged Partial Cycloid	64.80613	Chaos Terrain+Pull apart Terrain	N
339	Possible Fossa	-83.975601	21.469801	Jagged Partial Cycloid	81.67303	Chaos Terrain+Pull apart Terrain	Y
340	Possible Fossa	-103.545	0.706092	Jagged	29.060666	Pull apart Terrain + Chaos Terrain	P
341	Possible Fossa	-103.433	0.856639	LInear	10.044872	Pull apart Terrain + Chaos Terrain	P

342	Fossae	85.723517	9.540342	Jagged	27.752023	Pull apart Terrain	Y
343	Fossae	85.819755	9.71129	Jagged	21.561207	Pull apart Terrain	Y
344	Fossae	87.181169	9.179639	Jagged	15.383363	Pull apart Terrain	N
345	Fossae	87.228432	9.235153	Jagged	9.777847	Pull apart Terrain	N
346	Fossae	88.704862	9.306148	Linear	7.935355	Pull apart Terrain	Y
347	Fossae	88.676525	9.7112	Jagged	27.160672	Pull apart Terrain	Y
348	Fossae	84.989778	8.899864	Jagged	7.013963	Pull apart Terrain	N
349	Fossae	85.692582	9.128824	Jagged	8.706766	Pull apart Terrain	Y
350	Fossae	85.633068	9.167162	Jagged	7.090168	Pull apart Terrain	Y
351	Fossae	85.929208	9.176718	Jagged	10.324728	Pull apart Terrain	Y
352	Fossae	86.085488	9.126598	Linear	7.462758	Pull apart Terrain	N
353	Fossae	87.444741	9.445923	Jagged	25.323413	Pull apart Terrain	Y
354	Fossae	87.573747	9.227369	Jagged	16.414756	Pull apart Terrain	N
355	Fossae	88.097184	9.668841	Jagged	8.318259	Pull apart Terrain	N
356	Fossae	87.845474	9.495052	Jagged	9.75142	Pull apart Terrain	Y
357	Fossae	88.202589	9.600379	Jagged	6.378593	Pull apart Terrain	Y
358	Fossae	86.509022	9.626877	Cycloid	5.516485	Pull apart Terrain	N
359	Fossae	87.074132	9.099291	Jagged	24.261386	Pull apart Terrain	Y
360	Fossae	5.120971	43.445853	Jagged	327.31043	chaotic and pull apart terrain	Y

361	Fossae	6.732789	40.848442	Jagged	51.496197	chaotic and pull apart terrain	Y
362	Fossae or fracture	8.900657	43.249414	Jagged	56.57511	chaotic and pull apart terrain	Y